

Somatotopic Mapping of the Human Somatosensory Cortex

Using Functional Magnetic Resonance Imaging (fMRI)

by

Anil K. Gehi

Submitted to the Department of Electrical Engineering and Computer Science
in Partial Fulfillment of the Requirements for the Degrees of
Bachelor of Science in Electrical Science and Engineering
and Master of Engineering in Electrical Engineering and Computer Science
at the Massachusetts Institute of Technology

May 26, 1996

Copyright 1996 Anil K. Gehi. All rights reserved.

The author hereby grants to M.I.T. permission to reproduce
distribute publicly paper and electronic copies of this thesis
and to grant others the right to do so.

Author _____
Department of Electrical Engineering and Computer Science
May 17, 1996

Certified by _____
Suzanne Corkin
Thesis Supervisor

Accepted by _____
F. R. Morgenthaler
Chairman, Department Committee on Graduate Theses

MASSACHUSETTS INSTITUTE
OF TECHNOLOGY

JUN 11 1996

LIBRARIES

Eng.

Somatotopic Mapping of the Human Somatosensory Cortex

Using Functional Magnetic Resonance Imaging (fMRI)

by

Anil K. Gehi

Submitted to the
Department of Electrical Engineering and Computer Science

May 16, 1996

In Partial Fulfillment of the Requirements for the Degree of
Bachelor of Science in Computer [Electrical] Science and Engineering
and Master of Engineering in Electrical Engineering and Computer Science

Abstract

In recent years, functional magnetic resonance imaging (fMRI) has emerged as a powerful technique for localizing human functional brain activity non-invasively. Seminal studies by Woolsey et al. [58], Penfield et al. [38,39], Merzenich et al. [31], and Sur et al. [54] have shown that there exists a somatotopic map in the primary somatosensory cortex of humans and lower primates, and have described many of its organizing principles. Such studies, however, were done with macro and microelectrodes, which directly recorded electrical activity in the cerebral cortex. FMRI techniques measure cortical activation indirectly by non-invasively monitoring the regional cerebral blood flow (rCBF) within the cortex and overlaying this map on anatomical scans for localization. We report on experiments performed to better understand the fMRI signal evoked by somatosensory stimulation. We attempt to map somatotopically the palm of the hand, the volar surface of the forearm, and the glabrous surfaces of the thumb and forefinger. Further, we report on lateral inhibition in the somatosensory representation for the palm of the hand and the volar surface of the forearm. We propose empirical models to describe this lateral inhibition and discuss its potential neural and hemodynamic underpinnings.

Thesis Supervisor: Suzanne Corkin
Title: Professor of Behavioral Neuroscience

Table of Contents

1 Introduction

2 Background

2.1 Basic Anatomy

2.2 First Evidence of Maps

2.3 Organizational Principles of Somatosensory Maps

3 Evidence of the Importance of Maps for Human Perception

3.1 Somatosensory Homunculus

3.2 Effect of Parietal-Lobe Lesions on Somatosensory Thresholds

3.3 Plasticity of Cortical Maps

4 Toward a Non-Invasive Mapping of the Human Somatosensory Cortex

4.1 Connection between rCBF and Neuronal Activity

4.2 Localizing Functional Brain Activity Using fMRI

5 Previous Somatosensory or Motor Studies Using fMRI or PET

5.1 Somatotopic Mapping of Human Motor Cortex with PET

5.2 Somatotopic Mapping of Human Motor Cortex with fMRI

5.3 Somatotopic Mapping of Human Somatosensory Cortex with PET

5.4 Somatotopic Mapping of Human Somatosensory Cortex with fMRI

6 Methods and Approach

6.1 Experiment

6.1.1 Subjects

6.1.2 Apparatus

6.1.3 Imaging Paradigms

6.2 Analysis

6.2.1 Identifying the Postcentral Gyrus

6.2.2 Epoch Comparisons

6.2.3 Straightening the Postcentral Gyrus

6.2.4 Merging and Normalizing the Postcentral Gyrus

7 Results

7.1 Motor Control

7.2 Somatotopic Mapping

7.2.1 Noise in the Postcentral Gyrus

7.2.2 Somatotopy within Subjects

7.2.3 Somatotopy across Subjects

7.3 Lateral Inhibition

7.3.1 Possible Models

7.3.2 Box Plots, Histograms, ALP Plots of Hand, Forearm Comparisons

7.3.3 Correspondence with the Models

7.4 Possible Sources of Error

8 Discussion and Conclusions

8.1 Somatotopic Mapping of the Postcentral Gyrus with fMRI

8.2 Lateral Inhibition in the fMRI Signal

8.2.1 Neuronal Somatosensory Lateral Inhibition

8.2.2 Metabolic Somatosensory Lateral Inhibition

References

Appendix Individual Box Plots for All Subjects : Hand/ Forearm Paradigm

List of Tables

Table 1 : fMRI Experiments Performed

Table 2 : Comparison Abbreviations

Table 3 : Somatotopic Mapping of Each Subject

Table 4 : Somatotopic Mapping across All Activated Areas

Table 5 : Somatotopic Mapping across Individual Hemispheres

List of Figures

- Figure 1 : The Location of SI and SII on the Lateral Surface of the Cerebral Cortex
- Figure 2 : The Dorsal Column - Medial Lemniscal and Anterolateral Systems
- Figure 3 : The Penfield Somatosensory Homunculus
- Figure 4 : Example of Oblique Coronal Slices
- Figure 5 : Stimulation Paradigms
- Figure 6 : Example of K-S Map and Timecourse
- Figure 7 : Outlined Postcentral Gyrus
- Figure 8 : Straightening, Merging, and Normalizing Procedure
- Figure 9 : Box Plot of Auditory Task (Noise)
- Figure 10 : Comparison of Auditory Noise with Somatosensory Data
- Figure 11 : Histograms of Accumulated Hand/Baseline, Forearm/Baseline, Thumb/
Baseline, and Forefinger/Baseline Positive Activation
- Figure 12 : ALP Plots of Accumulated Hand/Baseline, Forearm/Baseline, Thumb/
Baseline, and Forefinger/Baseline Positive Activation
- Figure 13 : Histograms of Accumulated and Zeroed Hand/Baseline, Forearm/Baseline,
Thumb/Baseline, and Forefinger/Baseline Positive Activation
- Figure 14 : ALP Plots of Accumulated and Zeroed Hand/Baseline, Forearm/Baseline,
Thumb/Baseline, and Forefinger/Baseline Positive Activation
- Figure 15 : Histograms of Hand/Baseline, Forearm/Baseline, Thumb/Baseline, and
Forefinger/Baseline Accumulated Across Hemispheres
- Figure 16 : Comparison of the Center of Hand Representation with the Penfield
Homunculus
- Figure 17 : The Noninhibitory Model of Hand and Forearm Representation
- Figure 18 : The Inhibitory Model of Hand and Forearm Representation
- Figure 19 : Box Plots of Hand/Baseline and Forearm/Baseline Comparisons
- Figure 20 : Box Plots of Hand/Forearm and Hand+Forearm/Baseline Comparisons
- Figure 21 : Box Plots of Accumulated Hand/Baseline, Forearm/Baseline, Hand/
Forearm, and Hand+Forearm/Baseline Comparisons
- Figure 22 : Histograms of Accumulated Hand/Baseline, Forearm/Baseline, Hand/
Forearm, and Hand+Forearm/Baseline Comparisons
- Figure 23 : ALP Plots of Accumulated Hand/Baseline, Forearm/Baseline, Hand/
Forearm, and Hand+Forearm/Baseline Comparisons
- Figure 24 : ALP Plots of Accumulated and Zeroed Hand/Baseline, Forearm/Baseline,
Hand/Forearm, and Hand+Forearm/Baseline Comparisons
- Figure 25 : Empirically Corrected Inhibitory Model of Hand and Forearm
Representation
- Figure 26 : Diagram of Lateral Inhibition
- Figure 27 : Enlargement of Receptive Fields after Blocking Lateral Inhibition

Chapter 1

Introduction

The somatosensory cerebral map plays a vital role in human perception [8]. A method for acquiring a precise map of the human somatosensory cortex non-invasively and repeatedly would be tremendously useful to our understanding of somatosensory function. With the advent of functional magnetic resonance imaging (fMRI), this achievement may be possible. No detailed study of the somatotopic mapping capabilities of fMRI has been published. Because fMRI potentially allows for a non-invasive, repeatable study of the mapping of the cortex, many medical afflictions related to the mapping of somatosensory cortex (e.g. phantom pain, tumors) can be addressed and studied with this technique.

The fMRI technique measures metabolic changes associated with neuronal activity; therefore, a precise study of this metabolic signal and its connection to previously elaborated cortical maps is necessary. The somatosensory system has been studied extensively with a number of techniques, from macro and microelectrode electrical recordings to optical and

PET imaging. Through each method, our understanding of the relation between the cortical map and human perception has deepened as principles of organization have been revealed.

In this study, we examine fMRI activity in the postcentral gyrus during somatosensory stimulation. We report on the characteristics of this signal and present empirical models to explain some of the organizing principles of the somatosensory cortex as it is uncovered through the fMRI signal. We show that detailed somatotopic mapping of body regions are not possible with our fMRI methods. However, we show that we are able to approach the established human somatotopic map (Penfield et al., [39]) with precise localization of the hand representation and precise localization of the range of the forearm, thumb, and forefinger representations. Furthermore, we show that purely excitatory models of hand and forearm representation do not fully describe the response of the fMRI signal to hand and forearm somatosensory stimulation (Gehi et al., [18]). Rather, models incorporating lateral inhibition must be employed.

Chapter 2

Background

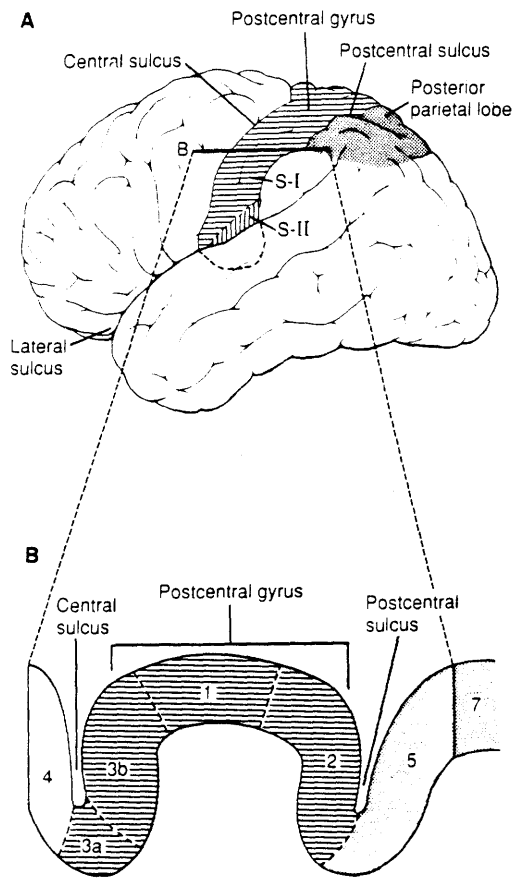
2.1 Basic Anatomy

Perceptions acquired through our sensory systems form the basis of our knowledge of the world. Perception begins in receptor cells that are sensitive to particular stimuli. From these receptor cells, the sensory pathways are linked by neurons from the periphery through intermediate stages (e.g., the thalamus) and to the cerebral cortex. The somatosensory system, in particular, mediates the sensations of touch, limb proprioception, temperature, and pain. Somatosensory information is relayed from the periphery receptors, through the spinal cord to the thalamus, and to the cerebral cortex by means of two somatosensory ascending pathways: the dorsal column-medial lemniscal system which mediates cutaneous touch, vibration, and limb proprioception, and the anterolateral system which mediates pain and cutaneous temperature [24].

The dorsal column-medial lemniscal system pathway ascends ipsilaterally in the spinal cord. The axons of this dorsal column ascend to the caudal medulla of the brain stem into the ipsilateral hemisphere and synapse on the cells of the dorsal column nuclei. From there, the medial lemniscus tract decussates and projects to the ventral posterior nucleus of the thalamus. Neurons in the ventral posterior nucleus project through the internal capsule to the primary somatosensory cortex (SI) (Figure 1), which constitutes the major portion of the postcentral gyrus. The secondary somatosensory cortex (SII) that is lateral to the primary somatosensory cortex, lying in the upper bank of the lateral sulcus (sylvian fissure), receives input primarily from SI (Figure 2) [22].

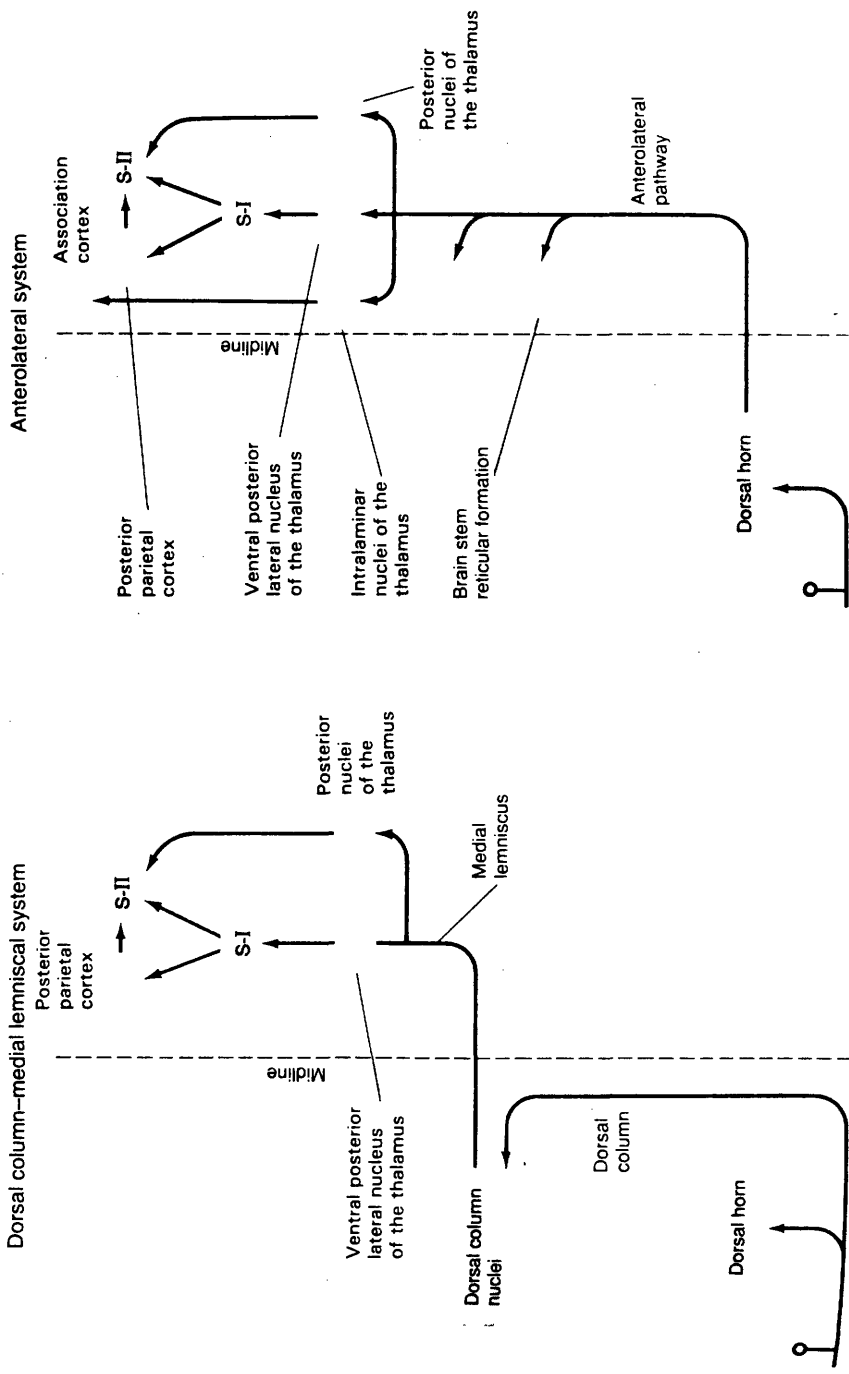
Perhaps the most striking feature of somatosensory systems is the orderly manner in which the peripheral receptor sheet (the body surface) is represented in the spinal cord, the thalamus, and finally the cerebral cortex. Various portions of the peripheral receptor sheet are represented such that contiguous surfaces in the periphery are represented by neighboring neurons in the central nervous system. This phenomenon is known as topographic organization; in the somatosensory system, this topography is known as somatotopy.

Figure 1. Diagram of the location of SI and SII on the lateral surface of the cerebral cortex [24].



Location of the Primary and Secondary Somatosensory Cortex

Figure 2. Diagram of the dorsal column-medial lemniscal and anterolateral systems showing the ascent of somatosensory input from the receptor to SI and SII [24].



Summary Diagram of Major Ascending Somatic Sensory Systems

2.2 First Evidence of Maps

In a landmark study by Woolsey, Marshall, and Bard [reviewed in 58], important features of the overall organization of the postcentral parietal cortex (SI) in macaque monkeys were found by recording evoked potentials from the surface of the brain. Woolsey et al. studied which portions of the body surface given a tactile or punctate stimulus, were capable of evoking responses at recording sites of the brain. The responses were detected with macroelectrodes placed in a closely spaced grid along the postcentral gyrus. By removing parts of the brain, they were able to explore even those cortical areas buried within the central sulcus that are also part of SI. These studies led to the following conclusions: First, the region of the postcentral gyrus activated by tactile stimuli include Brodmann areas 1, 3a, 3b, and 2. Second, the cortex is activated almost exclusively contralaterally. Third, there is an orderly representation of body parts within the somatosensory cortex with a medial-to-lateral sequence corresponding to tail-to-tongue of the body surface. Fourth, the cortical organization does not exactly reflect the body surface in that there are certain discontinuities in the cortical map. Fifth, the skin surfaces with the greatest tactile sensitivity have the greatest representation in the cortex [reviewed in 54].

2.3 Organizational Principles of Somatosensory Maps

A detailed study by Merzenich, Kaas, Sur, and Lin [31] added greater specificity to our understanding of the primate somatosensory representation in the postcentral gyrus by showing that the classical primary somatosensory region (SI) including Brodmann areas 1,

3a, 3b, and 2 of cerebral cortex contained as many as four separate representations of the body rather than one (Figure 1). This study consisted of an analysis of receptive field locations for extensive arrays of closely placed microelectrode recording sites in the parietal cortex of owl monkeys. With these techniques, the researchers were able to record from single neurons. Merzenich et al.'s study led to several important conclusions: First, the extensive mapping of the SI region of the owl monkey showed unequivocal evidence that there were at least two cutaneous representations of the body surface in owl monkeys, one in Brodmann area 1 and one in Brodmann area 3b. This study showed that the concept of a single sensory homunculus in SI, a specific representation of body regions in localized cerebral cortex, must be abandoned or placed in serious doubt for primates. Second, Brodmann area 3a is outside this cutaneous sensory strip, and there is an orderly representation of deep body structures probably coextensive with Brodmann area 2. Third, what previously had been described as a sensory homunculus did not represent the cutaneous representations found. The SI representation is better described as composites of subunits, each of which is internally somatotopic. Within each sector, progressions of recording sites correspond to progressions of receptive fields. Thus, cortical representations are organized to favor continuities in somatotopy. Disruptions, to a large extent, are a simple consequence of the impossibility of representing the three-dimensional skin surface on the two-dimensional cortex surface without splits. Further, the problem of preserving continuity in representation is increased when body representations become distorted as a consequence of greater or less sensory sensitivity [29, 52].

Sur, Merzenich, and Kaas [54] quantified the observation that receptive field size is

inversely proportional to magnification, and they delineated discontinuities in body representation. Again experimenting on owl monkeys, Sur et al., within the cortical, contralateral representation of body regions in the postcentral gyrus, derived receptive fields at many hundreds of cortical sites. The representations of the body surface in cortical areas 3b and 1 were reconstructed by demarcating the regions of cortex that received cutaneous input from given body parts. The cortical magnification factor for any skin surface was obtained by dividing its cortical representation by its skin surface area. Sur et al. found that regions with high cortical magnification, such as the glabrous hand or foot of the owl monkey, cannot maintain the same topography with the rest of the forelimb or hindlimb that exists on the skin. Thus, there are numerous discontinuities in receptive field progression. However, regions with more equal magnification factors, such as the forearm, arm, trunk, or leg, may maintain topography across cortical regions of representation. But perhaps the most important observation of the study was that the smaller the area of cortex devoted to a given region or subregion of the body surface, the larger the receptive fields on that part of the body. Further, the relation found between field size and inverse magnification was found to be a linear one [52]. Thus, definite organizational principles of somatosensory cortex were methodically laid out, suggesting that the search for more extensive constants among the representations of primate somatosensory cortex may be fruitful.

Chapter 3

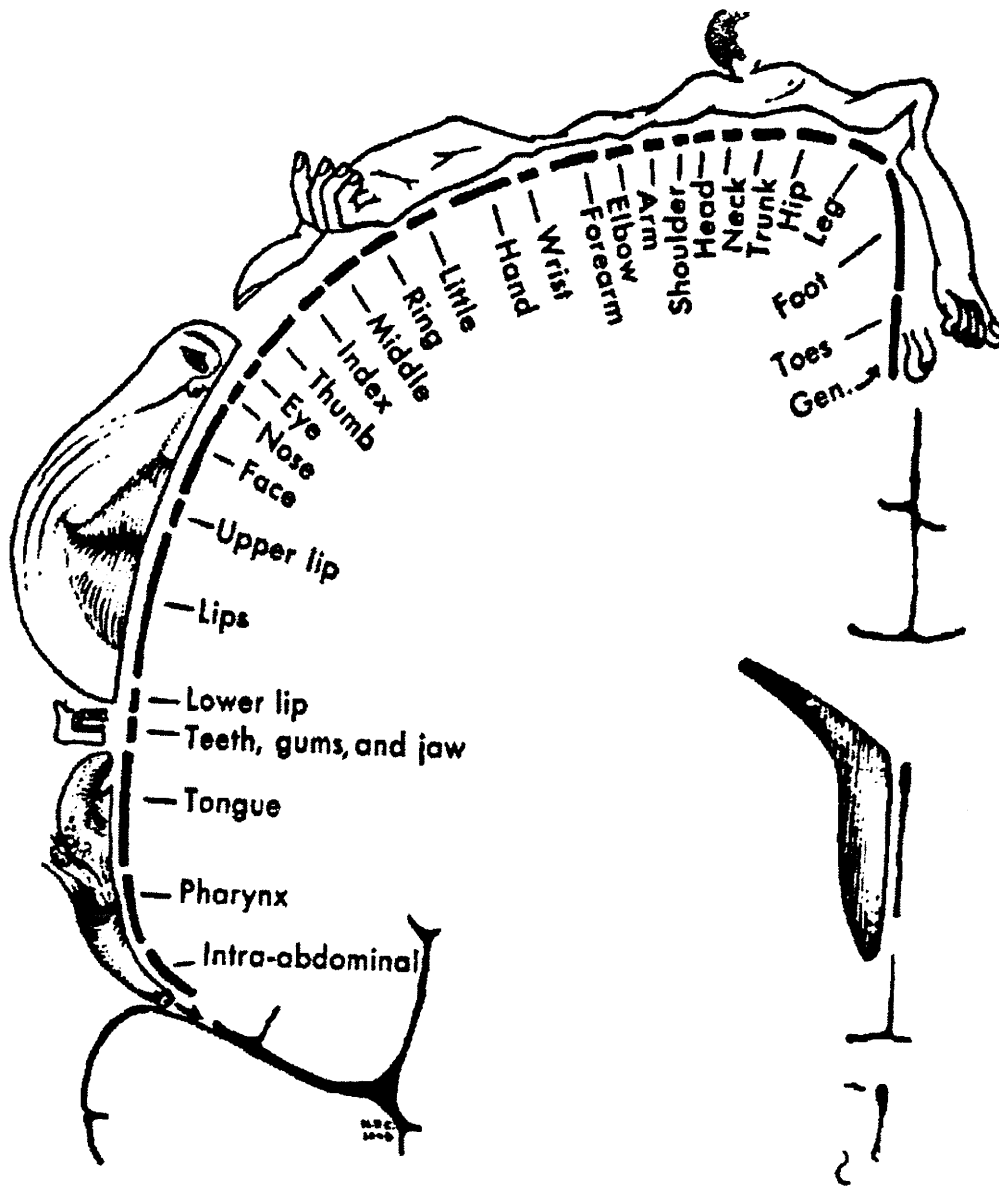
Evidence of the Importance of Maps for Human Perception

3.1 The Somatosensory Homunculus

A landmark study by Penfield and Rasmussen [39] was the first detailed study of the somatosensory mapping of the human cerebral cortex. They described detailed cortical stimulation protocols collected during operations for focal epilepsy in conscious patients. The surgical problem was to remove epileptogenic tissue without damaging the precentral and postcentral gyri, thereby avoiding paralysis and sensory loss. To this end, motor and sensory areas were mapped out carefully by stimulation. A bipolar electrode with the points separated approximately 3 mm was used for stimulation, and the sensation was described by the awake patient. Sensory responses were elicited primarily from the post-central cortex. Penfield and Rasmussen's mapping conclusions regarding the somatosensory representation of man in the postcentral gyrus are summarized in the somatosensory homunculus, derived by averaging their results across subject hemispheres (Figure 3).

This representation has come to be the established human somatosensory homunculus, the localization of human body representations to specific areas of SI. The right side of the figurine laid upon the cross section of the postcentral gyrus of the left hemisphere was drawn in proportion to the extent of cortex devoted to it. The length of the underlying block lines indicated more precisely the comparative extent of each body representation [38, 39]. This study revealed a link between human somatic perception and the gross mapping of the somatosensory cortex by demonstrating the correlation between locus of cortical stimulation and locus of body sensation.

Figure 3. The Penfield somatosensory homunculus derived from bipolar electrode stimulation of the postcentral gyrus [39].



The Penfield Somatosensory Homunculus

3.2 Effect of Parietal-Lobe Lesions on Somatosensory Thresholds

In a study conducted by Corkin, Milner, and Rasmussen [8], patients at the Montreal Neurological Institute undergoing surgery for the relief of focal epilepsy, were tested for pressure sensitivity, two-point discrimination, point localization, and position sense of the hand. These tests are indicative of the sensitivity of the somesthetic acuity of body regions. For instance, the tip of the forefinger, a particularly sensitive region, has a much lower threshold for pressure sensitivity than the forearm, a relatively insensitive region. The findings of Corkin et al. obtained from patients with well-defined unilateral cortical excisions were unequivocal in reaffirming the role of the postcentral gyrus in discriminative sensitivity. Lesions that included the postcentral hand area were associated with severe and lasting sensory loss on the contralateral hand. Further, parietal-lobe lesions that were thought to spare the hand area of the postcentral gyrus produced either transient sensory defects of the contralateral hand or none at all. Importantly, Corkin et al. found that a lesion in the postcentral gyrus that is relatively small in total extent can produce a profound and lasting somesthetic defect of the contralateral hand while a much larger posterior parietal lesion does not. This study suggested that it is the locus, and not the amount, of parietal cortex that is the important parameter in somatosensory perception. Perceptual deficits in a given body region arose from lesions to the corresponding region of the SI map. Again, the spatial organization of the SI map was intimately tied to perception [7, 8, 9].

3.3 Plasticity of Cortical Maps

Merzenich, Kaas, Wall, Sur, Nelson, and Felleman [32] described a remarkable plasticity of primate somatosensory cortical maps. Detailed maps of the hand surface representation in areas 3b and 1 of squirrel and owl monkeys were derived before, immediately after, and at subsequent intervals following median nerve section. The studies revealed that the details of the cortical map structure in areas 3b and 1 are dynamically maintained. It was found that while large cortical sectors were initially silenced by median nerve section, representations of bordering glabrous skin surfaces progressively expanded to larger and larger portions of the cortical area previously devoted to the median nerve. By 22 days, reoccupation of the former median nerve area was complete. As predicted by Sur et al. (1980), concomitant with changes in representational magnification over time were inverse changes in receptive field sizes [32].

Correlated to this neural reorganization of the somatosensory system of monkeys is the perceptual phenomenon of adult humans known as the phantom perception, the vivid perception derived from amputated body parts. Ramachandran et al. [43] showed that upper limb amputees had referred sensations in their phantom body part following stimuli that were delivered to the lower face on the same side of the amputation or to a region proximal to the stump of the amputated body part. The distribution of referred sensations suggested that a lateral-to-medial and a medial-to-lateral remapping of the deafferented somatosensory cortex had occurred [43]. Changes in the organization of maps observed by Merzenich et al. were shown to be correlated with the pattern of referred sensations in

amputees. Again, the mapping of the primary somatosensory cortex was a vital factor in the maintenance of somesthetic perception in humans.

Chapter 4

Toward a Non-Invasive Mapping of Human Somatosensory Cortex

Given the relation between map organization of the cerebral cortex and human somatosensory perception, there is a great need for a non-invasive procedure for documenting and monitoring the map. The need was met in the technique of functional magnetic resonance imaging (fMRI). The use of fMRI for monitoring brain activity stems from the studies correlating brain activity to regional cerebral blood oxygenation and blood flow (rCBF). The measurement of rCBF with fMRI has become an important tool for identifying brain areas associated with specific functions in humans *in vivo*.

4.1 Connection between rCBF and Neuronal Activity

Under normal conditions, the brain needs glucose as its source of energy. However,

because there is only minor glycogen storage in the human brain, a permanent supply of glucose via the blood is necessary. Such reasoning points to a connection between blood flow to the brain and neuronal activity. Studies done by Sokoloff et al. [reviewed in 22] confirmed this connection using 2-deoxy-glucose. By monitoring the accumulation of 2-deoxy-glucose, which cannot be catabolized as glucose but uses the same carrier system as glucose to enter the brain, Sokoloff et al. demonstrated a close correlation between rCBF and glucose consumption in the rat brain. They further demonstrated that changes in rCBF followed changes in neuronal activity by a few seconds. Leniger-Follert and Hossmann [reviewed in 22] found that after direct electrical stimulation of the sensorimotor cortex of the cat, blood flow increased within 1 sec and persisted until the end of stimulation. Thus, increases in neuronal activity led to increases in rCBF. However, whether the glucose was needed in the perikaryon, the axon, or the synapse of the neuron was unclear. A study done by Duncan et al. [reviewed in 22] of the cerebral metabolism at a cellular level showed that 2-deoxy-glucose uptake occurred not in cell bodies, but in areas rich in synapses, dendrites, and axons. Erulkar [reviewed in 22] showed that the glucose utilization is coupled mainly to presynaptic, not postsynaptic, neuronal activity. These studies suggested that presynaptic activity in cortical regions should increase neuronal glucose utilization and consequently rCBF [22], though they do not distinguish between excitatory and inhibitory presynaptic activity (Moore et al., [34]).

4.2 Localizing Functional Brain Activity Using fMRI

fMRI is a tool used to study changes in rCBF. When doing an fMRI scan, the subject is

placed into a strong, homogenous magnetic field, 1.5-4.0 Tesla (T). Consequently, various atomic nuclei, particularly the proton nuclei of hydrogen atoms, align themselves with this external field and reach a thermal equilibrium. The proton nuclei precess about the applied field at a characteristic frequency although at a random phase with respect to one another. The application of a brief radio frequency (rf) electromagnetic pulse induces a transient coherence to the spin magnetization, resulting in a brief rf signal. The rate at which the radio signal, also known as the magnetic resonance (MR) signal, decays ($T2^*$) depends upon a variety of physical factors of the medium. The presence of tissues with differing magnetizability causes local variations in the signal loss, allowing for the formation of a magnetic resonance anatomical image. In a study by Thulborn [reviewed in 3], it was demonstrated that the signal decay rate of deoxyhemoglobin is more rapid than that of oxyhemoglobin. Ogawa and Lee [reviewed in 3] subsequently reported that by monitoring $T2^*$, cortical blood vessels became more visible as blood oxygen was lowered. This effect became known as the blood oxygenation-level dependent (BOLD) method. Turner [reviewed in 3] demonstrated that with high-speed, echo-planar imaging, it was possible to observe the timecourse of these oxygenation changes. Thus using blood as an endogenous contrasting agent, it was possible to observe with rapid, functional MRI methods the transient changes in the MR signal that accompany the hemodynamic events of brain activity. fMRI allowed the non-invasive observation of the hemodynamic changes accompanying neuronal activity. Kwong et al. [reviewed in 3] found that variations in the prolonged rate at which the MR signal approaches equilibrium, $T1$, could also be used to observe the increased flow of blood into an imaging volume. Further, it was found that while $T2^*$ probably reflects the signal changes in the venous system, $T1$ is more biased

toward the arterial system, giving a truer account of neuronal activity. The hemodynamically induced signal changes at 2-5% were small, but with adequate signal-to-noise ratios in the MR images, these changes were clearly visible [3].

Chapter 5

Previous Somatosensory or Motor Studies Using fMRI or PET

There have been no detailed fMRI studies of primary somatosensory cortex of humans. This review describes PET and fMRI studies of primary somatosensory and motor cortex, having similar mapping properties to primary somatosensory cortex. PET, like fMRI, measures rCBF, an index of neuronal activity in primary somatosensory and motor cortex.

5.1 Somatotopic Mapping of Human Motor Cortex with PET

As shown in humans by Penfield et al. [38] in the study of epileptic patients, the human motor cortex, primarily occupying the precentral gyrus, is also somatotopically organized. Grafton et al. [19] conducted a PET study of the motor somatotopy of humans. In this study, several images of rCBF were obtained using PET in 12 normal subjects while they

performed a set of motor tracking tasks. Subjects were presented with a randomly moving, half-centimeter target displayed on a 13-in video monitor. In a control experiment, subjects followed the target with their eyes. In subsequent experiments, subjects followed the target under several conditions: with the index finger, allowing rotation only of the axis about the first metacarpophalangeal joint; with the hand, allowing rotation only at the shoulder joint; with the great toe; and with the tongue extended. The investigators measured the site of maximal activation in primary motor cortex and the peak percentage increase of rCBF, and then mapped the point maxima for each stimulation onto an MRI-generated coronal section. All subjects demonstrated focal increases in rCBF that followed the classic somatotopic representation of the motor cortex as defined by Penfield et al. In a similar study Grafton et al. [19] documented within-arm somatotopy in the human motor cortex with PET. Six subjects tracked a target, rotating only about the first metacarpophalangeal joint, the wrist, the elbow, or the shoulder. Again, maxima determined whether there was a consistent homuncular pattern. Grafton et al. found that the different responses in the motor cortex formed a well-defined homuncular representation, with the finger movements most inferolateral and shoulder movements most superior, in accordance with the established Penfield et al. homunculus. However, the “approximate area of the rCBF responses for each task overlapped extensively” [19].

5.2 Somatotopic Mapping of Human Motor Cortex with fMRI

A seminal study done by Kwong et al. [28] first reported rCBF changes observable with fMRI without an exogenous contrasting agent. Seven normal human subjects performed

visual and motor tasks to localize signal intensity changes. To visualize these changes, the investigators used a stimulation paradigm alternating between resting and stimulated states. Regions of cortical activity could then be revealed by magnitude subtraction of averaged baseline images from all subsequent activation images. The primary visual cortex (V1) was evaluated using flash photic stimulation. Image analysis revealed that the temporal response of V1 signal intensity changes was 4.4 sec delayed from activation. A similar subtraction and time series analysis was performed during a hand squeezing, motor activating task. The activated region corresponded to the expected homuncular region within the primary motor cortex. The temporal response of the motor task was similar to that of the visual task. All analyses were done on a single coronal or oblique coronal image that contained the respective motor or visual cortex [28].

Kim et al. [27] studied human motor cortical activity using a 4T whole-body MRI system. They instructed 6 human subjects to make repetitive opposing thumb and forefinger movements in three experimental conditions: with the right hand, left hand, and both hands. They calculated the difference between averaged baseline and averaged task-induced image intensities, and compared the baseline and activation conditions with a t -test ($p < .0001$). They then overlaid all pixels with statistically significant activation on an anatomical map. All subjects showed localized activation in the lateral region of the motor cortex. Kim et al. found the expected somatotopy of activation, though the area of motor cortex activated in the task was smaller than the area activated in electrical stimulation studies (Penfield et al. [39]) [27]. This effect, however, may have been due to the stringent threshold used in the experiment.

Rao et al. [44, 45] conducted a human motor cortex study on 8 subjects using a 1.5T MRI scanner. Again the paradigm consisted of multiple periods of baseline alternating with periods of muscle activation. The activation tasks required self-paced repetitive movements of the fingers, elbow, and toes on the subject's right, dominant side. The finger and toe movements consisted of repetitive flexion and extension of the metacarpophalangeal joints, except the thumb and great toe. The arm movements consisted of flexion and extension of approximately 25° at the elbow with the shoulder at a constant approximately 20° flex. Rao et al. found that movements of the toes produced signal changes in the left motor cortex that were more medial than those produced by finger movements, deriving again somatotopy in accordance with the established motor homunculus. Importantly, Rao et al. found that there was little or no spatial overlap observed between the activation sites for the toe and finger movements. Signal intensity changes for the elbow, however, situated between that of the fingers and toes, overlapped with the changes observed with the finger movements [44, 45].

5.3 Somatotopic Mapping of Human Somatosensory Cortex with PET

Roland and Seitz [47] measured activity in the human somatosensory cortex using PET. They stimulated 10 subjects with 3 stimulation paradigms in 3 experiments. In one experiment, subjects were passively stimulated by vibrating the hand. In a haptic condition, subjects actively explored the shape of blocks with the hand. In the third experiment, subjects opposed the thumb and forefinger at a constant frequency. Brain activation measured

by PET in the Roland and Seitz study was defined to be in any area encompassing at least three uncorrelated pixels and having a spot for which the change in rCBF between a baseline, control experiment and the stimulation experiment was larger than 5.0 mL. All three tasks produced SI activity in the hand area of approximately similar magnitude and location. Only passive vibration activated SII selectively [47].

5.4 Somatotopic Mapping of the Human Somatosensory Cortex with fMRI

Fried et al. [14] conducted an fMRI study of the entire Rolandic cortex, comprising the somatosensory and motor cortex. They asked 9 subjects to perform a motor activation task, consisting of repetitive flexion and extension of the toes of the dominant foot for the duration of the scan. A baseline, resting scan of equivalent duration was compared with the experimental condition. Fried et al. found that the most prominent changes in signal intensity occurred in regions known to represent the lower extremity in primary motor and somatosensory cortices. During the prolonged motor stimulation, Fried et al. found a decline in the MR signal, probably due to an increase in the deoxyhemoglobin content during conditions of sustained activity. Fried et al. warned that the temporal dynamics of the MR signal should be considered in analyzing functional scanning procedures. The delivery time and nature of the stimulus impose important effects on neuronal habituation as well as on changes in blood flow and metabolism [14].

Chapter 6

Methods and Approach

6.1 Experiment

The following experiments were performed with two goals: first, to study the somatotopic mapping of the palm of the hand, the volar surface of the forearm, and the glabrous surface of the thumb and forefinger with fMRI, and second, to document the detailed organization of this representation in the palm and volar forearm.

6.1.1 Subjects

Five normal, right-handed subjects (4 female, 1 male; ages 21 to 25) participated in the fMRI experiments. The subjects will be known as Subject1, Subject2, Subject3, Subject4, and Subject5, numbered in chronological order of experiment date. Subject2 had an ado-

lescent hand surgery to remove a swollen, painful nerve ganglion in the back of the left hand, immediately above the wrist joint. However, Subject2 reported no loss of sensation following the surgery and is included in this study. Subject3 had suffered a torn ligament in the left ring finger prior to the scan, but, the experimental stimulus did not contact this area of the hand. All other subjects reported no aberrations of the stimulated regions or of the nervous system.

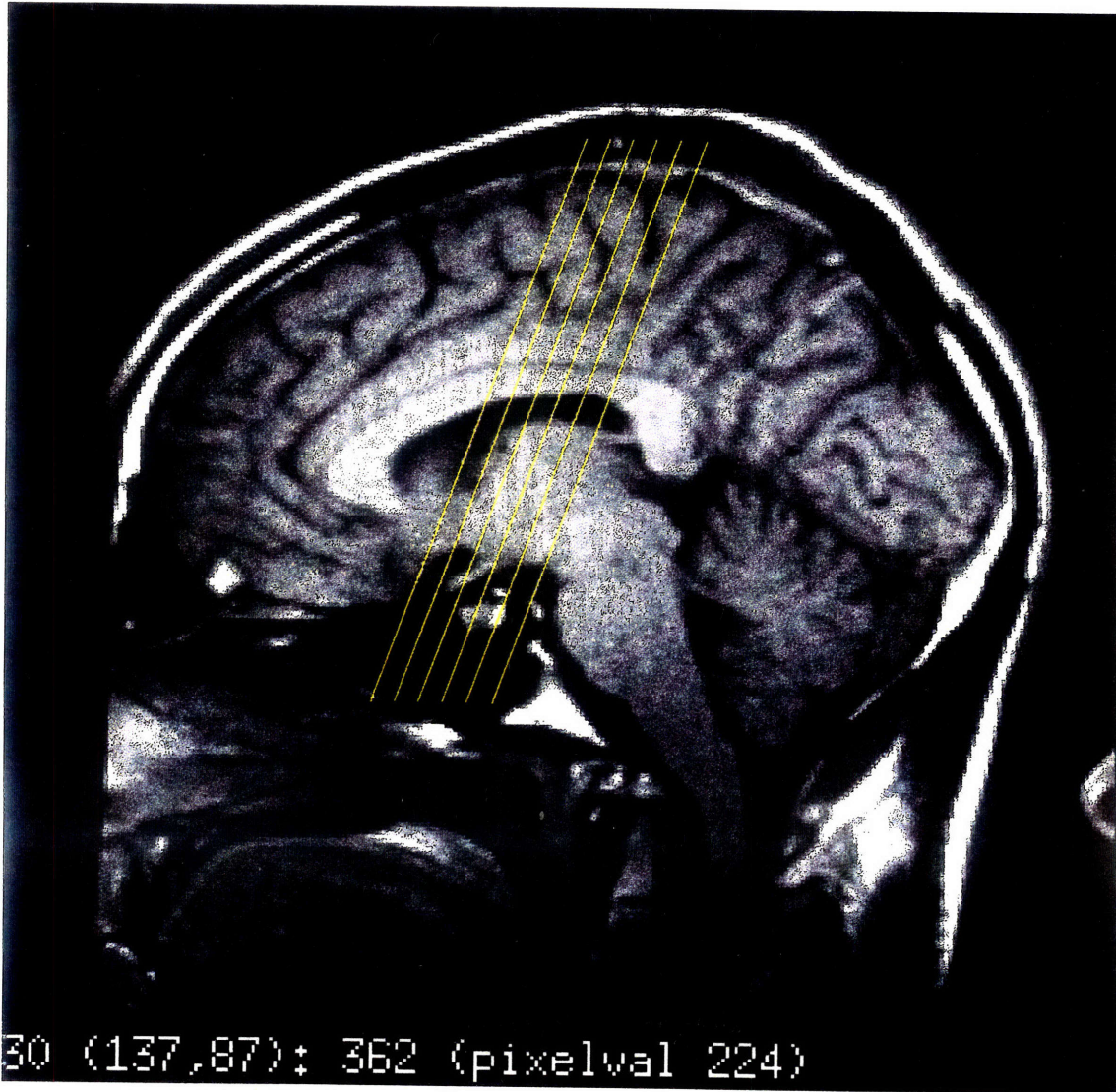
6.1.2 Experimental Apparatus

All fMRI experiments were performed at the MGH-NMR Center in Charlestown, MA, using a 1.5 T General Electric Signa, MRI scanner modified by Advanced NMR Systems. A full head coil (as opposed to a surface coil) allowed bilateral acquisitions to be made. High-speed, echo-planar MRI data were taken with a TR of 2500, a TE of 80, and 10 contiguous oblique coronal slices, each 7 mm thick, giving 96 images per slice for a 4 min scan. After sagittal localizer MRI images were acquired, we oriented the angle of the slices, so that they followed the postero-to-anterolateral progression of the postcentral gyrus (Figure 1). Oblique coronal slices aided in the subsequent analysis because the entire postcentral gyrus would often be contained in three or four slices. The resolution of the coronal slices was $3 \times 3 \text{ mm}^2$ per pixel of image. Figure 4 shows an example of the orientation of the oblique coronal slices for a single subject.

Each subject received somatosensory stimulation through repeated stimulation with a von Frey hair (gauge 15, $\log_{10} \text{ mg} = 5.88$) at approximately 3-5 Hz. The von Frey hair gave a

punctilious stimulus of a consistent pressure. This point stimulus should activate cutaneous receptors, giving activation primarily in areas 1 and 3b of SI.

Figure 4. Oblique coronal slices through the parietal cerebral cortex of Subject4. The 6 slices are oriented at an angle along that of the cingulate sulcus, completely encapsulate SI (see Figure 1).



Oblique Coronal Slices through the Parietal Cerebral Cortex

6.1.3 Imaging Paradigms

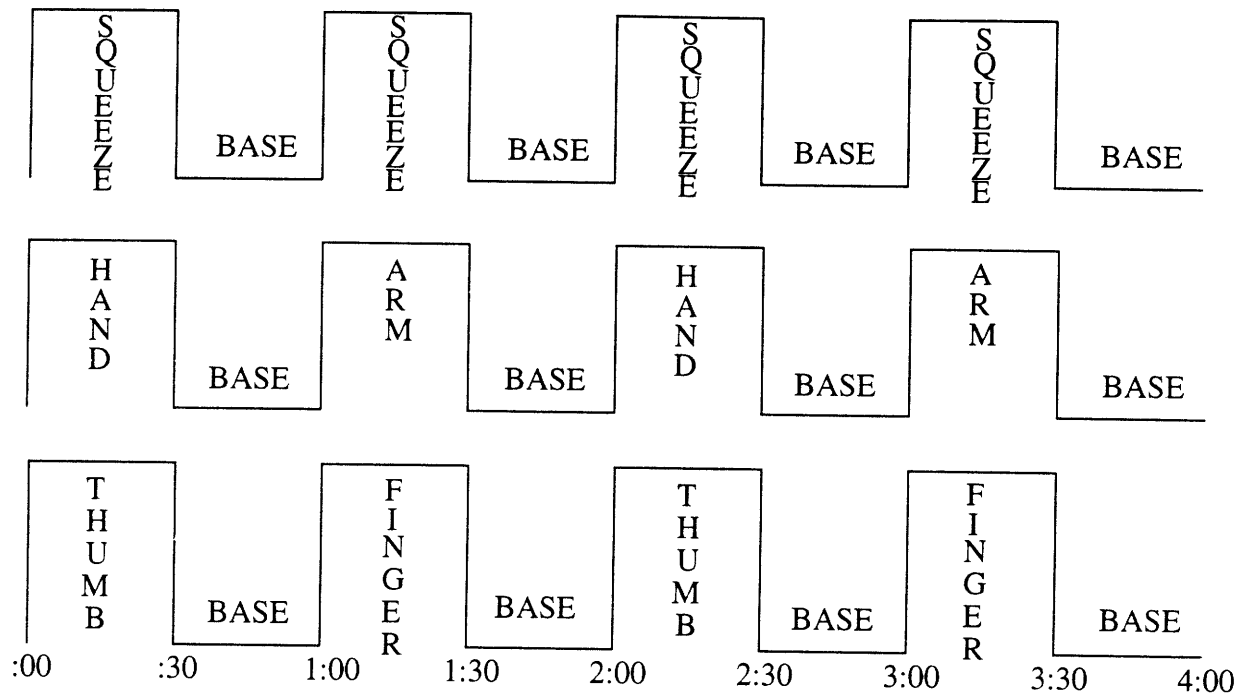
A motor stimulation paradigm was introduced into the experimental procedures. Similar to Kwong et al. [28], Grafton et al. [19], and Rao et al. [44, 45], the 4 min scanning time consisted of a series of alternating activation and baseline conditions. Prior to entering the scanner, subjects were told that during the activation epoch, they should constrict their hand as if squeezing a rubber ball, but that their fingers should not contact the hand or each other. In this manner, the squeezing motion should activate the primary motor cortex in the precentral gyrus. All paradigms were administered bilaterally. Figure 5 diagrams the motor stimulation paradigms.

The sensory stimulation paradigms were also designed with alternating stimulation and baseline. The hand/forearm paradigms used stimulation of the hand, forearm, and simultaneously hand and forearm. The thumb/forefinger paradigms used stimulation of the glabrous surface of the thumb, the glabrous surface of the forefinger, and simultaneously thumb and forefinger. All paradigms were performed bilaterally. For this study, only single area stimulations were analyzed (e.g., hand stimulation, forearm stimulation, but not simultaneous hand and forearm stimulation). Figure 5 shows diagrams of the hand/forearm and thumb/forefinger stimulation paradigms. The order of stimulation within the sensory stimulation paradigms were balanced across the 4 min scan to thwart drift in rCBF and neuronal habituation from corrupting the fMRI signal (Figure 5). Table 1 summarizes the experiments performed with each subject:

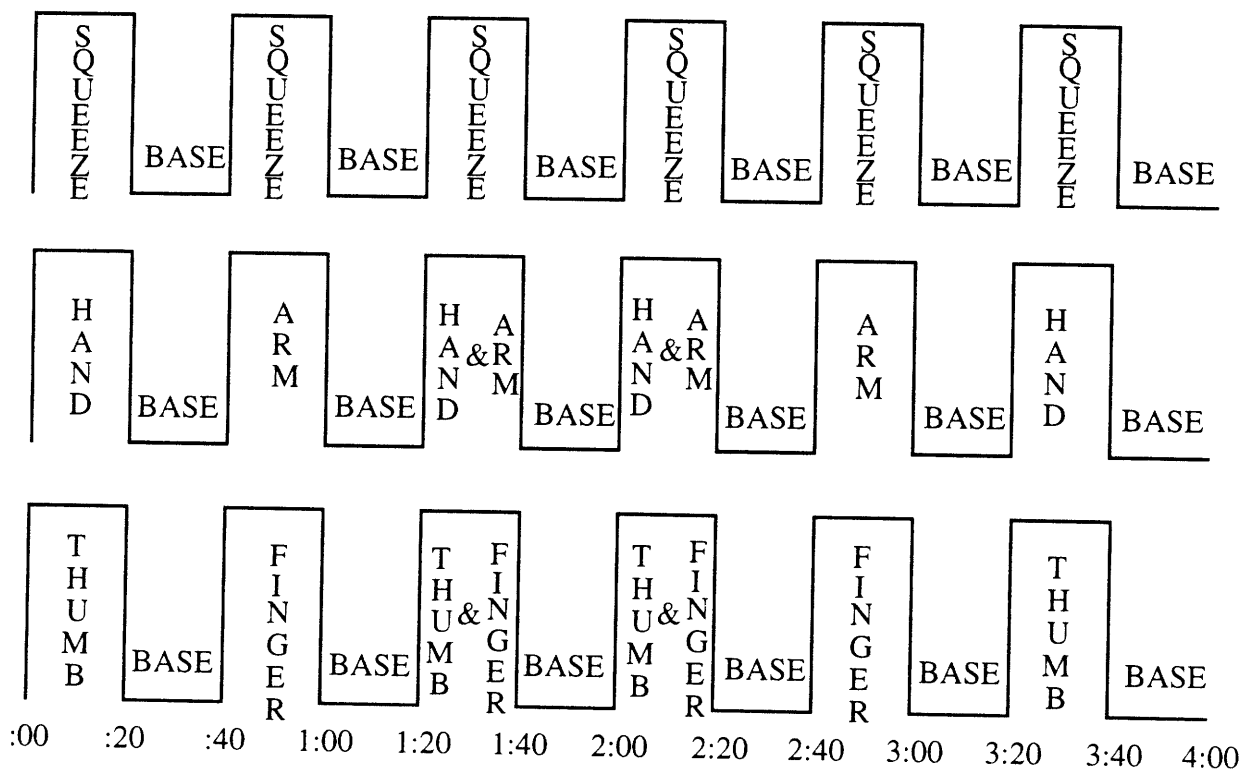
Table 1: fMRI Experiments Performed

Subject	Number of Scans	Areas of Stimulation	Length of Epochs (sec)
Subject1	4	hand/arm	30
	2	thumb/forefinger	30
Subject2	4	hand/arm	20
	2	thumb/forefinger	20
Subject3	2	hand/arm	20
	2	thumb/forefinger	20
Subject4	2	hand/arm	20
	2	thumb/forefinger	20
Subject5	2	hand/arm	20
	2	thumb/forefinger	20

Figure 5. Diagram of motor, hand/forearm, and thumb/forefinger stimulation paradigms for all subjects.



Motor, Hand/Forearm, Thumb/Forefinger Paradigms
Subject1



Motor, Hand/Forearm, Thumb/Forefinger Paradigms
Subject2, Subject3, Subject4, Subject5

6.2 Analysis

6.2.1 Identification of the Postcentral Gyrus

To analyze the functional data acquired from the fMRI scans, it was first necessary to identify the postcentral gyrus in the 10 oblique coronal slices for each subject. Due to variation in the sulci and gyri between subjects, the location of the postcentral gyrus in oblique coronal sections was inconsistent. There were, however, a number of techniques that one could use to identify and verify the location of the postcentral gyrus.

As previously discussed, the postcentral gyrus is located posterior to the central sulcus and anterior to the postcentral sulcus (Figure 1). It was virtually impossible to anatomically identify these sulci directly from the high resolution anatomical MRI images of the oblique coronal slices. To locate these sulci, we resliced the high resolution scans of the brain in three planes of section - coronal, sagittal, and axial. Once the brain could be viewed from all three perspectives, it was possible to identify with confidence the progression of the central, precentral, and postcentral sulci. This procedure was done by beginning on the most dorsal axial sections and progressing ventrally through the brain. Eventually a “T” crossing of the superior frontal sulcus with the precentral sulcus became evident. The central and postcentral sulci were identified as the two sulci immediately posterior to the precentral sulcus because the precentral, central, and postcentral sulci follow roughly parallel, medial-to-lateral and posterior-to-anterior paths. Once these sulci were identified, the precentral and postcentral gyri were localized on the high resolution

oblique coronal slices.

We also analyzed motor activation as a further verification of the location of the precentral and postcentral gyri. As demonstrated by Kwong et al. [28], Kim et al. [27], and Rao et al. [44, 45], functional mapping of the primary motor cortex with fMRI is robust. All five subjects showed significant activation ($p < .05$) within the precentral gyrus during motor activity, confirming the anatomical localization.

6.2.2 Epoch Comparisons

We used the statistical methods developed by Weisskoff et al. at the MGH-NMR center to analyze functional MRI raw data. This analysis compared epochs within a functional scan using the Kolmogorov-Smirnov (K-S) statistic. This statistic is similar to the student's t -test in that it is sensitive to changes in the mean. Unlike the student's t -test, however, this analysis also detects changes in the skew and variance. Unfortunately, such parametric analyses rely on pooling data points from the paradigm epochs, thereby losing any within-epoch temporal resolution. This pooling prevents detailed analysis of sensory transients. Such temporal resolution, however, was not necessary to this mapping study.

Before performing the K-S statistical analysis, we processed the functional raw data through a number of formatting conversions that prepared the data for the K-S map grinder. The K-S map grinder took as input the formatted raw data and parameters indicating which epochs to compare statistically, and then implemented a pixel-by-pixel com-

parison of the functional scan epochs for each oblique coronal slice. When this functional K-S map was superimposed on the high-resolution MRI coronal slice, areas of functional activity could be identified. "Functional activity" indicated regions of the brain that were significantly more active in one condition than in another (e.g., experimental vs. baseline). The K-S map displayed a color-coded map of the activated regions conveying levels of significance. For this study, significant functional differences were taken to be at or beyond $p < .05$ level of significance (above the 95% confidence threshold). We chose this permissive threshold for several reasons: First, as a first pass at somatosensory functional mapping, we wanted to be lax in our exclusion of activated areas. Second, the head coil had a low signal to noise ratio, so we were looking for changes on the order of 1-2%. Third, preliminary studies showed that, with the exception of hand stimulation, using a more stringent threshold would give an extremely poor sampling of activation.

The K-S map software also permitted a specific region of interest (ROI) of the functional image to be studied. The functional data corresponding to the pixels within this ROI could be averaged and the timecourse of the raw data viewed. The timecourse displayed the image-by-image (96 total for 4 min) signal intensity for the averaged ROI. For example, Figure 6 illustrates hand activation (Subject3: right-hand stimulation). The timecourse shows a response to hand and simultaneous hand and forearm stimulation.

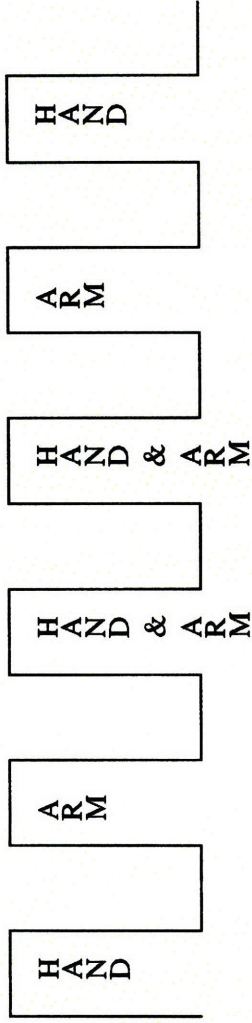
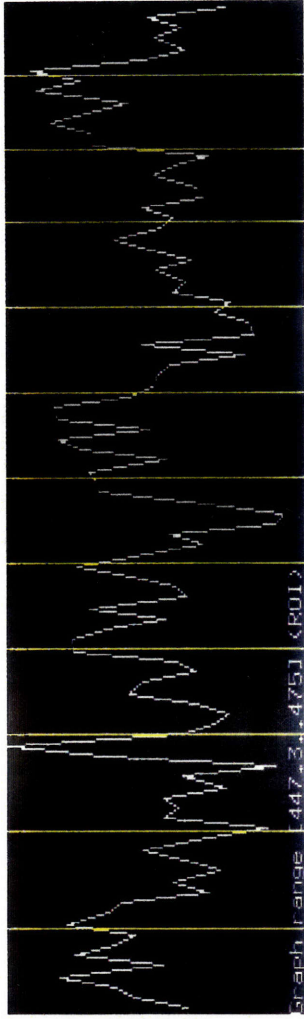
We performed a number of different epoch comparisons with the K-S mapping technique. We did a motor(squeeze)/baseline comparison for the motor paradigms. For the hand/arm paradigm, we did a hand/baseline comparison, a hand/arm comparison, and a summed

(not simultaneous) hand+arm/baseline comparison. Equivalent K-S comparisons were done for the thumb/forefinger paradigm with thumb analogous to hand and finger analogous to arm. A table outlining abbreviations that will be used hereafter for the comparisons follows:


Table 2: Comparison Abbreviations

Comparison	Abbreviation
hand/baseline positive	H/B
hand/baseline negative	B/H
forearm/baseline positive	A/B
forearm/baseline negative	B/A
hand/forearm positive	H/A
hand/forearm negative	A/H
hand+forearm/baseline positive	H+A/B
hand+forearm/baseline negative	B/H+A
thumb/baseline positive	T/B
thumb/baseline negative	B/T
forefinger/baseline positive	F/B
forefinger/baseline negative	B/F

Figure 6. Example of K-S map and timecourse generated in the analysis of a right-side hand/forearm experiment on Subject3. The highlighted region of interest (ROI) corresponds to the hand representation in the contralateral postcentral gyrus. The timecourse of the fMRI signal closely follows epochs of hand and simultaneous hand and forearm stimulation.



Hand/Arm Stimulation Paradigm

 = region of interest (ROI)

Somatosensory Activation in the Postcentral Gyrus

6.2.3 Straightening the Postcentral Gyrus

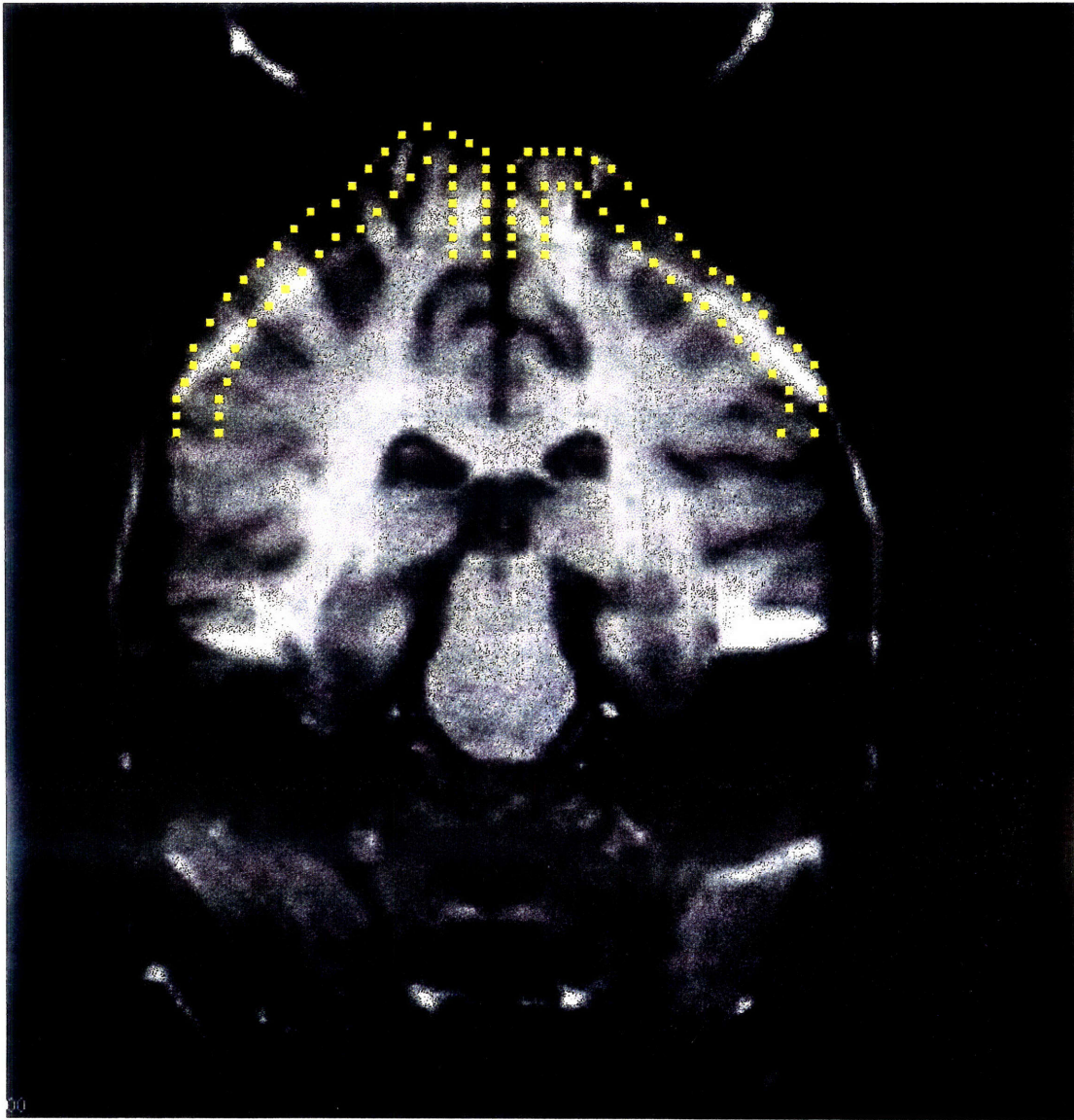
In order to compare the localization of activation along the postcentral gyrus between hemispheres, it was desirable to *straighten* the postcentral gyrus in each oblique coronal slice, *merge* the slices into one slice, and *normalize* the length of the postcentral gyrus. The human postcentral gyrus located between the central and postcentral sulcus travels in a medial-to-lateral, anterior-to-posterior manner from the cingulate sulcus to the sylvian fissure [37]. The postcentral gyrus has a thickness of approximately 3-5 mm [37]. Thus, an outline was overlaid on the region of the slices that was believed to contain the postcentral gyrus. This region was taken to be the outer edge of the cortex from the cingulate sulcus to approximately 6 mm dorsal to the sylvian fissure. In an effort to exclude SII, located in the upper bank of the sylvian fissure (Figure 1), the outlined region stopped short of the sylvian fissure. Figure 7 shows our definition of the postcentral gyrus in yellow.

Once the postcentral gyrus was outlined, areas of activation ($p < .05$) were identified within the borders of the outlined region. Localization of the areas of activation was defined as the linear distance along the superficial edge of the postcentral gyrus.

Once straightened, a *box plot* of a particular comparison could be constructed. The postcentral gyrus progresses from those slices most posterior to those most anterior and from the more medial region of the outlined area to the more lateral region. However, the postcentral gyrus also displays a characteristic double S-shaped path along this progression.

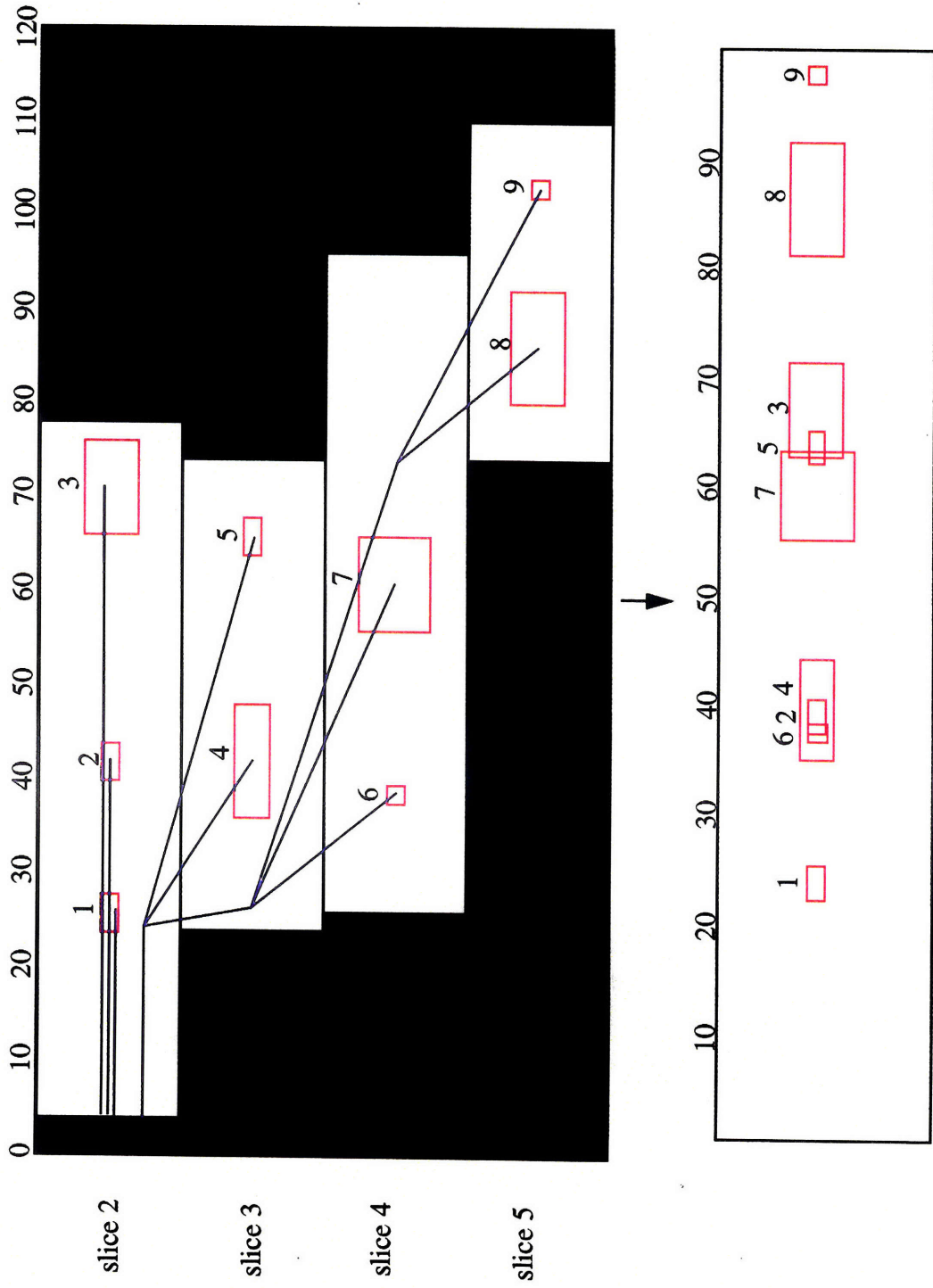
Therefore, regions of the postcentral gyrus often jump back and forth between the oblique coronal slices. Figure 8 shows an example of a straightened postcentral gyrus (Subject5, left hemisphere). Location along the postcentral gyrus has one degree of freedom in our reconstruction, i.e., the length along the postcentral gyrus.

Figure 7. Grid overlay for measurement of the postcentral gyrus. Pixels are $1.5 \times 1.5 \text{ mm}^2$. Our measurement of the postcentral gyrus stops at 5 mm prior to the start of the sylvian fissure, underestimating the full extent of the postcentral gyrus.



Sample Outline of Postcentral Gyrus

Figure 8. Straightening, merging, and normalizing procedure. Red boxes represent areas of activation along each oblique coronal slice. The area of each box corresponds to the area of the activated region. The postcentral gyrus of Subject5 was completely contained in slices 2, 3, 4, and 5, with 2 being the most posterior and dorsal. The edge of each slice at 0 mm represents the most medial extent of the outlined postcentral gyrus; the edge at 120 mm represents the most lateral extent. Blue lines indicate the extent along the merged slice of each activated area. The length of each line was found by taking the hypotenuse of a right triangle with one leg as the distance along a slice and the other leg as the thickness of each slice, 7 mm. Once merged into a single slice, the length was normalized to 100 mm.



Straightening, Merging, and Normalizing Procedure

6.2.4 Merging and Normalizing the Postcentral Gyrus

Due to deviations in the path, shape, and length of the postcentral gyrus, it was necessary to merge the slices and normalize the postcentral gyrus to make comparisons among subjects and to acquire a better sampling of data. To this end, we developed a technique to collapse the activated areas on each slice into a single slice. One could imagine drawing a smooth curve along the center of the straightened slices along the entire postcentral gyrus, adding 7 mm, the thickness of each slice, whenever a border between slices was crossed, and calling this the single slice. Subsequently drawing the closest perpendicular from an activated area to this smooth curve would indicate where along the smooth curve, or the single slice, the activated areas would lie. To approximate this ideal systematically and consistently, the following procedure was used: First, we selected the slice extending most medially as the reference slice. All other slices were merged into this reference slice. Second, the localization of any activated areas in the reference slice was taken to be at their location on the unmerged plot. Third, localization of activated areas in all other slices were referenced to this reference slice by taking the linear distance until the slice crossed the reference slice, and summing this with the hypotenuse of a right triangle constructed from the thickness of each slice (7 mm) as one leg and the linear distance along the non-reference slice as the other leg. This procedure is best understood with the illustration in Figure 8. The extent of the progression along the merged slices is shown for each activated area in blue. Once the slices were merged into one slice, the extent of the postcentral gyrus was normalized to a length of 100 “postcentral gyrus units”. Because our outlined postcentral gyrus was approximately 100 mm in length (90 - 120 mm) for

each subject, a “postcentral gyrus unit” roughly corresponded to 1 mm (Figure 8 shows a box plot of the complete straightened, merged, and normalized postcentral gyrus).

Chapter 7

Results

With the resulting straightened and merged data describing the activated areas in the post-central gyrus, meaningful results could be ascertained, not only for a single scan, but also across scans and subjects. The central questions of the study regarding somatotopic mapping and lateral inhibition will be addressed with these results.

7.1 Motor Control

In addition to providing anatomical verification, the motor paradigm controlled for the quality of the fMRI signal in response to external stimulation of each subject. As was shown by Kwong et al. [28], this motor task is a robust activator of the fMRI signal. In 5/5 subjects, 10/10 hemispheres, clear activation due to the motor stimulation task was present in the precentral gyrus. The clarity of the response is apparent not only in the intensity of the activity shown in the K-S map but also in the ROI timecourse. Clear divi-

sions occur between motor stimulation and baseline epochs.

7.2 Somatotopic Mapping

The results of a somatotopic mapping study of the hand, forearm, thumb, and forefinger stem from the positive comparisons of a single stimulated region with baseline. Box plots of the straightened, merged, and normalized K-S maps ($p < .05$) obtained with the hand/arm paradigm for all subjects are in the Appendix.

7.2.1 Noise in the Postcentral Gyrus

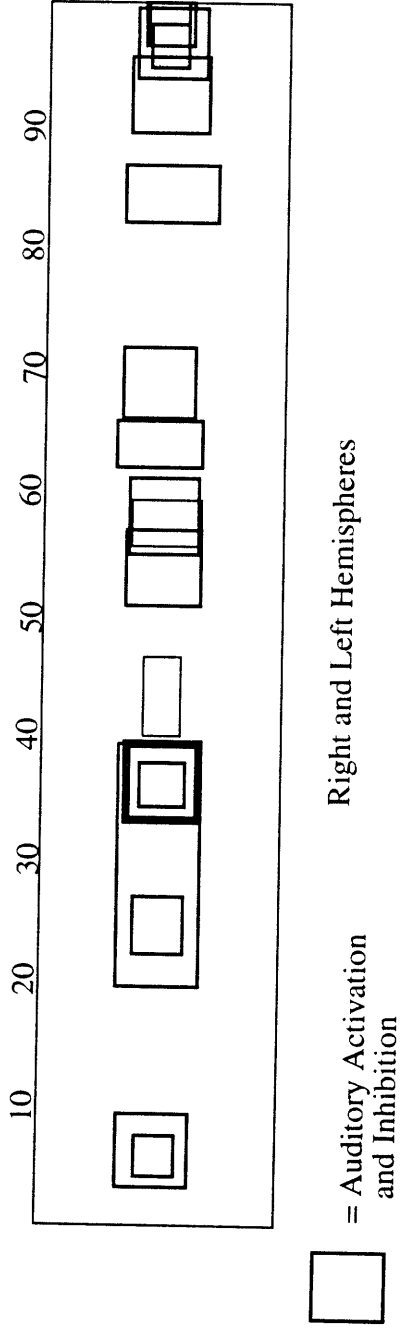
Before evaluating the somatotopic map, we analyzed the noise along the postcentral gyrus that surpassed our threshold of activation ($p < .05$). A subject scanned with identical epoch lengths but with an auditory task, completely unrelated to our somatosensory paradigm was analyzed by comparing alternating epochs. Because auditory stimulation is known not to project to the postcentral gyrus, we considered activation in the postcentral gyrus to be noise. A box plot of this auditory task is shown in Figure 9. The activated areas spread along the entire the postcentral gyrus (Figure 10). The location of the activated areas does not have a normal (Gaussian) distribution (mean, 56.58 mm; SD, 29.56 mm) for the data from the two hemispheres.

To get an indication of the extent to which noise influenced our results, we generated another plot relating the location of the activated regions to the product of the area and the

$-\log_{10}(p\text{-value})$, $p < .05$. These plots will be known as ALP (Area, Localization, P-value) plots. Such ALP plots incorporate the area, intensity (p -value and number of activated areas), and location of activated regions in the postcentral gyrus, the three central factors in our determination of somatotopy. The ALP plot of the postcentral gyrus during the auditory task is shown in Figure 10. The noise lacks a Gaussian distribution.

This noise distribution can be compared with the distribution of a body region representation. For example, the H/B comparison data accumulated over all subjects, both hemispheres, showed a much more localized, Gaussian distribution. Figure 10 shows a histogram and ALP plot of the localization of the hand along the postcentral gyrus. Here the histogram has a more Gaussian, focused shape of the histogram (mean: 62.94 mm, SD: 21.02 mm).

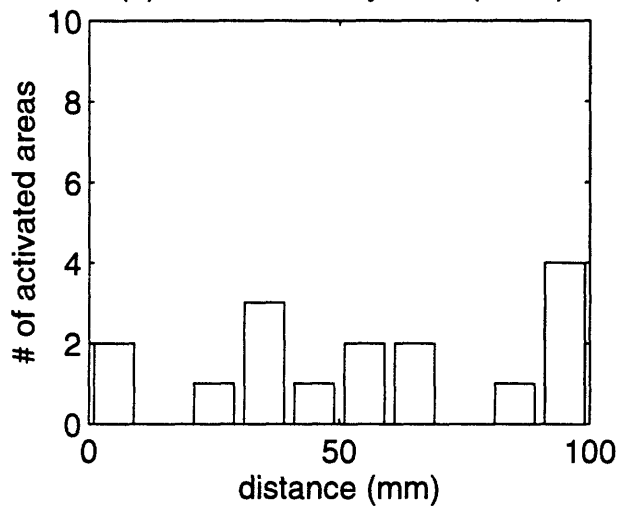
Figure 9. Box plot of auditory task (noise) activated areas in the postcentral gyrus. Activated areas spread along the entire extent of the gyrus. Line thickness of rectangles is proportional to $-\log_{10}(\text{p-value})$ of the K-S statistic.



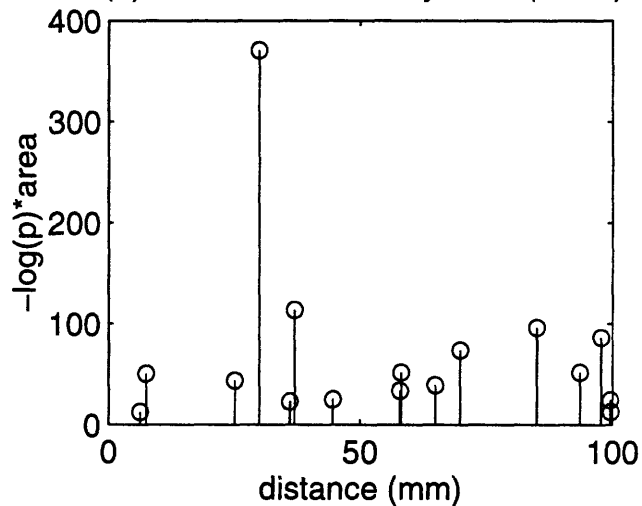
Box Plot of Auditory Task (Noise)

Figure 10. (a) Histogram of the localization of auditory task (noise) activated areas in the postcentral gyrus. Activated areas do not have a normal distribution. (b) ALP plot of the localization of auditory task (noise) activated areas in the postcentral gyrus. Activated areas scaled by area and level of significance still do not have a normal distribution. (c) Histogram of the localization of accumulated hand/baseline positively activated areas in the postcentral gyrus for all subjects. Gaussian distribution (mean : 62.94, SD : 21.02) is shown for comparison. (d) ALP (Area, Localization, P-value) plot of the localization of accumulated hand/baseline positively activated areas in the postcentral gyrus for all subjects. When activated areas are scaled by area and level of significance, the distribution is Gaussian in appearance.

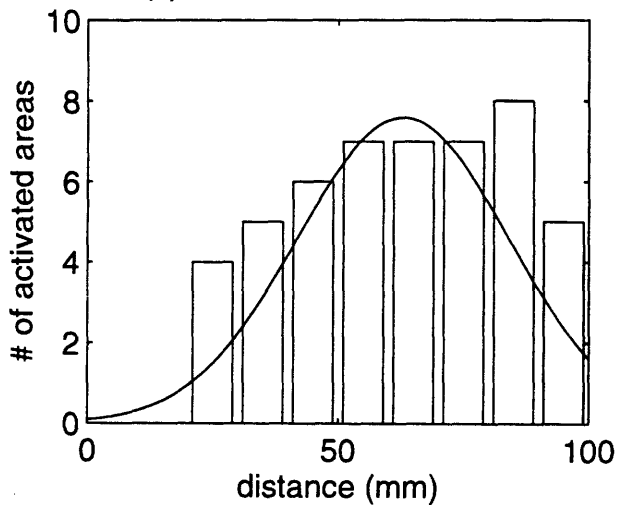
(a) Hist of Auditory Task (noise)



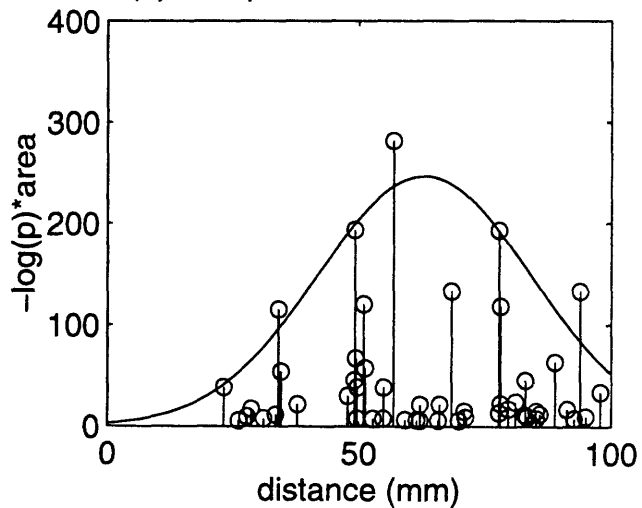
(b) ALP Plot of Auditory Task (noise)



(c) Hist of Accumulated H/B



(d) ALP plot of Accumulated H/B



7.2.2 Somatotopy within Subjects

Table 3 shows the mean location of activated areas for H/B, A/B, T/B, and F/B comparisons, for individual hemispheres of each subject. The expected order, medially to laterally, of the representation along the postcentral gyrus for body regions, in accordance with the established Penfield homunculus, is: forearm, hand, forefinger, thumb (Figure 3) [39].

Table 3: Somatotopic Mapping of Each Subject

Subject	Hemisphere	Forearm (mm)	Hand (mm)	Forefinger (mm)	Thumb (mm)
Subject1	right	mean: 12.60 SD: 0.52 (n=2)	mean: 73.85 SD: 20.24 (n=8)	mean: 65.30 SD: 12.77 (n=3)	mean: 66.90 SD: 37.90 (n=3)
	left	mean: 60.77 SD: N/A (n=1)	mean: 75.48 SD: 3.25 (n=3)	mean: 80.48 SD: N/A (n=1)	mean: 84.16 SD: 12.82 (n=2)
Subject2	right	mean: 54.07 SD: N/A (n=1)	mean: 60.31 SD: 1.15 (n=2)	mean: 59.42 SD: 24.60 (n=4)	mean: 54.39 SD: 6.77 (n=3)
	left	mean: 79.10 SD: 16.42 (n=6)	mean: 62.83 SD: 23.81 (n=16)	mean: 41.01 SD: 32.41 (n=4)	mean: 67.97 SD: 22.76 (n=4)
Subject3	right	mean: 64.13 SD: 12.38 (n=2)	mean: 64.29 SD: 17.54 (n=3)	mean: 62.76 SD: 20.73 (n=3)	mean: 79.78 SD: N/A (n=1)
	left	mean: N/A SD: N/A (n=0)	mean: 59.08 SD: 13.38 (n=3)	mean: 71.11 SD: 13.31 (n=2)	mean: 84.43 SD: N/A (n=1)
Subject4	right	mean: 52.41 SD: N/A (n=1)	mean: 45.54 SD: 17.62 (n=6)	mean: 46.40 SD: 6.01 (n=2)	mean: N/A SD: N/A (n=0)
	left	mean: 75.40 SD: 19.39 (n=2)	mean: 65.43 SD: 20.00 (n=5)	mean: 77.22 SD: 19.93 (n=3)	mean: 61.81 SD: 18.02 (n=2)
Subject5	right	mean: N/A SD: N/A (n=0)	mean: 52.80 SD: N/A (n=1)	mean: N/A SD: N/A (n=0)	mean: 44.51 SD: 36.41 (n=3)
	left	mean: N/A SD: N/A (n=0)	mean: 60.27 SD: 5.44 (n=2)	mean: 36.68 SD: 19.97 (n=3)	mean: 75.33 SD: N/A (n=1)

Only hand stimulation activated all 10 hemispheres ($p < .05$), with the number of activated areas ranging from 1-16 per hemisphere (Subject1 and Subject2 had 4 hand/arm paradigm scans while the other subjects had 2). Forearm, thumb, and forefinger activation were equally consistent among all subjects, ranging from 0-4 areas of activation per hemisphere ($p < .05$).

Somatotopy results were: 4/7 hemispheres showed hand/forearm somatotopy; 6/8 hemispheres showed thumb/forefinger somatotopy; 5/7 hemispheres showed hand/thumb somatotopy. Only 1/6 hemispheres (Subject1, left hemisphere) showed complete somatotopy corresponding to the Penfield homunculus. Similar to Grafton et al. [19], when studying somatotopy, we compared the means of the distributions, disregarding the standard deviations, because representations were significantly overlapping.

Although these results are interesting, the lack of activated areas in the postcentral gyrus for the stimulated areas (with the exception of hand) made within-subject, within-hemisphere somatotopic mapping difficult to interpret. As previously shown, noise is inherently present in the fMRI signal within the postcentral gyrus, making clear somatotopic mapping of a single hemisphere inconclusive with these methods.

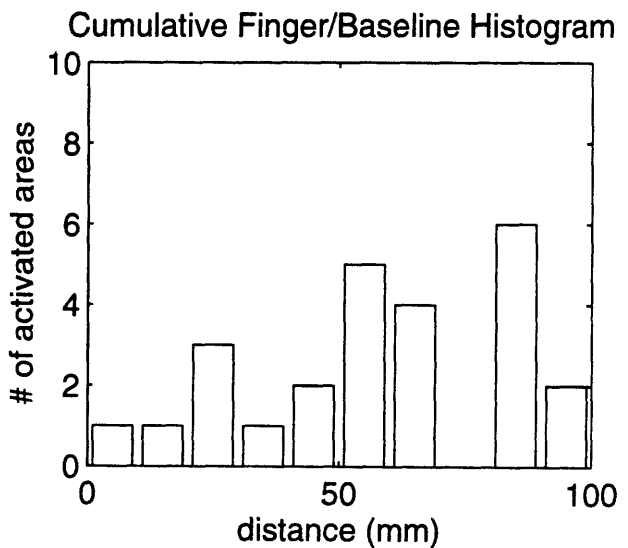
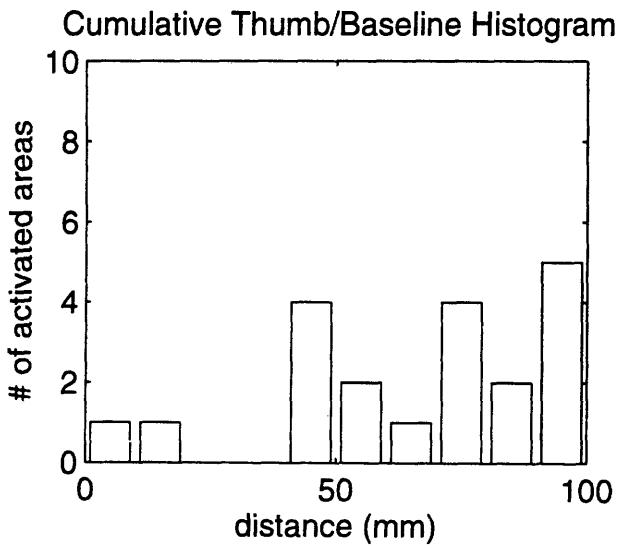
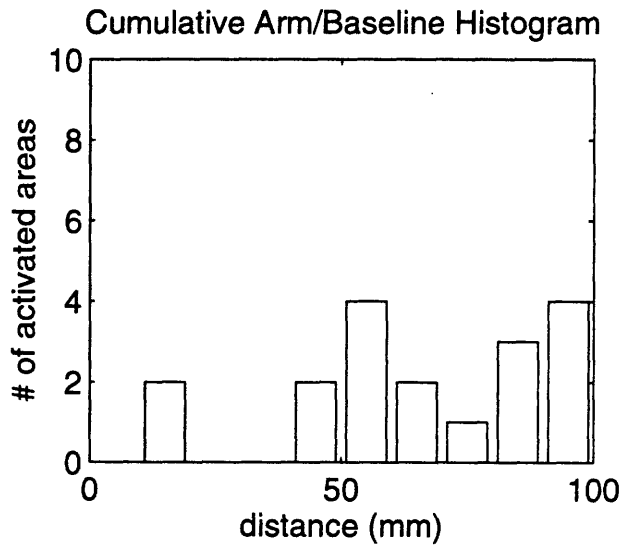
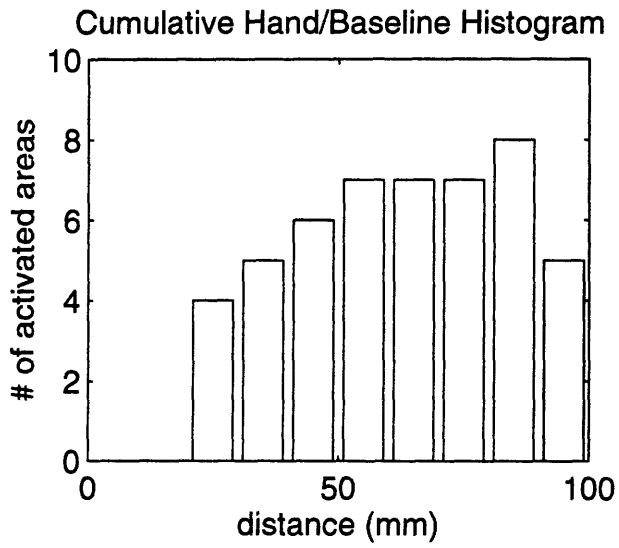
7.2.3 Somatotopy across Subjects

To get more meaningful somatotopic mapping results, the stimulation/baseline positive comparisons data for each subject were accumulated. The histograms (Figure 11) show

the discrepancy between the number of areas activated by hand stimulation and those activated by other stimulations. The histogram of the response to hand stimulation have distinctly Gaussian distribution. Forearm, forefinger, and thumb stimulations produce a less pronounced distribution. Nevertheless, these representations are localized to the lateral half of the postcentral gyrus with a few outliers (compare with Figure 10). From the accumulated data, 78% of the forearm activated areas, 70% of the thumb activated areas, and 68% of the forefinger activated areas lie in the lateral half of the postcentral gyrus. All stimulations effected areas covering nearly the entire length of the postcentral gyrus.

We conclude, in accordance with Grafton et al. [19], that the fMRI response to somatosensory stimulations of neighboring regions are significantly overlapping. Thus representations are not consistent with the findings of Woolsey et al. [reviewed in 58], Penfield et al. [38], or Merzenich et al. [31] who used extracellular recordings and defined nonoverlapping, suprathreshold representations in SI. Perhaps with fMRI, we are seeing overlapping, subthreshold representations similar to the intracellular recordings of Moore et al. [35], though the noise inherent in the signal prevents more concrete claims.

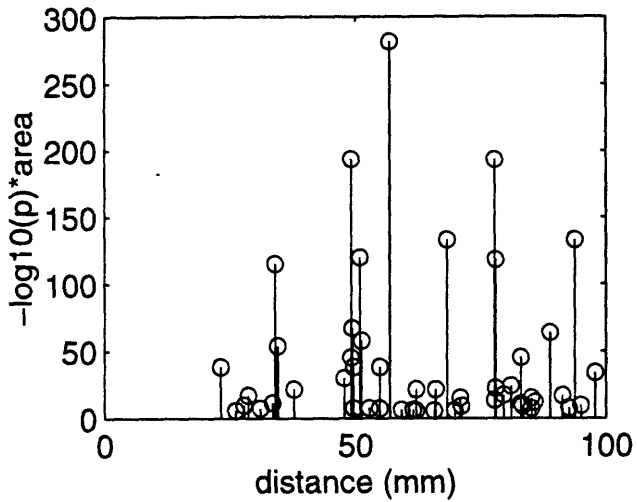
Figure 11. Histograms of the localization of accumulated hand/baseline, forearm/baseline, thumb/baseline, and forefinger/baseline positively activated areas in the postcentral gyrus for all subjects. Only hand has a Gaussian distribution although forearm, thumb, and forefinger are localized primarily to the lateral half of the gyrus. All representations are overlapping.



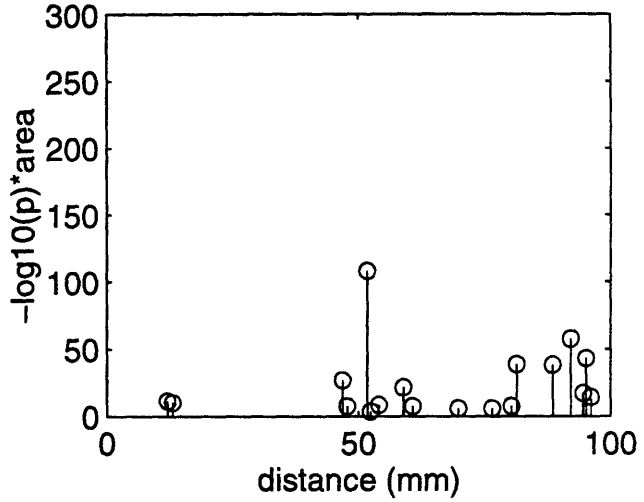
ALP plots (Figure 12) give a less discretized distribution of the activated areas along the postcentral gyrus. Additionally, area and p-value parameters from the K-S statistical map amplify particular data points. From the hand ALP plot, we see an even more distinct Gaussian distribution. The distribution of regions of the postcentral gyrus that respond to hand stimulation is centered at approximately 60-65 mm along the normalized postcentral gyrus. The distributions of the forearm, thumb, and forefinger stimulation regions are, again, not Gaussian but generally localized to the lateral half of the postcentral gyrus. The representation of the different stimulations through the fMRI signal are overlapping. From the ALP plots, we can also compare the intensity of the fMRI signal in response to different stimuli. Hand stimulation gives a much more intense response than forearm, thumb, or forefinger stimulation (mean of $-\log_{10}(\text{p-value}) \cdot \text{area}$: 44.07 - hand, 24.07 - forearm, 29.07 - thumb, 27.71 - forefinger).

Figure 12. ALP plots of the localization of accumulated hand/baseline, forearm/baseline, thumb/baseline, and forefinger/baseline positively activated areas in the postcentral gyrus for all subjects. Only hand has a Gaussian distribution; forearm, thumb, and forefinger are localized primarily to the later half of the gyrus. When activated areas are scaled by area and level of significance, hand/baseline positive activation is more intense than other body regions.

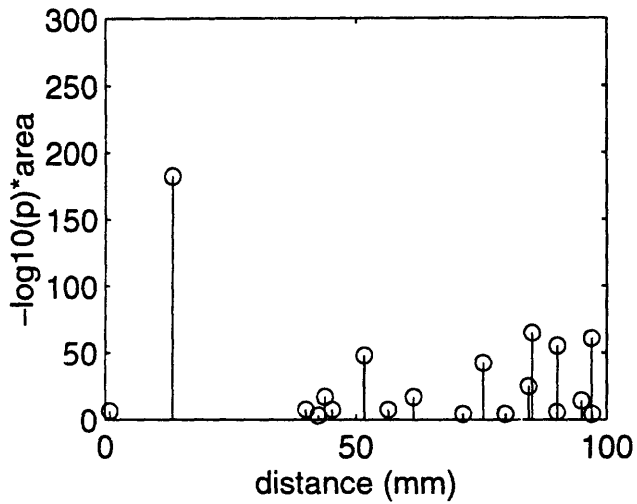
Cumulative Hand/Baseline ALP Plot



Cumulative Arm/Baseline ALP Plot



Cumulative Thumb/Baseline ALP Plot



Cumulative Finger/Baseline ALP Plot

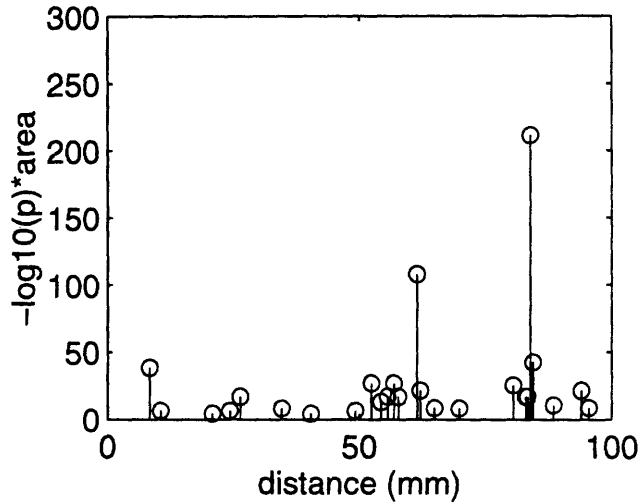


Table 4 compares the mean and SD of location along the normalized postcentral gyrus for the accumulated single stimulation data.

Table 4: Somatotopic Mapping across All Activated Areas

Forearm (mm)	Hand (mm)	Forefinger (mm)	Thumb (mm)
mean: 65.13 SD: 25.81 (n=18)	mean: 62.94 SD: 21.02 (n=49)	mean: 57.72 SD: 25.97 (n=25)	mean: 65.04 SD: 27.70 (n=20)

The results indicate that the detailed somatotopic mapping predicted by the Penfield homunculus is not observed.

We aligned the hemispheres to control intersubject and interhemispheric variability of the position of representations along the postcentral gyrus. Because the hand localization using the H/B comparison was the most robust somatotopic mapping indicator, the mean of the hand activated areas within each hemisphere was taken as an origin for alignment. This alignment provides a more accurate assessment of the size of the hand representation and reduces the representation jitter, allowing more subtle aspects (e.g., somatotopy, lateral inhibition) of organization to be observed. In this manner, hemispheres were “zeroed” before the subject data were accumulated. In histograms and ALP plots, the postcentral gyrus now extends from approximately -60 to 40 mm. Histograms and ALP plots of the zeroed hemispheres for H/B, A/B, T/B, and F/B comparisons are cleaner, but the results are the same (Figures 13 and 14).

Figure 13. Histograms of the localization of accumulated hand, forearm, thumb, and forefinger positive comparisons data for all subjects. Histograms have been aligned to the individual centers of hand activation to reduce smearing of the distributions.

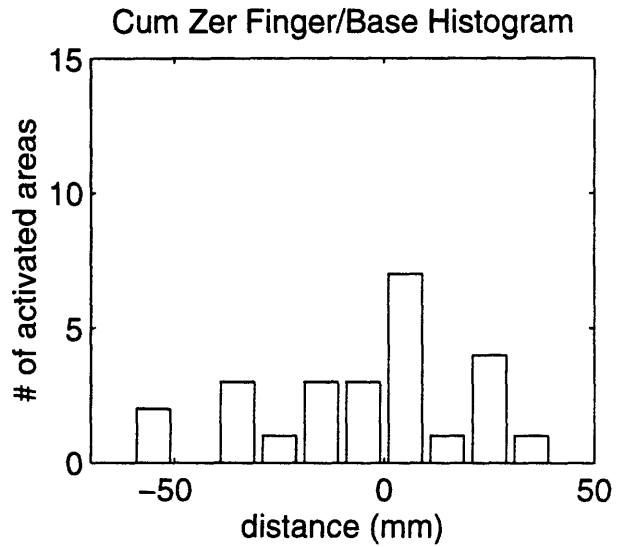
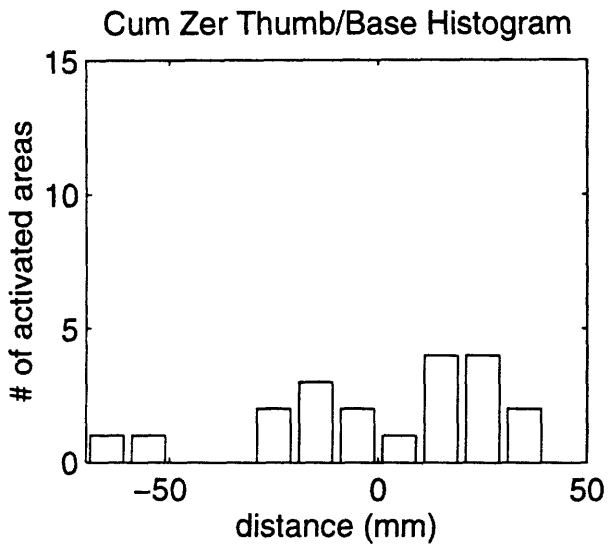
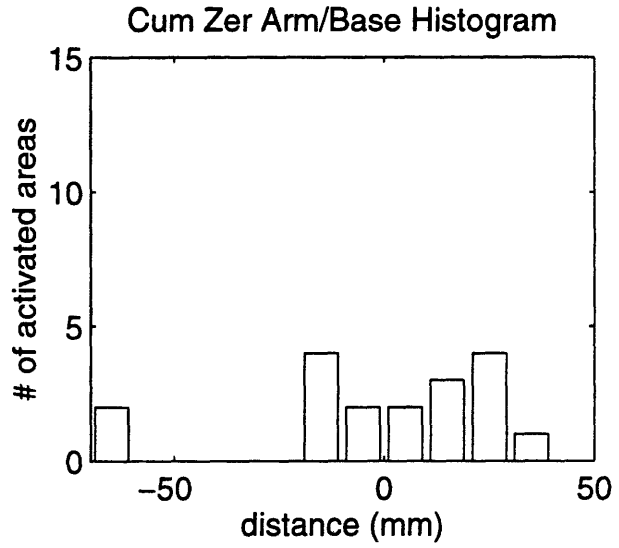
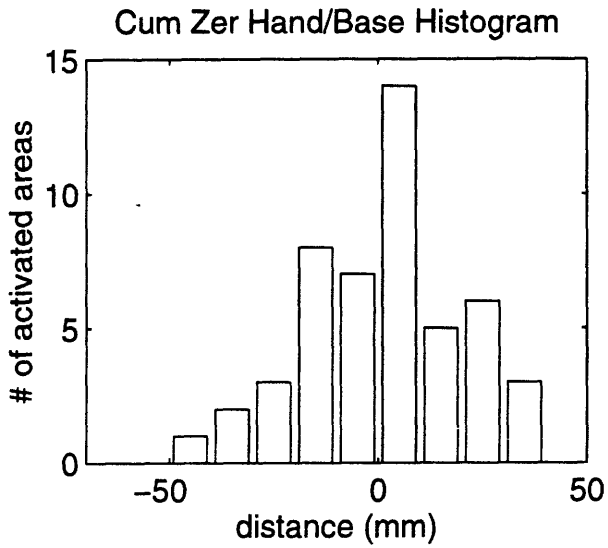
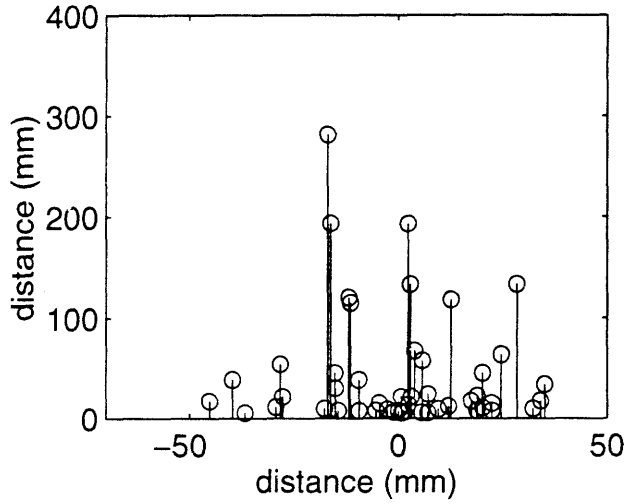
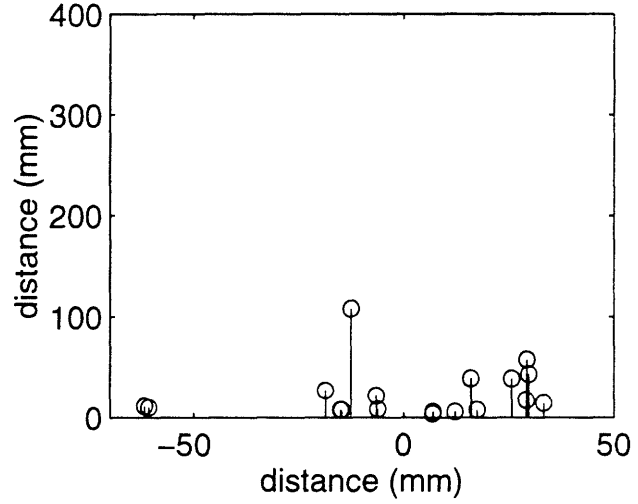


Figure 14. ALP plots of the localization of accumulated hand, forearm, thumb, and forefinger positive comparisons with baseline for all subjects. ALP plots have been aligned to the individual centers of hand activation to reduce smearing of the distributions.

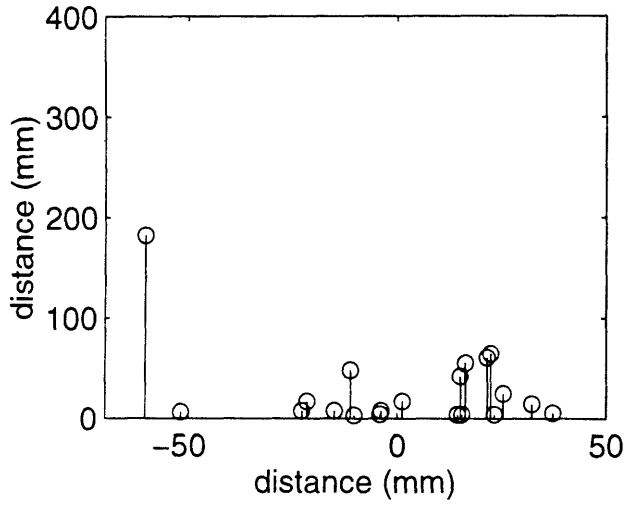
Cum Zer Hand/Base ALP Plot



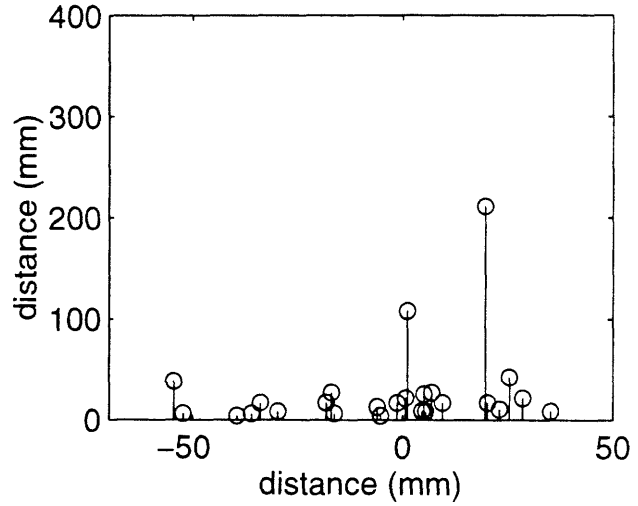
Cum Zer Arm/Base ALP Plot



Cum Zer Thumb/Base ALP Plot



Cum Zer Finger/Base ALP Plot



Additionally, we averaged across the means of each individual hemisphere (Figure 15, means are shown in Table 2). Table 5 compares the mean and SD of the localization of each body region representation when averaged across individual hemispheres.

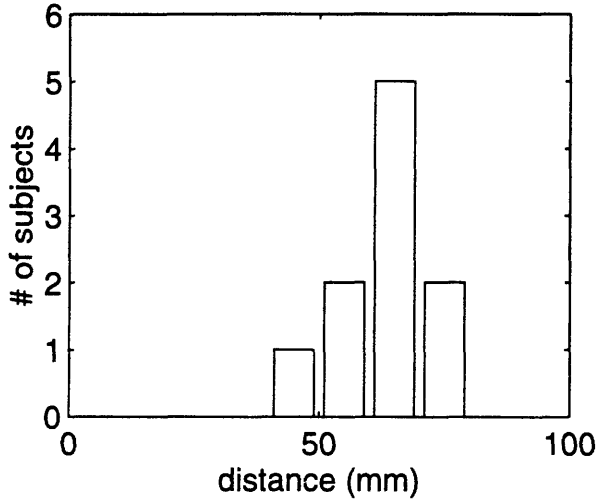
Table 5: Somatotopic Mapping Across Individual Hemispheres

Forearm (mm)	Hand (mm)	Forefinger (mm)	Thumb (mm)
mean: 56.93 SD: 21.96	mean: 62.99 SD: 8.88	mean: 60.04 SD: 15.67	mean: 68.81 SD: 13.67

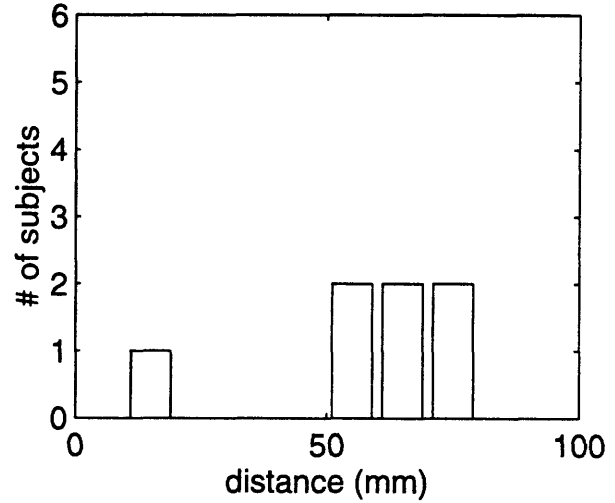
Hand localization is focused while thumb, forefinger, and particularly forearm activation, is more spread. And again, all regions are localized to the lateral half of the normalized postcentral gyrus. With this averaging procedure, however, we recovered almost complete somatotopic mapping of body regions in accordance with the Penfield homunculus: Forearm is medial to hand, forefinger is medial to thumb, but hand is not medial to forefinger. With different averaging procedures, we recovered different somatotopic mappings of the forearm, forefinger, and thumb. Averaging across the means of the individual hemispheres, the procedure used by Penfield et al. [39], gave somatotopic mapping most closely in accordance with the Penfield homunculus.

Figure 15. Histograms of the localization of hand, forearm, thumb, and forefinger positive baseline comparisons, averaging across each hemisphere.

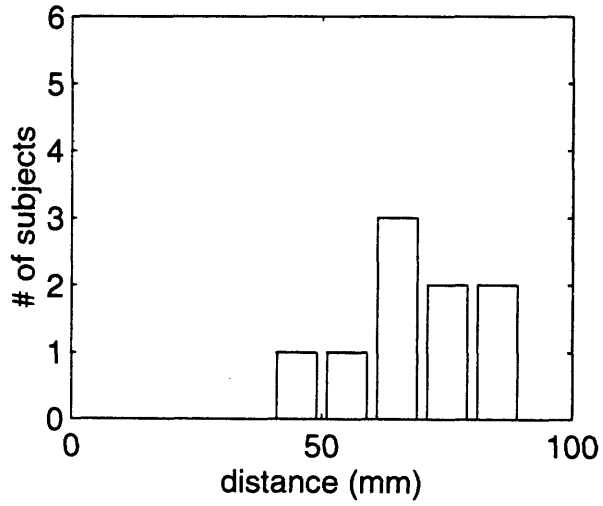
Hist of Centers of Hand/Base Pos Act



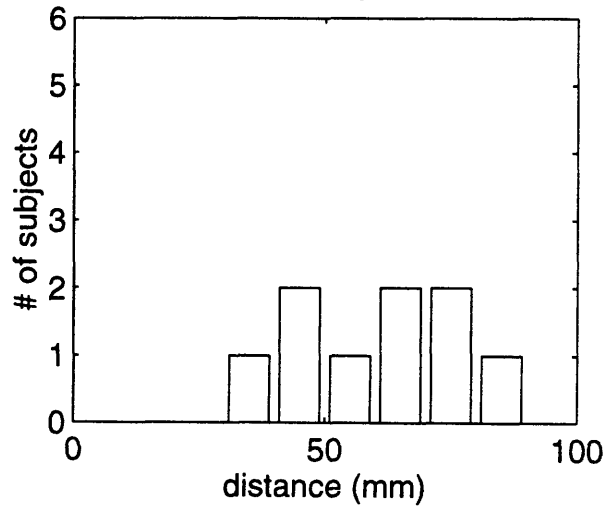
Hist of Centers of Arm/Base Pos Act



Hist of Centers of Thumb/Base Pos Act

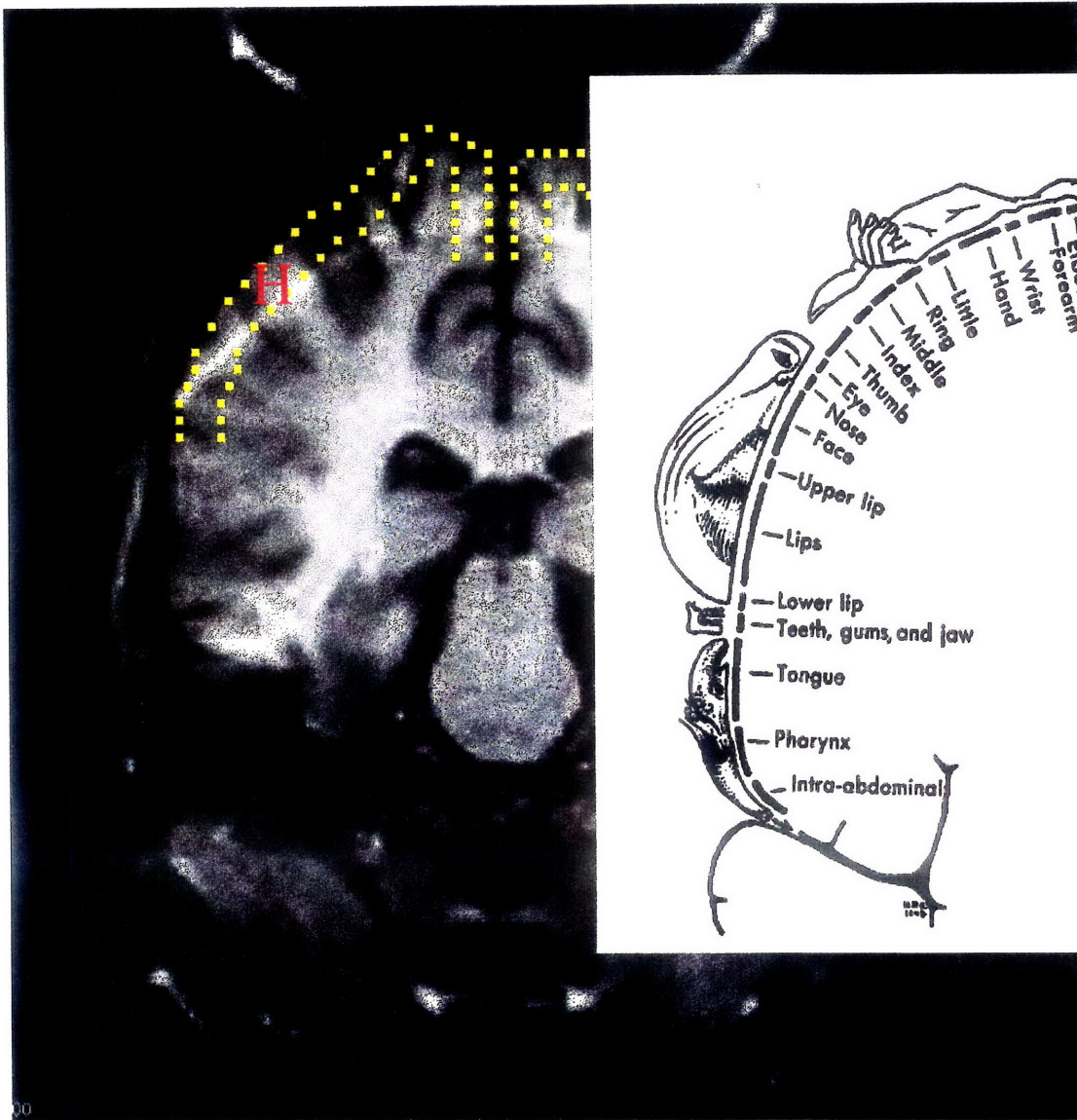


Hist of Centers of Finger/Base Pos Act



Our data support several conclusions regarding a somatotopic mapping of forearm, hand, forefinger, and thumb with fMRI. First, forearm, hand, thumb, and forefinger have overlapping representations on the normalized postcentral gyrus. Second, the representations of forearm, thumb, and forefinger are localized to the lateral half of the normalized postcentral gyrus. Third, the representation of hand is approximately two-thirds along the length of the postcentral gyrus. Comparing these results with those expected in accordance with the Penfield homunculus (Figure 16), we see that we correctly identified the hand representation at two-thirds of the length of the normalized gyrus, and that we correctly identified the forearm, thumb, and forefinger as in the vicinity of the hand. By averaging across hemispheres, we approached detailed somatotopy.

Figure 16. Comparison of the localization of the center of the hand representation found through our fMRI methods with the Penfield homunculus. The red “H” represents the localization of the hand region at 62.95 mm along our normalized postcentral gyrus. The Penfield homunculus is represented along the outline in yellow, extending past the outline to the sylvian fissure.



Localization of Hand in the Postcentral Gyrus

7.3 Lateral Inhibition

Somatotopic mapping was done with H/B, A/B, T/B, and F/B comparisons. We also performed a number of other comparisons done in the data analysis. These other comparisons were used to understand the organization of somatosensory representation in the postcentral gyrus. In particular, we studied the interaction between the hand and forearm representations. Three forms of presentation will be used to display the data: box plots, histograms, and ALP plots.

7.3.1 Possible Models

Two possible models are proposed here and compared with the data. The two models considered are the noninhibitory and inhibitory models.

In the noninhibitory model (Figure 17), the hand representation is modelled with a large spatial spread along the postcentral gyrus and a definite center. The forearm representation is modelled as less spatially spread, in accordance with the Penfield homunculus. The forearm representation overlaps the hand representation although the centers of the distributions are distinct. This overlap is predicted by a correlation between the hemodynamic fMRI signal and a subthreshold somatosensory representation (Erulkar et al., [reviewed in 20]) rather than with the suprathreshold somatosensory representation correlated with extracellular recordings (Merzenich et al., [31]). Figure 17 also shows what one would expect for H/A, A/H, H+A/B, and B/H+A comparisons: H/A comparisons would lead to a

decreased intensity and spread of signal compared to H/B comparisons; H+A/B comparisons would lead to an increased intensity and spread of signal compared to H/B and A/B comparisons.

In the inhibitory model (Figure 18), the hand representation is similar to that in the noninhibitory model, but displays regions of lateral inhibition (negative activation). The forearm representation is also similar to that in the noninhibitory model, but displays regions of lateral inhibition. Figure 18 also shows what one would expect for H/A, A/H, H+A/B, and B/H+A comparisons: H/A comparisons would lead to an increased intensity of signal compared to H/B comparisons; H+A/B comparisons would lead to an increased spread of signal compared to H/B and A/B comparisons; B/H+A comparisons would lead to an increased intensity and medial shift of signal compared to B/H and B/A comparisons.

Figure 17. Noninhibitory model of hand and forearm representation. The forearm representation is modeled as medial to the hand representation (Penfield et al. [39]) but overlapping (Grafton et al. [19]). The hand representation is modeled as wider and more responsive than forearm with regard to its density of cutaneous receptors. Expected fMRI signal response with a hand/forearm and hand+forearm/baseline comparison is also shown.

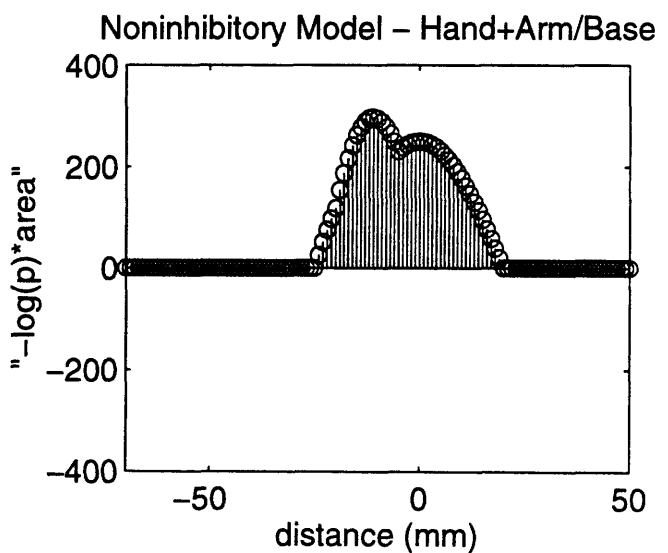
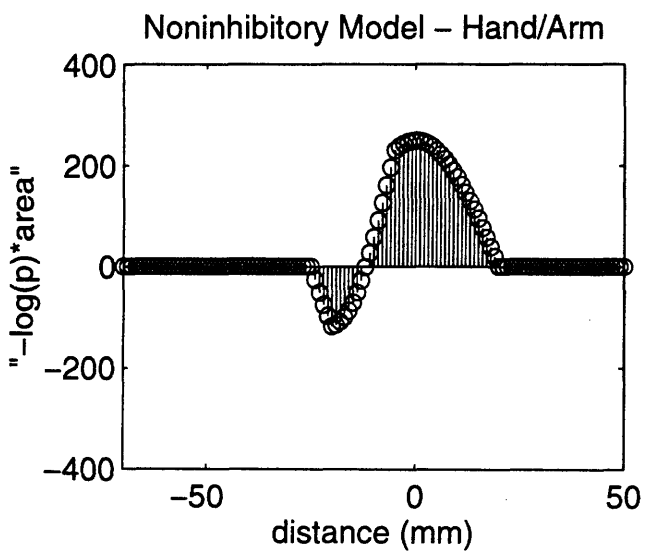
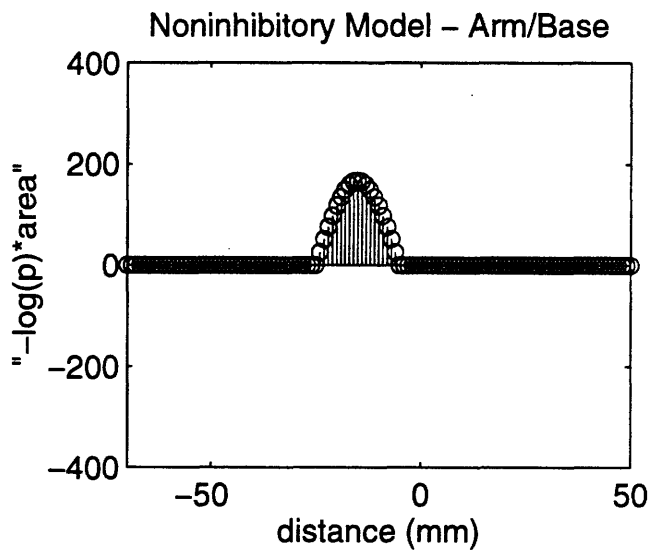
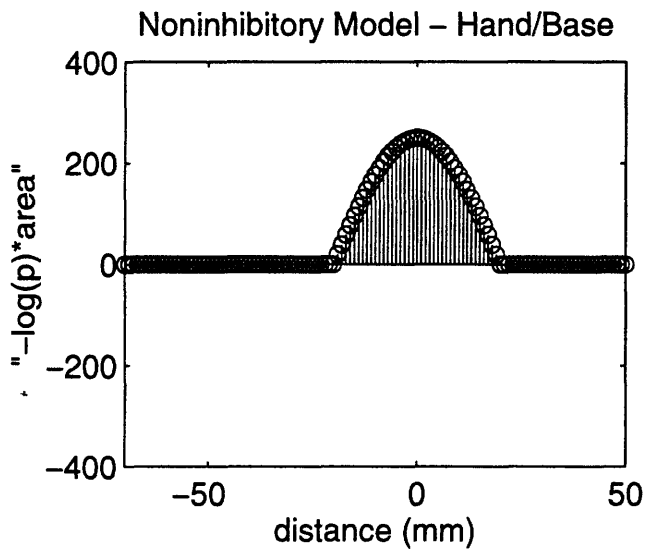
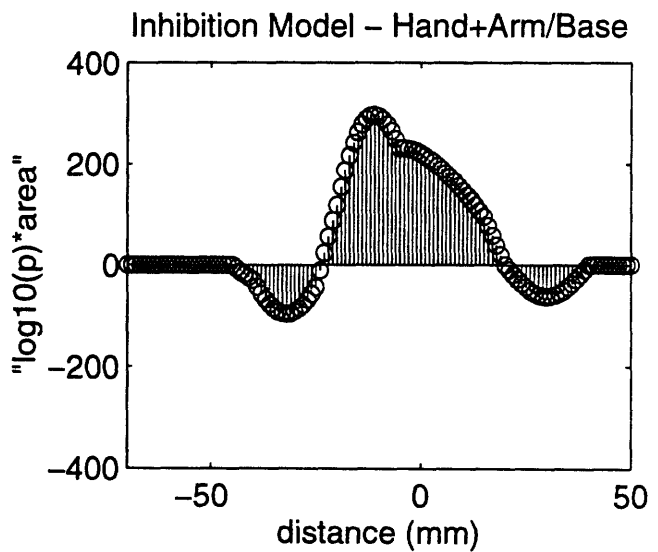
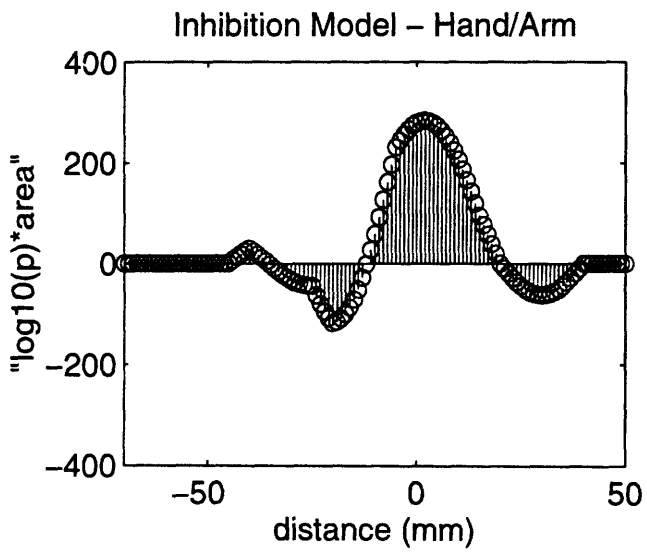
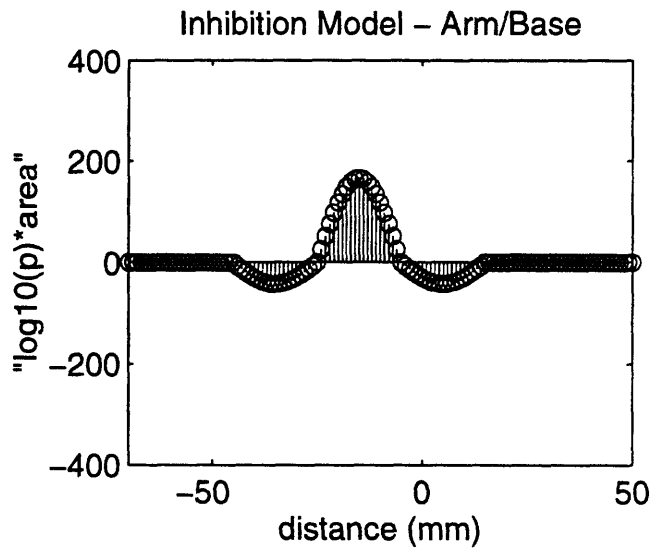
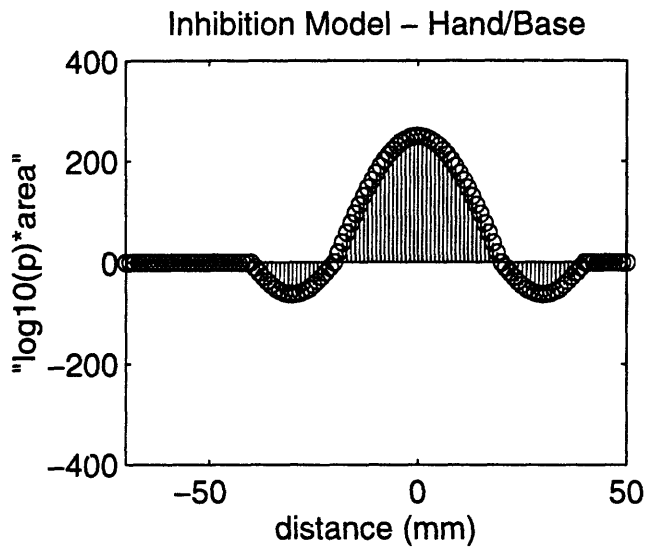


Figure 18. Inhibitory model of hand and forearm representation. The inhibitory model is identical to the noninhibitory model except for regions of lateral inhibition that have been included. The expected fMRI signal response with a hand/forearm and hand+forearm/ baseline comparison is shown.

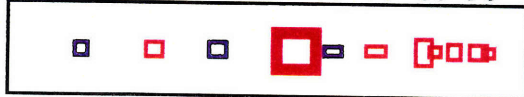


7.3.2 Box Plots, Histograms, and ALP Plots of Hand, Forearm Comparisons

The box plots of the H/B, B/H, A/B, and B/A comparisons (Figure 19) illustrate the relative frequency of inhibited areas in the B/A comparison compared with inhibited areas in the B/H comparison. Inhibition in the B/A comparison often overlaps activation in the H/B comparison. The box plots of the H/A, A/H, H+A/B, and B/H+A comparisons (Figure 20) show the striking increase in the number of activated areas in the H/A comparison relative to the H/B comparison. Not only are there more areas of activation ($n=93$ vs. $n=49$), but the activation is more robust (thicker lines correspond to lower p -values). However, the number of activated areas of A/H comparison ($n=18$) relative to the A/B comparison ($n=15$) is roughly equivalent. Thus performing H/A and A/H comparisons increase the intensity of the hand representation but do effect the arm representation. The H+A/B comparisons show roughly the same intensity ($n=39$ vs. $n=49$) as the H/B comparisons but with a more spread distribution. The B/H+A comparisons shows intense inhibition. In the B/H+A comparisons, inhibition is more medial than in the B/H and B/A comparisons (mean B/H+A inhibition: 44.72 mm, mean B/H inhibition: 49.20, mean B/A inhibition: 55.25).

Figure 19. Box plots of hand/baseline and forearm/baseline positive and negative comparisons for all 5 subjects, all 10 hemispheres. Red rectangles indicate hand activation; blue rectangles indicate hand inhibition. Red circles indicate forearm activation; blue circles indicate forearm inhibition. Line thickness of rectangles and circles is proportional to $-\log(p\text{-value})$ of the KS statistic. Forearm inhibition overlaps hand activation. Hand activation is increased relative to arm activation.

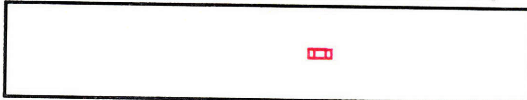
10 20 30 40 50 60 70 80 90



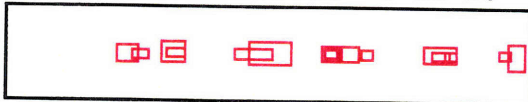
10 20 30 40 50 60 70 80 90



10 20 30 40 50 60 70 80 90



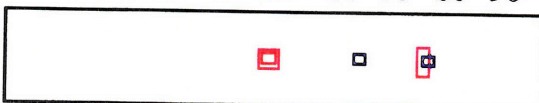
10 20 30 40 50 60 70 80 90



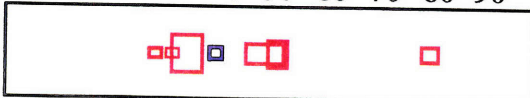
10 20 30 40 50 60 70 80 90



10 20 30 40 50 60 70 80 90



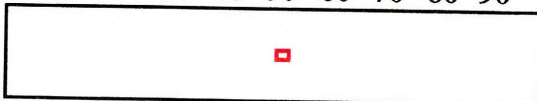
10 20 30 40 50 60 70 80 90



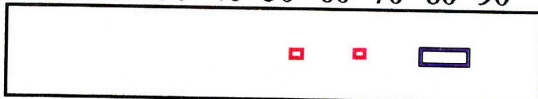
10 20 30 40 50 60 70 80 90



10 20 30 40 50 60 70 80 90

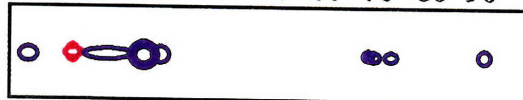


10 20 30 40 50 60 70 80 90



Hand/Base All Subjects

10 20 30 40 50 60 70 80 90



10 20 30 40 50 60 70 80 90



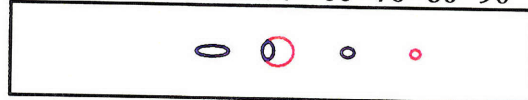
10 20 30 40 50 60 70 80 90



10 20 30 40 50 60 70 80 90



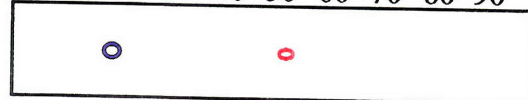
10 20 30 40 50 60 70 80 90



10 20 30 40 50 60 70 80 90



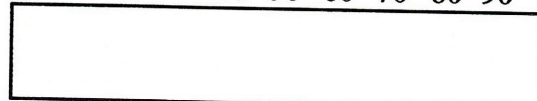
10 20 30 40 50 60 70 80 90



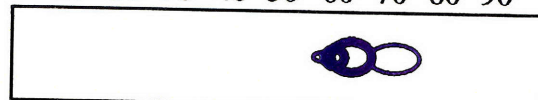
10 20 30 40 50 60 70 80 90



10 20 30 40 50 60 70 80 90

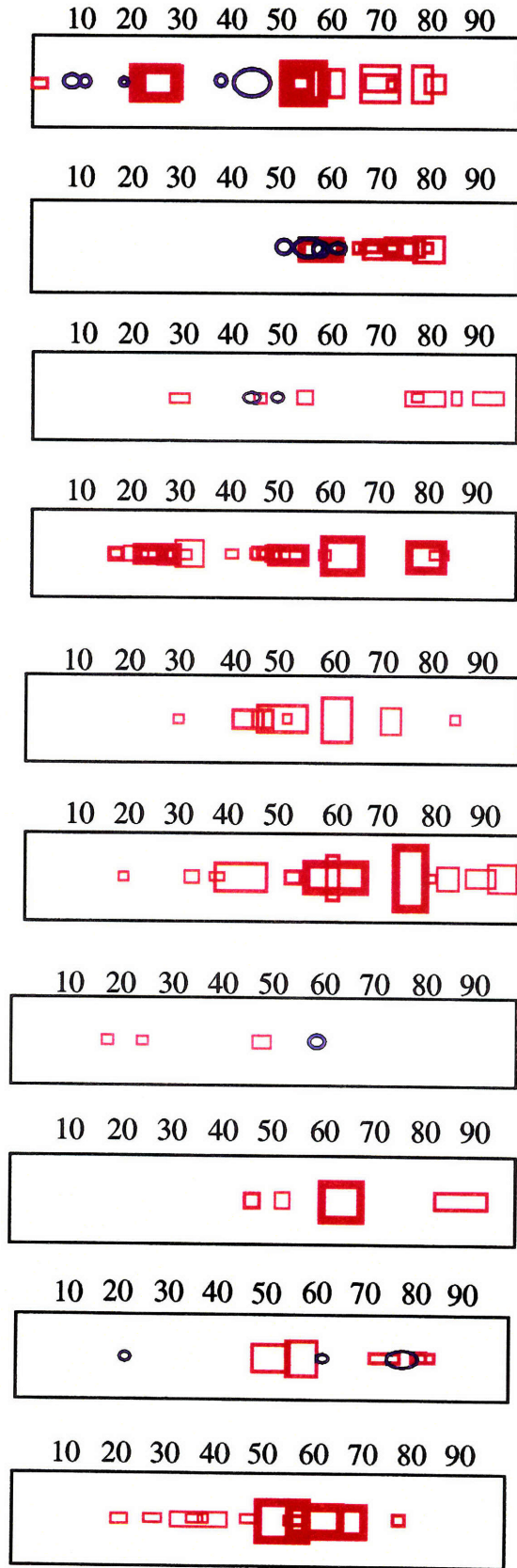


10 20 30 40 50 60 70 80 90

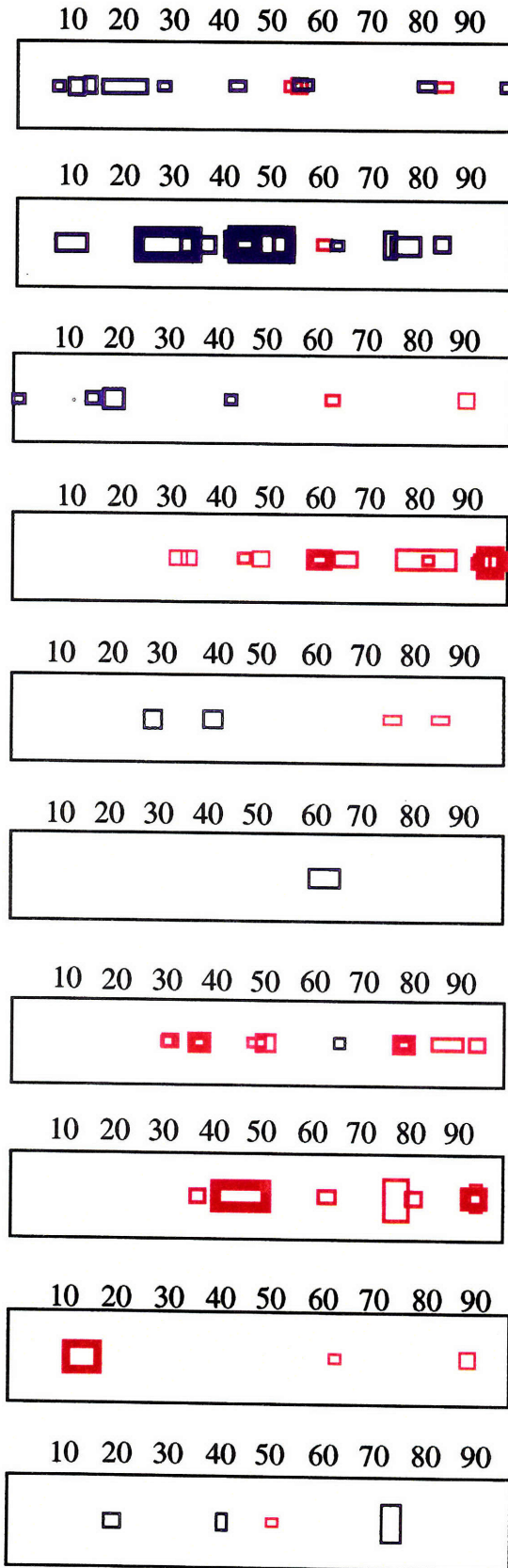


Arm/Base All Subject

Figure 20. Box plots of hand/forearm and hand+forearm/baseline positive and negative comparisons for all 5 subjects, all 10 hemispheres. Red rectangles on the hand/forearm comparisons indicate hand activation; blue circles on the hand/arm comparisons indicate forearm activation. Red rectangles on the hand+forearm/baseline comparisons indicate hand and forearm activation; blue rectangle on the hand+forearm/baseline comparisons indicate hand and forearm inhibition. Line thickness of rectangles and circles is proportional to $-\log(p\text{-value})$ of the KS statistic. The frequency of hand activation in the hand/arm comparisons is increased relative to the hand/baseline comparisons of Figure 24. Hand and forearm inhibition in the hand+forearm/baseline is increased relative to the hand/baseline and forearm/baseline comparisons of Figure 24.



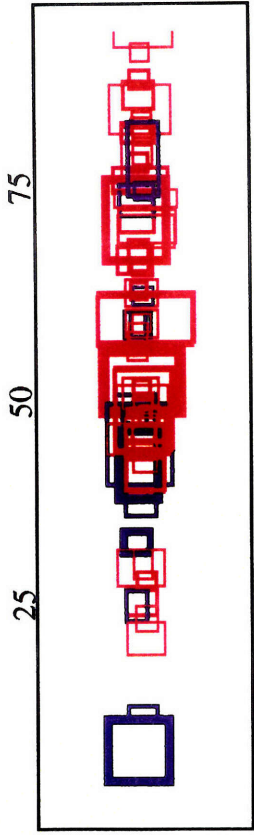
Hand/Arm All Subjects



Hand+Arm/Base All Subjects

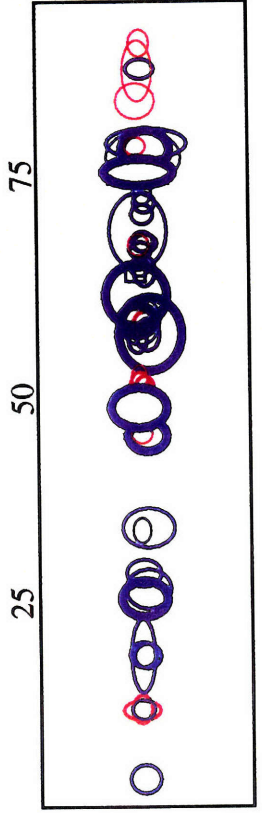
Accumulated data box plots (Figure 21) displaying activation and inhibition for the eight comparisons further emphasize these trends. Inhibition in the B/A comparison is centered in the hand area defined by the activation in the H/B comparison. The intensity of activation in H/A comparisons increases in relation to the H/B comparisons. In the B/H+A comparisons, there is a medial shift and increased intensity of inhibition in relation to inhibition in the B/H and B/A comparisons.

Figure 21. Accumulated data box plots across all 5 subjects, all 10 hemispheres of the four hand/arm paradigm comparisons shown in Figures 24 and 24. The trends described for Figures 19 and 20 become clearer in these accumulated data box plots.



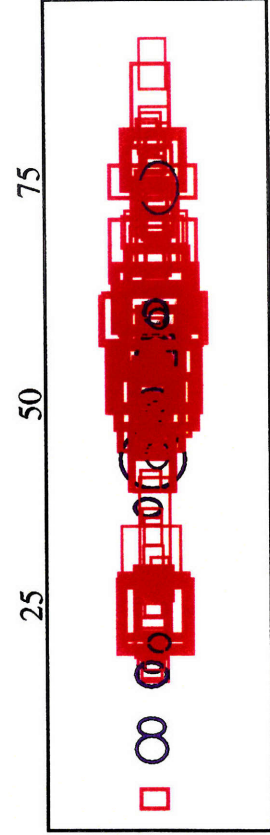
Cumulative Hand/Base Comparison

□ = Hand Activation □ = Hand Inhibition



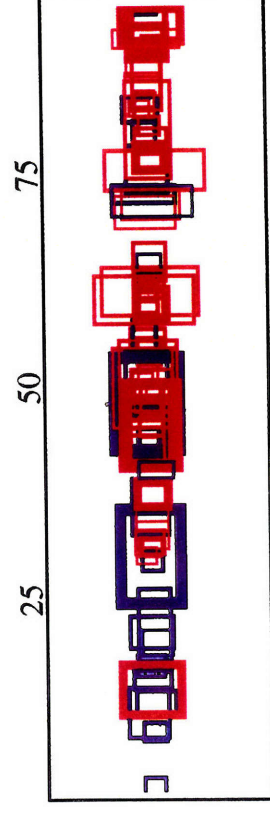
Cumulative Arm/Base Comparison

○ = Arm Activation ○ = Arm Inhibition



Cumulative Hand/Arm Comparison

□ = Hand Activation ○ = Arm Activation

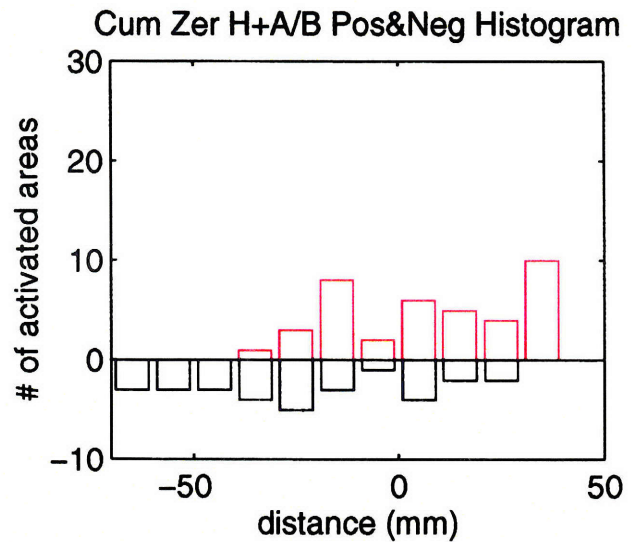
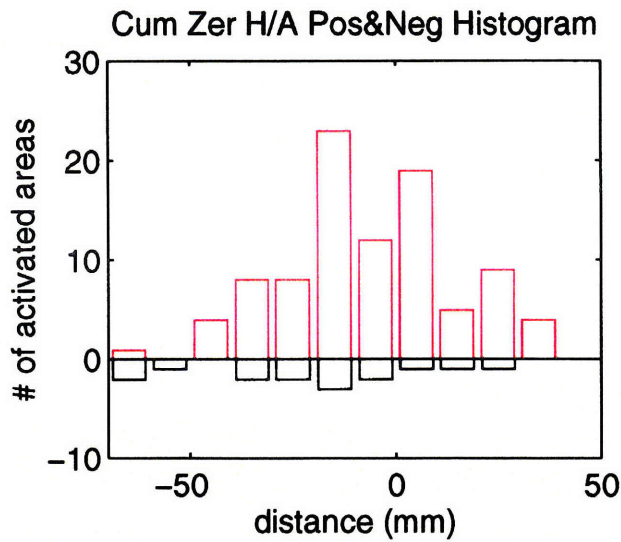
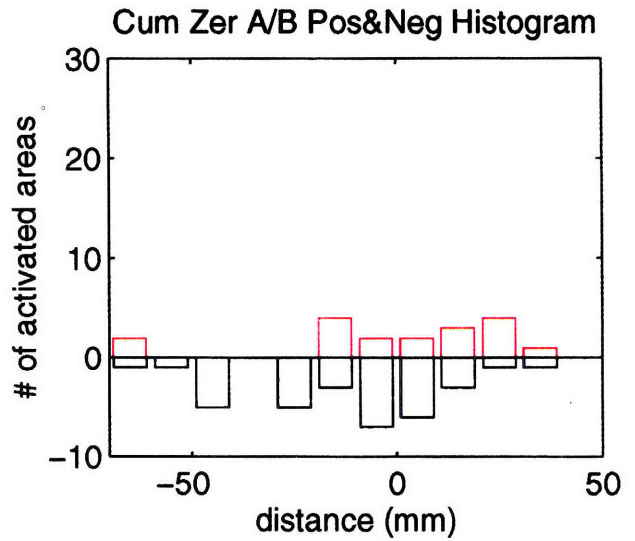
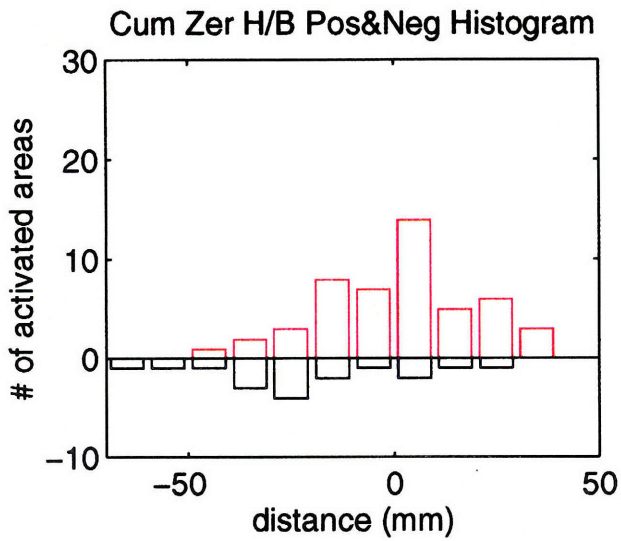


Cumulative Hand+Arm/Base Comparison

□ = Hand+Arm Activation □ = Hand+Arm Inhibition

The zeroed and accumulated data histograms (Figure 22) of the 10 hemispheres for the 8 positive and negative comparisons: H/B, B/H, A/B, B/A, H/A, A/H, H+A/B, and B/H+A illustrate the findings found in the accumulated box plots. Arm inhibition in the B/A histogram is localized to the hand representation revealed in the H/B comparison. Arm activation is flanked by arm inhibition as revealed in the A/B and B/A comparisons. Hand activation is intensified in the H/A comparison in relation to the H/B comparison. Forearm activation is similar in intensity in the A/B comparison in relation to the A/H comparison. Hand and forearm inhibition is slightly intensified and shifted medially in the B/H+A comparison in relation to the H+A/B comparison. Also, H/B and B/H comparisons reveal inhibition in the hand representation medial to the hand activation. This last result was not clearly seen in the box plots.

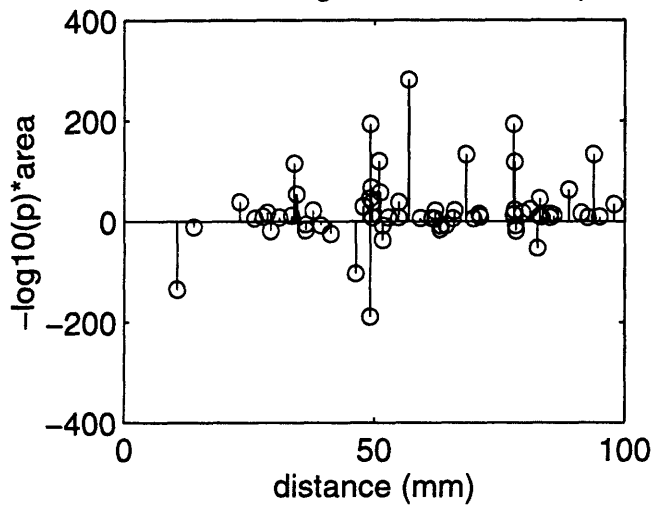
Figure 22. Histograms of the eight hand/arm paradigm accumulated data comparisons after localization was zeroed in each hemisphere to the center of hand/baseline positive activation. Positive activation is shown in red; negative activation is shown in blue. Arm inhibition overlaps hand activation. Hand activation in the hand/arm comparison is more intense relative to the hand/baseline comparison. Forearm inhibition is shifted medially and is more intense than hand inhibition and arm inhibition.



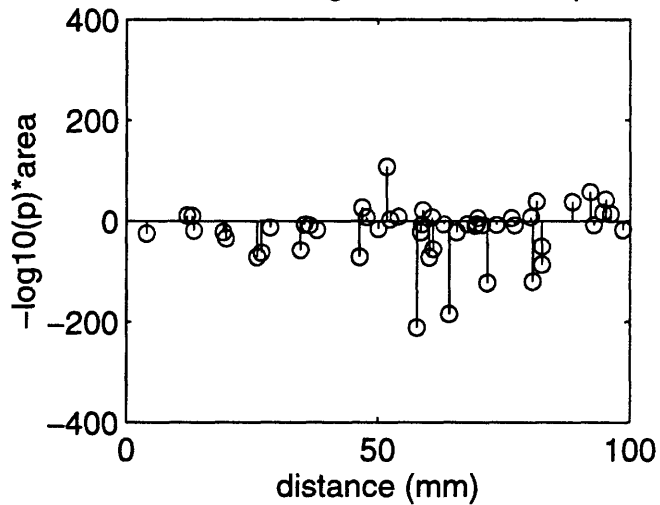
The presence of inhibition found in the cumulative box plots and cumulative histograms were evident in the ALP plots (Figures 23 and 24). Inhibition dominated the B/A ALP plot. Inhibition in the B/H ALP plot was localized medial to the activation in the H/B ALP plot. Arm inhibition was again more intense in relation to hand inhibition. The intensity of the hand activation in the H/A ALP plot was magnified in relation to the hand activation in the H/B plot. Arm activation, however, was not present in the A/H ALP plot. The B/H+A comparison displayed a more medial and more intense inhibition than the B/H or B/A comparisons.

Figure 23. ALP plots of the eight hand/arm paradigm accumulated comparisons prior to zeroing to hand activation. The same trends witnessed in the box plots and histograms are evident here. Compare these ALP plots with the noninhibitory and the inhibitory models in Figures 17 and 18.

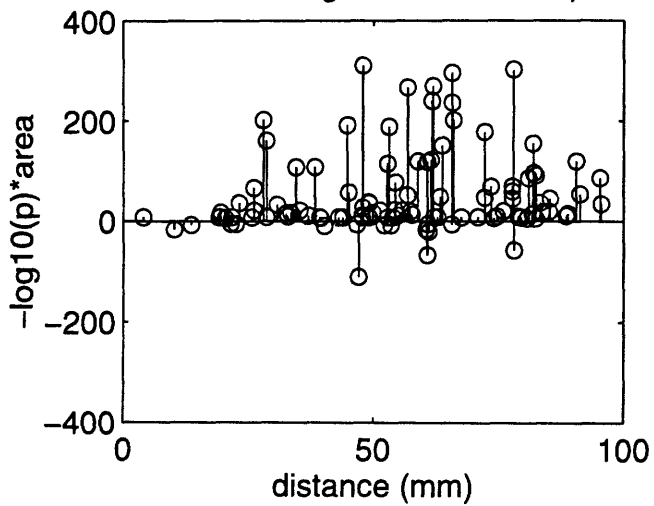
Cum Pos&Neg Hand/Base ALP plot



Cum Pos&Neg Arm/Base ALP plot



Cum Pos&Neg Hand/Arm ALP plot



Cum Pos&Neg Hand+Arm/Base ALP plot

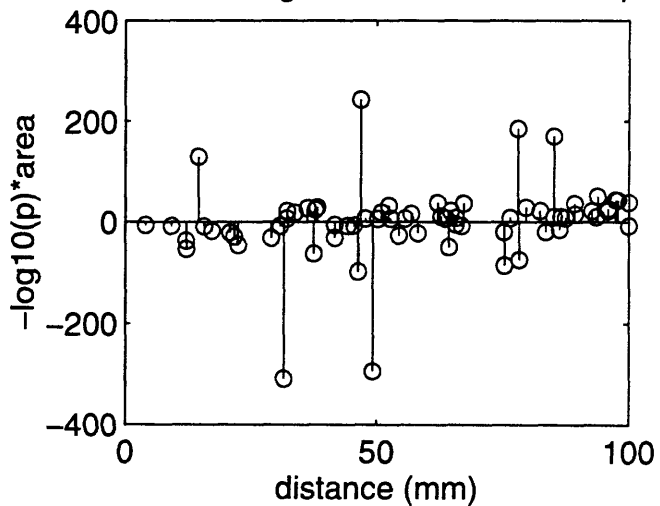
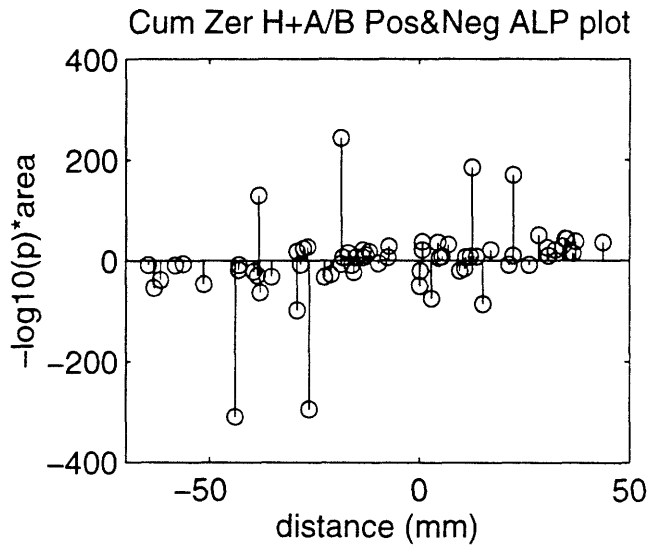
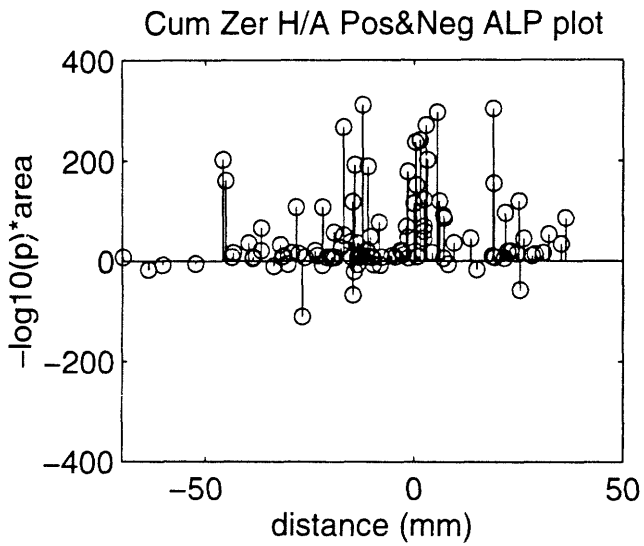
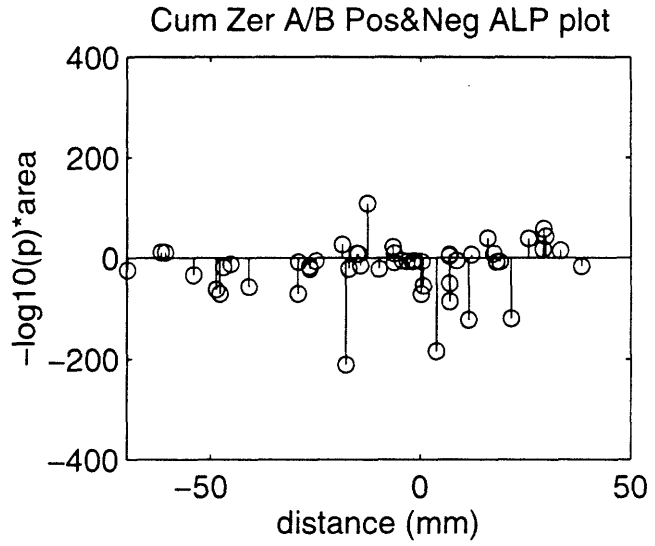
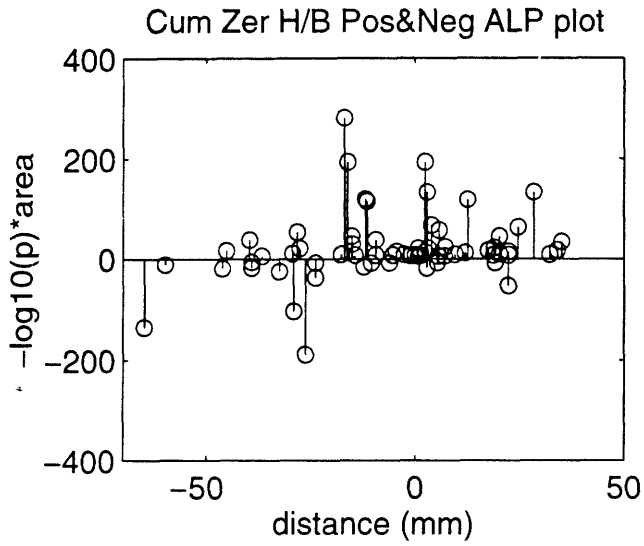


Figure 24. ALP plots of the eight hand/arm paradigm accumulated comparisons after localization was zeroed in each hemisphere to the center of hand/baseline positive activation. The discussed trends of organization are even clearer than in Figure 23. Compare these ALP plots with Figures 17 and 18.



7.3.3 Correspondence with the Models

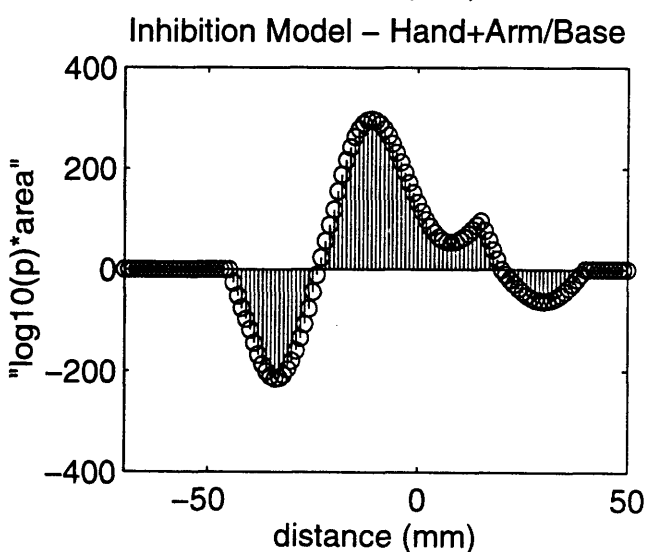
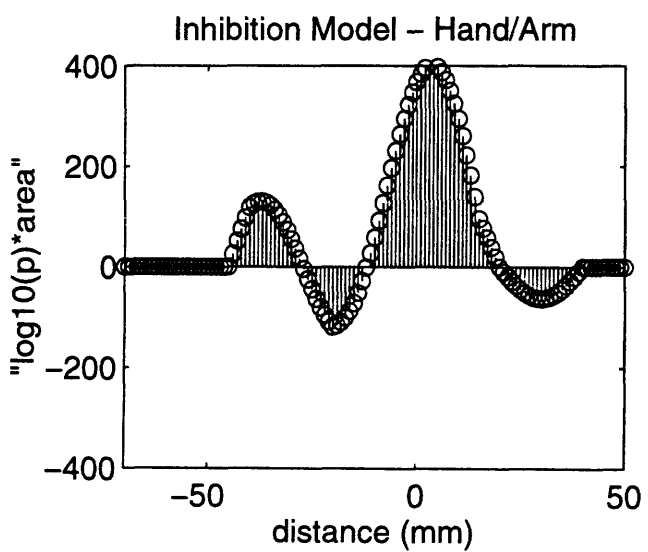
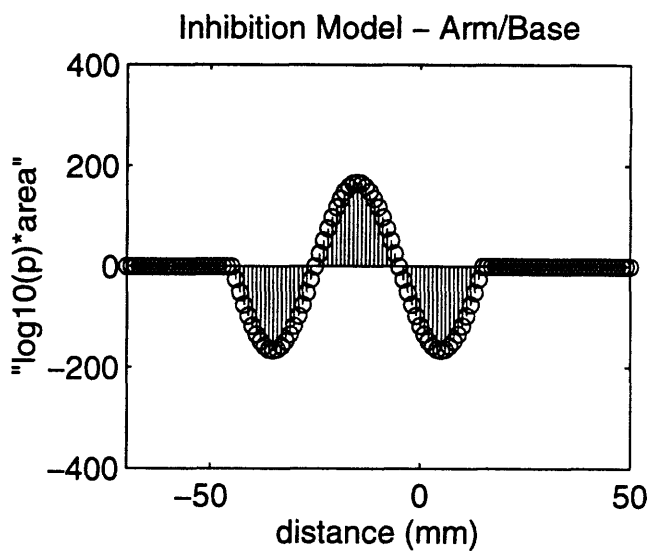
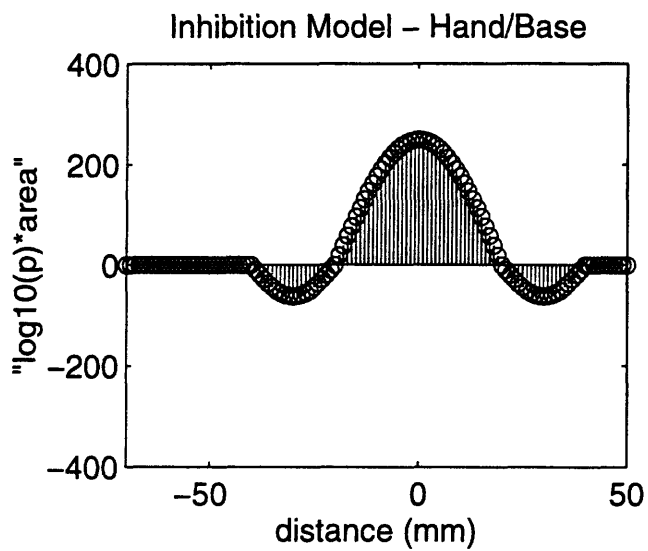
The data from the various hand/forearm comparisons presented with box plots, histograms, and ALP plots all pointed to a model including a spatially localized inhibitory component. B/A comparisons generated substantial inhibition that consistently overlapped the hand representation, a first indication of the presence of inhibition. Why forearm inhibition dominated forearm activation was unclear. B/H comparisons generated a well-localized inhibition medial to the hand representation. Although these B/H comparisons did not show inhibition lateral to the hand representation, this may have resulted from our premature section of the postcentral gyrus at its lateral extent (done to reduce corruption of our data by activation in SII). H/A comparisons showed increased intensity in the fMRI signal, a result predicted only by the inhibitory model. When hand activation was compared with the overlapping forearm inhibition, the hand activation became more pronounced. Forearm activation did not occur in the A/H comparisons. When forearm activation was compared with the broader and more pronounced, overlapping hand activation, forearm activation was obscured. H+A/B comparisons, by contrast, did not show an increase in intensity predicted by the noninhibitory model. B/H+A comparisons showed an increased intensity and medial shift of inhibition, which is predicted by the inhibitory model.

With these results, we modified the inhibitory model to fit the data more closely. Based on the substantial inhibition shown by the B/A comparisons, we increased the amplitude of the forearm inhibitory sidebands. We also shifted the location of the forearm representa-

tion so that the hand inhibitory sideband did not overlap the forearm activation region.

Figure 25 shows the final empirical inhibitory model of hand and forearm representation.

Figure 25. An empirically corrected version of the inhibitory model first presented in Figure 18. The extent of overlap of forearm and hand, and the intensity of arm inhibition were varied to more closely fit the data. This final empirical model of the representation of hand and forearm as seen through the fMRI signal shows striking similarities to the experimental ALP plots of Figure 24.



7.4 Possible Sources of Error

There were several sources of error in these experiments and subsequent analysis that may have corrupted our data. Our experimental procedures were not ideal. Stimulation of body regions with a von Frey hair was not a completely consistent somatosensory, cutaneous input. Stimulation of the hand and forearm were more easily accomplished than stimulation of the thumb and forefinger because the forearm and hand were relatively larger and flatter. During stimulation of the thumb and forefinger, the von Frey hair would sometimes slide off so that the goal of stimulation with only a point stimulus was not achieved. This inconsistency may explain the inconclusive somatotopic findings of the thumb and forefinger in comparison with the hand and forearm.

No study of the interference of the fMRI signal from the presence of experimenters has been done. It is possible that one or two experimenters applying the somatosensory stimulus during the functional scans could affect the validity of the fMRI signal. We did not, however, find any consistent perversion to the timecourse of the signal due to such interference, and there was, a priori, reason to believe that experimenter presence should not affect signal strength (Kwong, personal communication).

There were a number of misrepresentations of data that could have occurred when doing the K-S analyses. Because fMRI techniques are reporting on changes in rCBF of approximately 2-5%, noise in the data could have resulted in noise in the K-S map, as was previously shown. This noise could have come in various forms. For instance, a large spike of

rCBF or a gradual drift in the rCBF in a studied region may have affected the K-S map. In general, any substantial change in the rCBF not on the order of 20 or 30 sec might have resulted in error. With our threshold at $p < .05$, such noise in the data would have been eliminated from the K-S map with 95% confidence. Also, our stimulation paradigms were designed so that stimulation epochs were balanced in the 4 min scan to reduce the effect of drift.

The straightening and merging procedure with the postcentral gyrus also introduced a potential source of error. In this procedure we made a basic assumption that the postcentral gyrus took no sharp turns in its medial to lateral course. A postcentral gyrus with sharp turns would have been warped by the merging. In addition, as activated areas extended far from the line they were meant to be mapped to, the error in their placement along the straightened postcentral gyrus was increased. This basic assumption was a generalization of the anatomy of the cerebral cortex, a practice that is never completely dependable. In the subjects of this study, however, such turns of the postcentral gyrus were not observed.

Chapter 8

Discussion and Conclusions

8.1 Somatotopic Mapping of the Postcentral Gyrus with fMRI

A complete, detailed mapping of the forearm, hand, thumb, and forefinger was not possible with these fMRI methods. Rather, we were able to precisely localize only the hand region along the postcentral gyrus while the forearm, thumb, and forefinger areas were found to be in the vicinity of the hand, on the lateral half of the normalized postcentral gyrus. These findings are consistent with the established location of the represented regions on the Penfield homunculus (Figure 16).

But why was it possible to localize the hand while the forearm, forefinger, and thumb localizations were inconclusive with these methods? As previously discussed, we expected certain body representations to be devoted a larger cortical area due to an increased acuity in sensation from increased innervation [24]. For example, the hand

region, an extensively innervated region of the body that plays an important role in fine tactile acuity was represented with a larger cortical area than the forearm region, a less extensively innervated body region. The Penfield homunculus clearly demonstrates this phenomenon. Perhaps if a body region has a more extensive cortical area devoted to the mapping of cutaneous stimulation, the fMRI signal would be more robust. We saw this phenomenon in our results: hand stimulation elicited 49 activated areas; forearm stimulation elicited 25 activated areas; forefinger stimulation elicited 18 activated areas. With only 18-25 activated areas, we were not able to surpass the crucial signal to noise ratio in the fMRI signal to give detailed somatotopy.

It is also possible that we were limited by the resolution of the fMRI signal. Resolution of the functional scans was $3 \times 3 \times 7 \text{ mm}^3$. If the representation of the forefinger or forearm did not extend well beyond this limiting resolution among the majority of the 10 hemispheres, we should not have expected that we could localize these regions within the postcentral gyrus.

The representation of the thumb, however, is comparable in spatial extent to the hand. We would expect to see thumb activation in as broad a region as hand activation. The Penfield homunculus shows, in fact, that the thumb and hand are among those body regions with the largest relative magnification in their cortical representation. The only explanation that we can put forth for this discrepancy is experimental error.

We conclude from the somatotopic mapping study that detailed somatotopy across 5 sub-

jects, 10 hemispheres is difficult to realize with these fMRI methods. While a distinct hand representation was localized, forearm, thumb, and forefinger activation did not overcome the noise in the fMRI signal. Greater sampling of subjects may be the answer to this problem.

8.2 Lateral Inhibition in the fMRI Signal

Lateral inhibition of body representations as seen through the fMRI signal was definitely present in our data. There are two alternative hypotheses that predict inhibition in the signal: inhibition from neuronal interactions, or inhibition from metabolic fluctuations.

8.2.1 Neuronal Somatosensory Lateral Inhibition

The presence of neuronal lateral inhibition in the somatosensory system is a well-reported phenomenon [10, 53, 34, 48]. Neuronal lateral inhibition arises from the divergence of signals that occur at each relay station as a cutaneous receptor signal travels to the cerebral cortex. For example, a point stimulus such as a von Frey hair, will activate several touch receptors in the area around the stimulus. The impulses from these touch receptors will discharge a group of cells in a dorsal column nucleus, which discharge a group of cells in the ventral posterior nucleus of the thalamus, and which discharge a group of cells in the primary somatosensory cortex. The population of cells that are activated at each relay station is controlled by two factors: first, the afferent pathway that was activated initially by the stimulus connects anatomically to a certain population of cells; and second, the popu-

lation of neurons at each relay station directly activated by the initial stimulus also discharge inhibitory neurons that will restrict the final population of responding neuronal cells. This inhibitory phenomenon produces the resolution and localization of the stimulus at each relay station of the central nervous system and eventually in the cerebral cortex (Figure 26) [24].

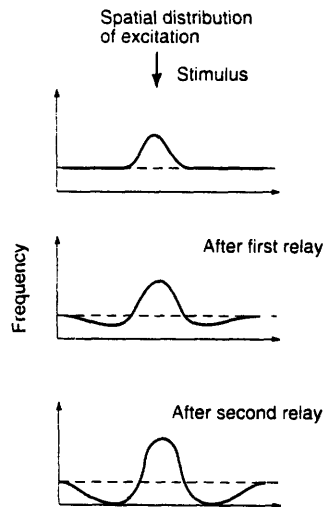
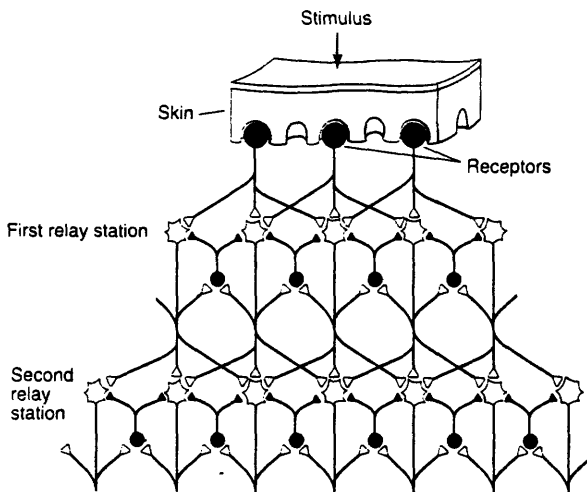
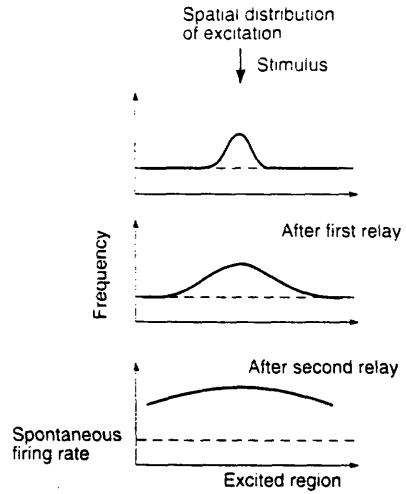
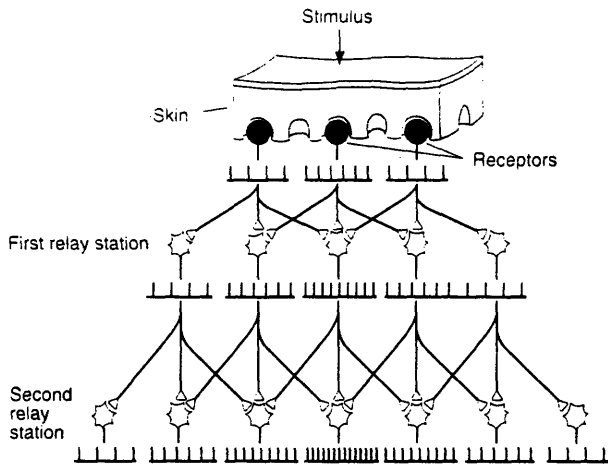
Dykes et al. [10] reported on the role of γ -amino-butyric acid (GABA) in cat primary somatosensory cortex. They found that GABA mediated the local inhibitory influences of neuronal response to cutaneous stimuli. Extracellular recordings revealed that bicuculline methiodide (BMI) antagonized the GABA mediated influences and enlarged the size of the neuronal receptive-fields. Thus, Dykes et al. demonstrated the presence of lateral inhibition by demonstrating the predicted enlargement of the receptive field when antagonizing inhibition (Figure 27) [10]. Additionally, Sur [53] reported center-surround organization in somatosensory neurons within the somatosensory cortex of macaque monkeys, and Moore et al. [34] reported the presence of lateral inhibition in intracellular recordings of rat somatosensory cortex, results consistent with the presence of neuronal lateral inhibition.

Schroeder et al. [48] reported the presence of intracortical inhibition in the somatosensory cortex of squirrel monkeys in a study of the organization of latent inputs within area 3b after median or ulnar nerve section. They found that input from the radial nerve had access to the cortical regions normally driven by input from the median and ulnar nerves; the representation of the glabrous hand was inhibited by nondominant input from the

radial nerve and dominant input from the median or ulnar nerves [48].

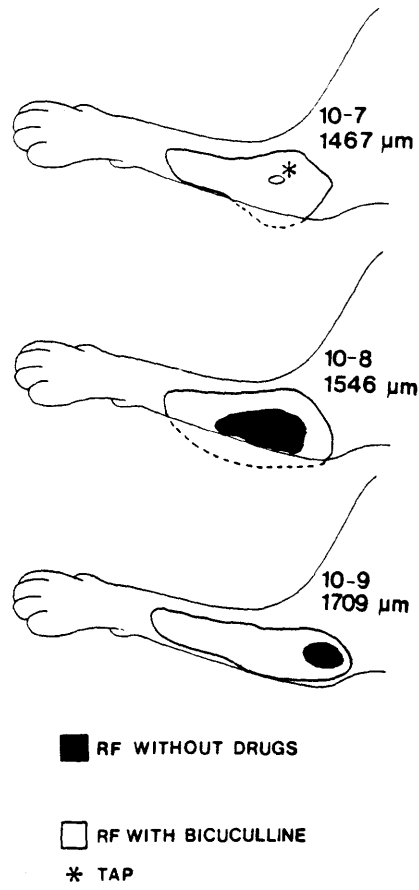
These studies clearly demonstrated lateral inhibition of neighboring representations in the postcentral gyrus. It is possible that the lateral inhibition we witnessed in the study of the organization of hand and forearm in the somatosensory cortex through fMRI is also due to this neuronal inhibition. However, there are several potential problems with this idea. FMRI is a measure of rCBF fluctuation in the cortex. As previously discussed, the correlation of rCBF to neuronal activity has been well-researched and well-established. Nonetheless, inhibitory surround of individual neurons may not scale to the spatial extent of the inhibition we see with the fMRI signal, although the inhibition by nondominant input reported by Schroeder et al. is the correct spatial magnitude. Further, inhibition in the cortex is mediated by local inhibitory interneurons. Although these interneurons inhibit the surrounding neurons, they themselves are the most highly metabolically active neurons in the brain [24] and may increase the strength of the metabolic signal while inhibiting the neurons around them.

Figure 26. Neuronal inhibition due to the discharge of inhibitory neurons at each relay station of the central nervous system. This diagram shows how inhibition at the point of stimulation is conveyed through the neuronal pathways [24].



Effect of Lateral Inhibition

Figure 27. Enlargement of neuronal receptive fields when inhibition is antagonized. Dykes et al. found that bicuculline methiodide (BMI) blocks GABA mediated inhibition in cat primary somatosensory cortex. These studies support the presence of intracortical surrounding lateral inhibition [10].



Enlargement of Receptive Fields
After Blocking Lateral Inhibition

8.3.2 Metabolic Somatosensory Lateral Inhibition

Changes in rCBF indicate relative changes in regional cerebral oxygen metabolism. Seitz et al. [49] found that rCBF increases in primary somatosensory cortex could be detected with PET in response to vibratory somatosensory stimulation. Further, these rCBF increases were accompanied by rCBF decreases in the superior parietal cortex, the paralingual association area, and the left globus pallidus. Thus, the increases and decreases in rCBF were balanced so that the mean global CBF did not change during somatosensory stimulation compared with rest [49]. These findings support similar conclusions of Ingvar et al. in a study of language production using an intracarotid Xenon injection technique [reviewed in 49].

Kawashima et al. [25] similarly demonstrated cross-modality inhibition in selective attentional tasks using PET studies of rCBF. A series of PET studies were performed on human subjects engaged in a somatosensory task in “eyes open” and “eyes closed” conditions. During these tasks, Kawashima et al. found a significant decrease of rCBF in the visual cortex during eyes opened and eyes closed conditions, suggesting that decreases in rCBF in unattended areas during somatosensory tasks would occur, irrespective of input to the unattended areas. Thus, Kawashima et al. demonstrated not only clear selective activation of cortical regions known to participate in modality specific tasks, but also selective deactivation of unattended areas across modalities [25].

Drevets et al. [11] found focal activation and inhibition within the somatosensory cortex.

They monitored PET measurements in primary and secondary somatosensory cortices during the period when somatosensory stimuli were expected. They found that in *anticipation* of innocuous touching or localized, painful shocks, rCBF decreased in parts of the somatosensory cortex homunculus map located laterally, outside the regions devoted to representation of the skin area corresponding to the locus of expected stimulation. For example, they found that an anticipated stimulus to the fingers resulted in a decreased rCBF in the face area; anticipated stimulus to the toes resulted in a decreased rCBF in the finger and face area. However, no significant changes in rCBF occurred in the regions of the cortex representing the anticipated stimulus region. Such findings support the notion that analysis of the form of suppressing background activity may facilitate the processing of signals that respond to external stimuli [11].

Our findings of lateral inhibition in response to cutaneous stimuli of adjacent representations in the postcentral gyrus followed from the work of Seitz et al. [49], Kawashima et al. [25], and Drevets et al. [11]. We found that during the period in which somatosensory stimulation was administered to a given skin surface, fMRI signal intensity in regions of the postcentral gyrus mapped to the stimulated surface increased while signal intensity in those regions adjacent decreased. Such inhibition may be due to a local rationing of oxygenated blood similar to that described by Seitz et al., Kawashima et al., and Drevets et al. This report is the first demonstration of lateral inhibition in the fMRI signal from somatosensory stimulation.

We conclude that lateral inhibition of rCBF, and thus the fMRI signal, following hand and

forearm stimulation is a logical and coherent finding. Furthermore, by using the lateral inhibition of representations in the cortex as a baseline for comparative analyses, the detection of somatosensory response in an fMRI signal can be facilitated by boosting the intensity of a desired representation (as in our H/F comparisons). With our somatotopic mapping methods, we were able to derive crude somatotopic maps in accordance with the Penfield homunculus. It has not escaped our attention that the effects of lateral inhibition could be utilized further to generate a more complete, detailed somatotopic map with fMRI.

References

1. Aglioti, S., Cortese, F., Franchini, C. Rapid sensory remapping in the adult human brain as inferred from phantom breast perception. *Neuroreport* 5 : 473-476, 1994.
2. Cao, Y., Vikingstad, E. M., Huttenlocher, P. R., Towle, V. L. Functional magnetic resonance studies of the reorganization of the human hand sensorimotor area after unilateral brain injury in the perinatal period. *Proc. Natl. Acad. Sci. USA* 91 : 9612-9616, 1994.
3. Cohen, M. S., Bookheimer, S. Y. Localization of brain function using magnetic resonance imaging. *Trends in Neuroscience* 17 : 7, 1994
4. Colebatch, J. G., Deiber, M. P., Passingham, R. E., Friston, K. J., Frackowiak, R. S. J. Regional cerebral blood flow during voluntary arm and hand movements in human subjects. *J. of Neurophysiology* 65 : 6, 1991.
5. Connors, B. W., Gutnick, M. J. Intrinsic firing patterns of diverse neocortical neurons. *Trends in Neuroscience* 13 : 3, 1990.
6. Corkin, S. Chapter 4 : the role of different cerebral structures in somesthetic perception. *Handbook of Perception. Vol. VIB* : Academic Press, Inc., 1978.
7. Corkin, S., Milner, B., Taylor, L. Bilateral sensory loss after unilateral cerebral lesion in man. *Transactions of the American Neurological Association* 98 : 25-29, 1973.
8. Corkin, S., Milner, B., Rasmussen, T. Effects of different cortical excisions on sensory thresholds in man. *Transactions of the American Neurological Association*, 1964.
9. Corkin, S., Milner, B., Rasmussen, T. Somatosensory thresholds. *Archives of Neurology* 23 : 41-58, 1970.
10. Dykes, R. W., Landry, P., Metherate, R., Hicks, T. P. Function role of GABA in cat primary somatosensory cortex: shaping receptive fields of cortical neurons. *J. Neurophysiology* 52 : 1066-1093, 1984.
11. Drevets, W. C., Burton, H., Videen, T. O., Snyder, A. Z., Simpson, J. R., Raichle, M. E. Blood flow changes in human somatosensory cortex during anticipated stimulation. *Nature* 373 : 249-252, 1995.
12. Elbert, T., Flor, H., Birbaumer, N., Knecht, S., Hampson, S., Larbig, W., Taub, E. Extensive reorganization of the somatosensory cortex in adult humans after nervous system injury. *Neuroreport* 5 : 2593-2597, 1994.

13. Flor, H., Elbert, T., Knecht, S., Wienbruch, C., Pantev, C., Birbaumer, N., Larbig, W., Taub, E. Phantom-limb pain as a perceptual correlate of cortical reorganization following arm amputation. *Nature* 375 : 482-484, 1995.
14. Fried, I., Gozal, D., Kirlew, K. A. T., Hathout, G. M., Tang, H., Zhang, J., Harper, R. M. Dynamic magnetic resonance imaging of human Rolandic cortex. *Neuroreport* 5 : 1593-1596, 1994.
15. Friston, K. J., Frith, C. D., Frackowiak, S. J., Turner, R. Characterizing dynamic brain responses with fMRI : a multivariate approach. *Neuroimage* 2 : 166-172, 1995.
16. Friston, K. J., Frith, C. D., Frackowiak, S. J., Turner, R. Characterizing evoked hemodynamics with fMRI. *Neuroimage* 2, 157-165, 1995.
17. Frostig, R. D., Lieke, E. E., Tso, D. Y., Grinvald, A. Cortical functional architecture and local coupling between neuronal activity and the microcirculation revealed by in vivo high-resolution optical imaging of intrinsic signals. *Proc. Natl. Acad. Sci. USA* 87 : 6082-6086, 1990.
18. Gehi, A., Moore, C. I., Corkin, S., Rosen, B. R., Stern, C. E. FMRI of somatosensory cortex: somatotopy and lateral inhibition within the postcentral gyrus. Submitted, *Society for Neuroscience*, 1996.
19. Grafton, S. T., Woods, R. P., Mazziotta J. C. Within-arm somatotopy in human motor areas determined by positron emission tomography imaging of cerebral blood flow. *Experimental Brain Research* 95 : 172-176, 1993.
20. Horwitz, B. Data analysis paradigms for metabolic-flow data : combining neural modeling and functional neuroimaging. *Human Brain Mapping* 2 : 112-122, 1994.
21. Jack, C. R., Thompson, R. M., Butts, R. K., Sharbrough, F. W., Kelly, P. J., Hanson, D. P., Riederer, S. J., Ehman, R. L., Hangiandreou, N. J., Cascino, G. D. Sensory motor cortex: correlation of presurgical mapping with functional MR imaging and invasive cortical mapping. *Radiology* 190 : 85-92, 1994.
22. Jueptner, M., Weiller, C. Review : does measurement of regional cerebral blood flow reflect synaptic activity? - implications for PET and fMRI. *Neuroimage* 2 : 148-156, 1995.
23. Kaas, J. H., Garraghty, P. E. Hierarchical, parallel, and serial arrangements of sensory cortical areas : connection patterns and functional aspects. *Current Opinion in Neurobiology* 1 : 248-251, 1991.
24. Kandel, E. R., Schwartz, J. H., Jessell, T. M., *Principles of Neural Science, Third Edition*. Norwalk, CT : Appleton & Lange, 1991.

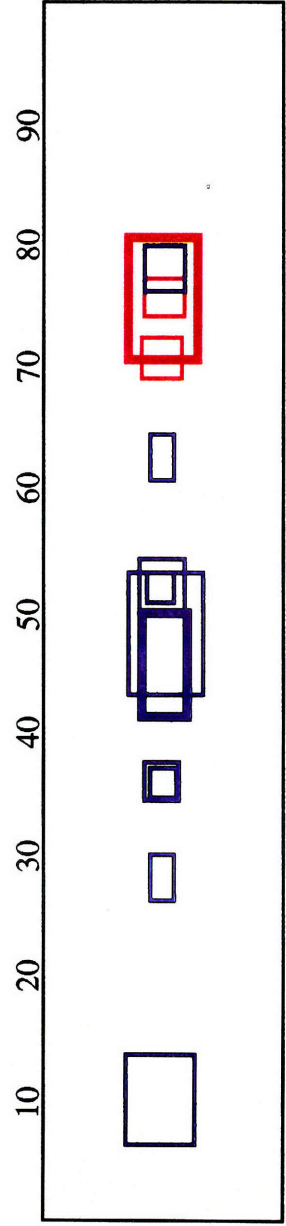
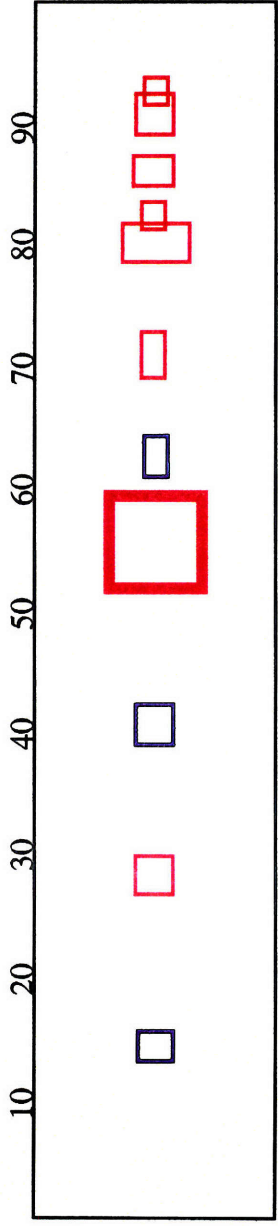
25. Kawashima, R., O'Sullivan, B. T., Roland, P. E. Positron-emission tomography studies of cross-modality inhibition in selective attentional tasks : closing the "mind's eye". *Proc. Natl. Acad. Sci. USA. Neurobiology*, 92 : 5969-5972, 1995.
26. Kew, J. J. M, Ridding, M. C., Rothwell, J. C., Rassingham, R. E., Leigh, P. N., Sooria-kumanran, S., Frackowiak, R. S. J., Brooks, D. J. Reorganization of cortical blood flow and transcranial magnetic stimulation maps in human subjects after upper limb amputation. *J. of Neurophysiology* 72 : 2517-2524, 1994.
27. Kim, S., Ashe, J., Georgopoulos, A. P., Merkle, H., Ellermann, J. M., Menon, R. S., Ogawa, S., Ugurbil, K. Functional imaging of human motor cortex at high magnetic field. *J. of Neurophysiology* 69 : 1, 1993.
28. Kwong, K. K., Belliveau, J. W., Chesler, D. A., Goldberg, I. E., Weisskoff, R. M., Poncelet, B. P., Kennedy, D. N., Hoppel, B. E., Cohen, M. S., Turner, R., Cheng, H., Brady, T. J., Rosen, B. R. Dynamic magnetic resonance imaging of human brain activity during primary sensory stimulation. *Proc. Natl. Acad. Sci. USA* 89 : 5675-5679, 1992.
29. Kristeva-Feige, R., Walter, H., Lutkenhoner, B., Hampson, S., Ross, B., Knorr, U., Steinmetz, H., Cheyne, D. A neuromagnetic study of the functional organization of the sensorimotor cortex. *Eur. J. of Neuroscience* 6 : 632-639, 1993.
30. Le Bihan, D., Karni, A. Applications of magnetic resonance imaging to the study of human brain function. *Current Opinion in Neurobiology* 5 : 231-237, 1995.
31. Merzenich, M. M., Kass, J. H., Sur, M., Lin, C. Double representation of the body surface within cytoarchitectonic areas 3b and 1 in "SI" in the owl monkey. *J. of Comparative Neurology* 181 : 41-74, 1978.
32. Merzenich, M. M., Kaas, J. H., Wall, J. T., Sur, M., Nelson, R. J., Felleman, D. J. Progression of change following median nerve section in the cortical representation of the hand in areas 3b and 1 in adult owl and squirrel monkeys. *Neuroscience* 10 : 639-665, 1993.
33. Merzenich, M. M., Recanzone, G., Jenkins, W. M., Allard, T. T., Nudo, R. J. Cortical representational plasticity. *Neurobiology of Neocortex*, John Wiley & Sons Limited : 41-67, 1988.
34. Moore, C. I., Gehi, A., Guimereas, A., R., Corkin, S., Rosen, B. R., Stern, C. E. Somatotopic mapping of cortical areas SI and SII using fMRI. *2nd Int. Conf. on Functional Mapping of the Human Brain*, 1996.
35. Moore, C. I., Nelson, S. B. In vivo whole cell recording of vibrissa-evoked synaptic responses in rat somatosensory cortex. *Society for Neuroscience*, 1994.

36. Ogawa, S., Tank, D. W., Menon, R., Ellermann, J. M., Kim, S., Merkle, H., Ugurbil, K. Intrinsic signal changes accompanying sensory stimulation : functional brain mapping with magnetic resonance imaging. *Proc. Natl. Acad. Sci. USA* 89 : 5951-5955, 1992.
37. Paxinas, G. *The Human Nervous System*. San Diego : Academic Press Inc., 1990.
38. Penfield, W., Boldrey, E. Somatic motor and sensory representation in the cerebral cortex of man as studied by electrical stimulation. *Brain* 60 : 369, 1937.
39. Penfield, W., Rasmussen, T. *The Cerebral Cortex of Man : A Clinical Study of Localization of Function*. New York : Hafner Publishing Company, 1950.
40. Pettit, M. J., Schwark, H. D. Receptive field reorganization in dorsal column nuclei during temporary denervation. *Science* 262 : , 1993.
41. Pons, T. P., Garraghty, P. E., Ommaya, A. K., Kaas, J. H., Taub, E., Mishkin, M. Massive cortical reorganization after sensory deafferentation in adult macaques. *Science*, 252 : 1857-1860, 1991.
42. Postone, N. Phantom limb pain. A review. *International J. of Psychiatry in Medicine* 17 : 1, 1987.
43. Ramachandran, V. S. Behavioral and magnetoencephalographic correlates of plasticity in the adult human brain. *Proc. Natl. Acad. Sci., USA* 90 : 10313-10420, 1993.
44. Rao, Sm. M., Binder, J. R., Hammeke, T. A., Bandettini, P. A., Bobholz, J. A., Frost, J. A., Myklebust, B. M., Jacobson, R. D., Hyde, J. S. Functional magnetic resonance imaging of complex human movements. *Neurology* 43 : 2311-2318, 1993.
45. Rao, Sm. M., Binder, J. R., Hammeke, T. A., Bandettini, P. A., Bobholz, J. A., Frost, J. A., Myklebust, B. M., Jacobson, R. D., Hyde, J. S. Somatotopic mapping of the human primary motor cortex with functional magnetic resonance imaging. *Neurology* 45 : 919-924, 1995.
46. Roland, P. E., Eriksson, L., Stone-Elander, S., Widen, L. Does mental activity change the oxidative metabolism of the brain? *J. of Neuroscience* 7 : 2373-2389, 1987.
47. Roland, P. E., Seitz, R. J. Positron emission tomography studies of the somatosensory system in man. *Exploring brain functional anatomy with positron tomography* (Ciba Foundation Symposium 163) : 113-124, 1991.
48. Schroeder, C. E., Seto, S., Arezzo, J. C., Garraghty, P. E. Electrophysiological evidence for overlapping dominant and latent inputs to somatosensory cortex in squirrel monkeys. *J. Neurophysiology* 74 : 722-732, 1995.

49. Seitz, R. J., Roland, P. E. Vibratory stimulation increases and decreases the regional cerebral blood flow and oxidative metabolism : a positron emission tomography (PET) study. *Acta Neurol Scand* 82 : 60-67, 1992.
50. Sereno, M. I., Dale, A. M., Reppas, J. B., Kwong, K. K., Belliveau, J. M., Brady, T. J., Rosen, B. R., Tootell, R. B. H. Borders of multiple visual areas in human revealed by functional magnetic resonance imaging. *Science* 268 : 889-893, 1995.
51. Stehling, M. K., Turner, R., Mansfield, P. Echo-planar imaging : magnetic resonance imaging in a fraction of a second. *Science* 254 : 43-50, 1991.
52. Sur, M. Maps of time and space. *Nature*. 378 : 13-14, 1995
53. Sur, M. *Some principles of organization of somatosensory cortex*. Unpublished doctoral dissertation, Vanderbilt University, 1978.
54. Sur, M., Merzenich, M. M., Kaas, J. H. Magnification, receptive-field area, and "hypercolumn" size in areas 3b and 1 of somatosensory cortex in owl monkeys. *J. of Neurophysiology* 44 : 2, 1980.
55. Talbot, J. D., marrett, S., Evans, A. C., Meter, E., Bushnell, M. C., Duncan, G. H. Multiple representations of pain in human cerebral cortex. *Science* 251 : 1355-1357, 1991.
56. Uematsu, S., Lesser, R. P., Gordon, B. Localization of sensorimotor cortex : the influence of sherrington and cushing on the modern concept. *Neurosurgery* 30 : 6, 1992.
57. White, J. C., Sweet, W. H. *Pain and the Neurosurgeon*. C. C. Thomas, 1969.
58. Woolsey, C. N. *Cortical Sensory Organization : Volume 1 - Multiple Somatic Areas*. Clifton, New Jersey : Humana Press, 1981.
59. Yang, T. T., Gallen, C. C., Ramachandran, V. S., Cobb, S., Schwartz, B. J., Bloom, F. E. Non-invasive detection of cerebral plasticity in adult human somatosensory cortex. *Neuroreport* 5 : 701-704, 1994.

Appendix

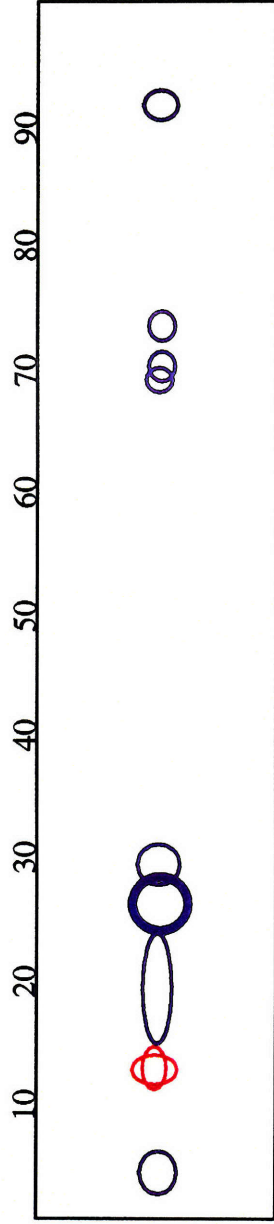
Appendix. Red rectangles on the hand/baseline comparisons indicate hand activation; blue rectangles indicate hand inhibition. Red circles on the forearm/baseline comparisons indicate forearm activation; blue circles indicate forearm inhibition. Red rectangles on the hand/forearm comparisons indicate hand activation; blue circles indicate forearm activation. Red rectangles on the hand+forearm/baseline comparisons indicate hand and forearm activation; blue rectangle indicate hand and forearm inhibition. Line thickness of rectangles and circles is proportional to $-\log(\text{p-value})$ of the KS statistic.



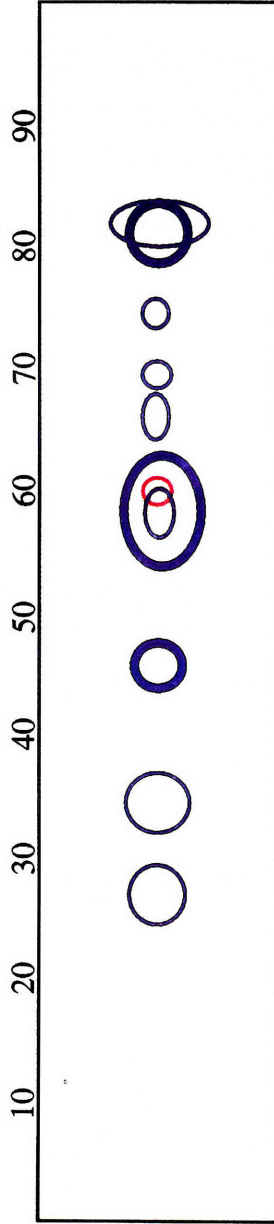
□ = Hand Activation

□ = Hand Inhibition

Subject1 : Hand/Base Comparison



Right Hemisphere

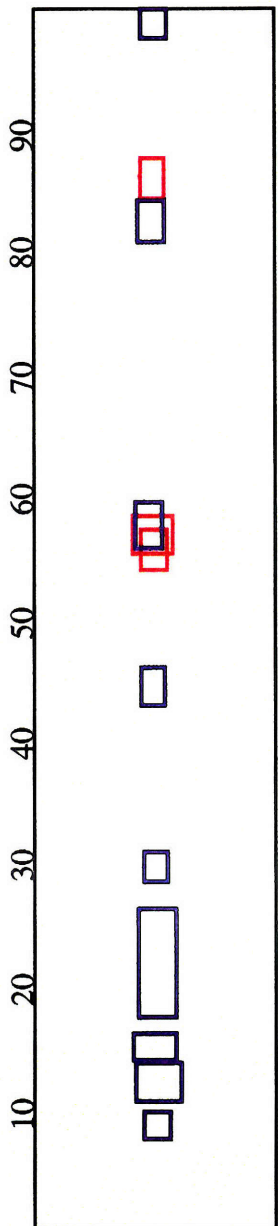


Left Hemisphere

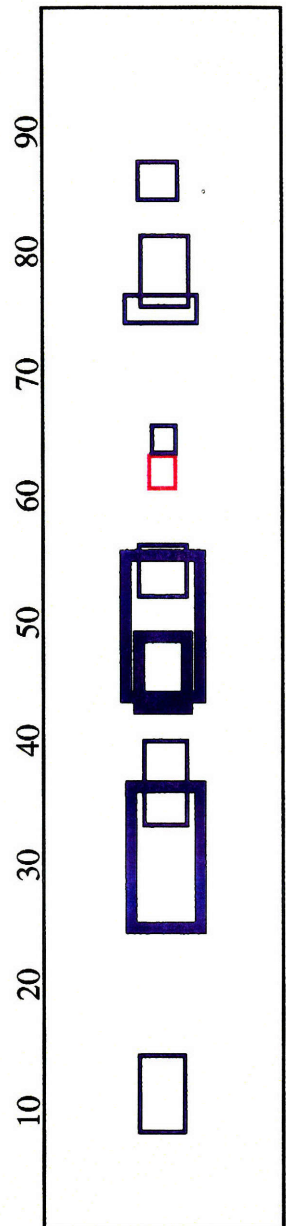
○ = Arm Activation

○ = Arm Inhibition

Subject1 : Arm/Base Comparison



Right Hemisphere

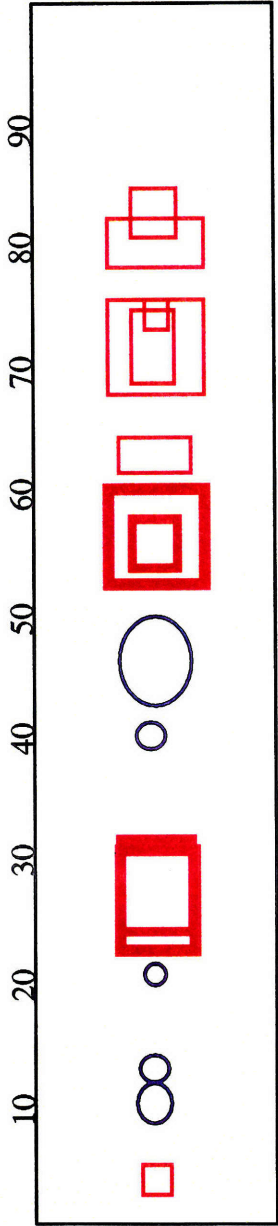


Left Hemisphere

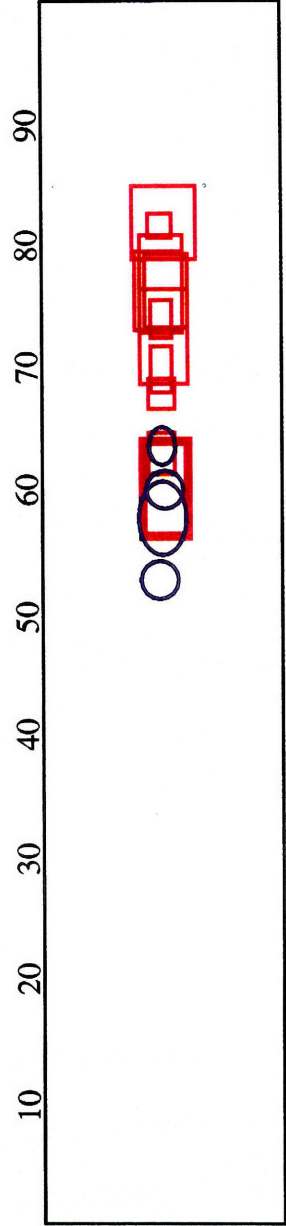
□ = Hand+Arm Activation

□ = Hand+Arm Inhibition

Subject1 : Hand+Arm/Base Comparison



Right Hemisphere

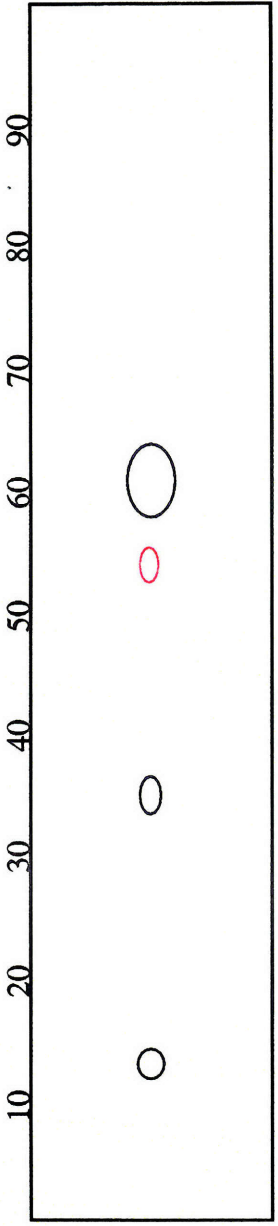


Left Hemisphere

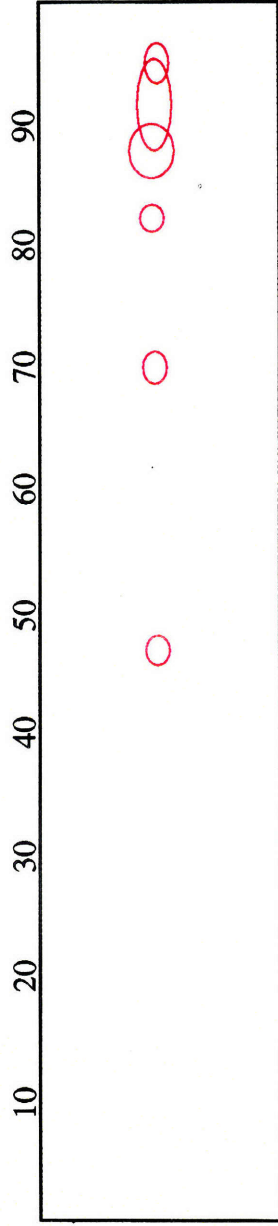
 = Hand Activation

 = Arm Activation

Subject1 : Hand/Arm Comparison



Right Hemisphere

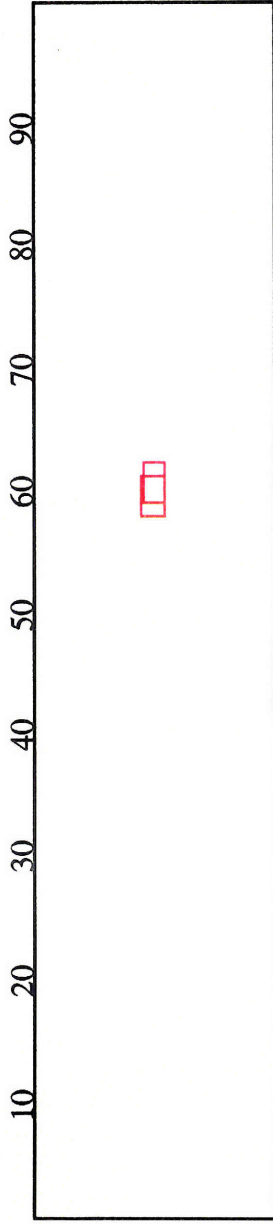


Left Hemisphere

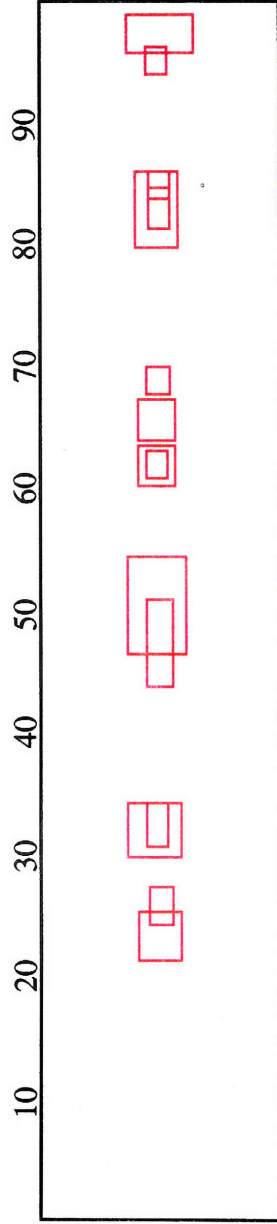
○ = Arm Activation

○ = Arm Inhibition

Subject2 : Arm/Base Comparison



Right Hemisphere

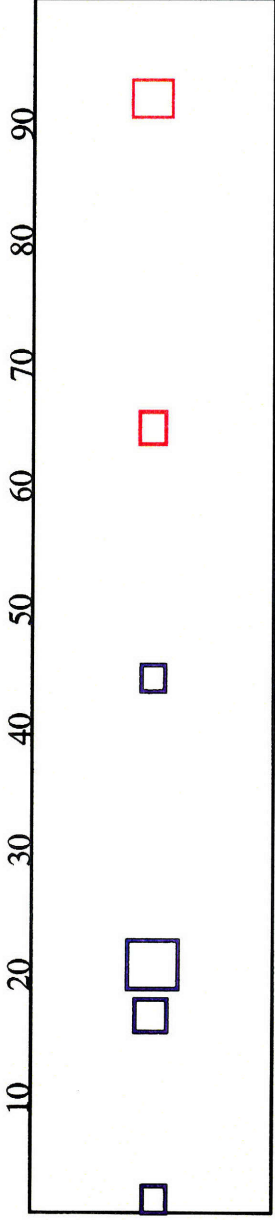


Left Hemisphere

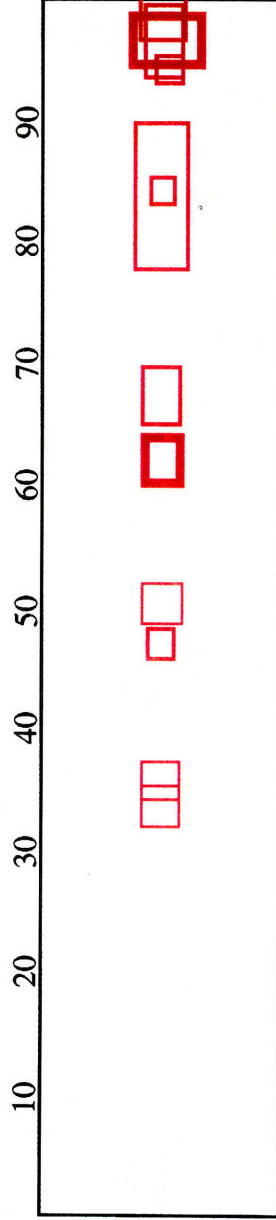
 = Hand Activation

 = Hand Inhibition

Subject2 : Hand/Base Comparison



Right Hemisphere

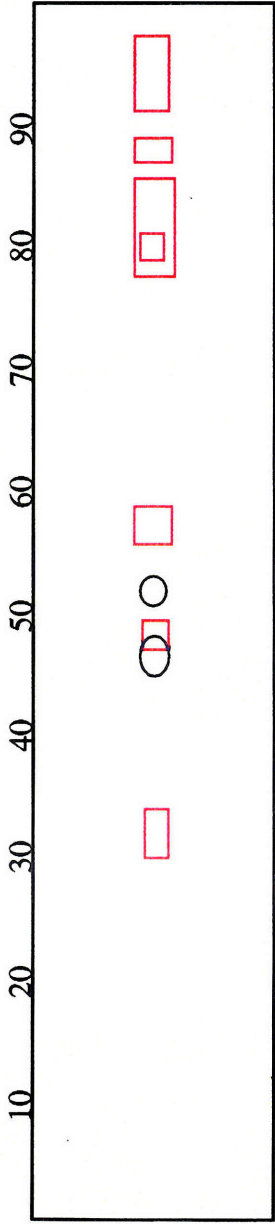


Left Hemisphere

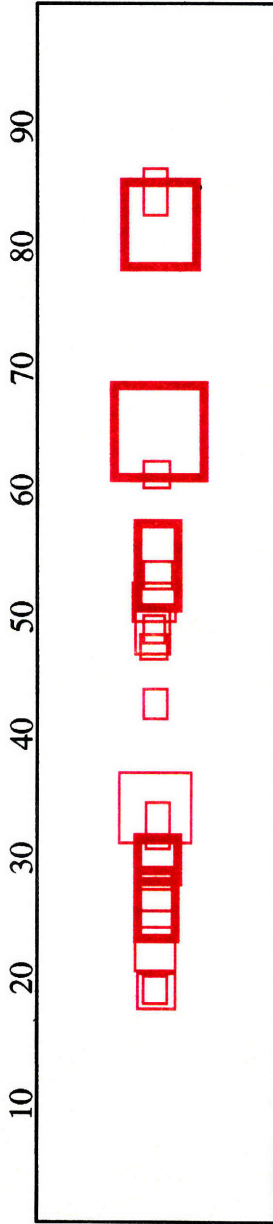
□ = Hand+Arm Activation

□ = Hand+Arm Inhibition

Subject2 : Hand+Arm/Base Comparison



Right Hemisphere

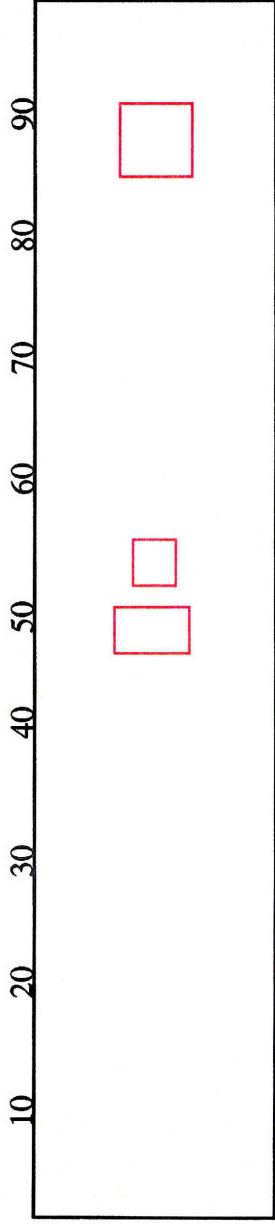


Left Hemisphere

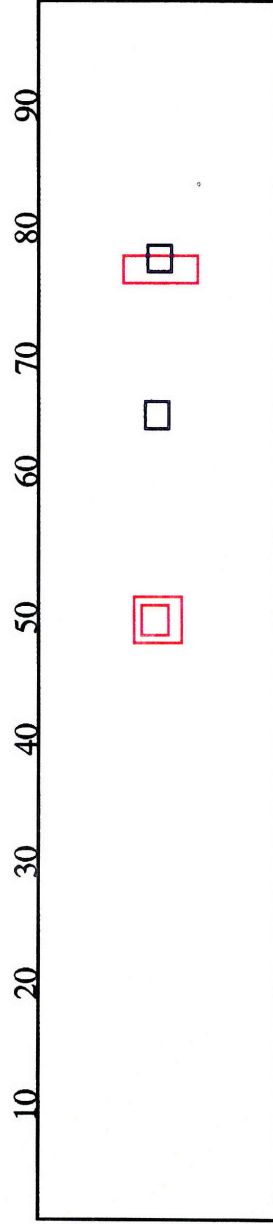
□ = Hand Activation

○ = Arm Activation

Subject2 : Hand/Arm Comparison



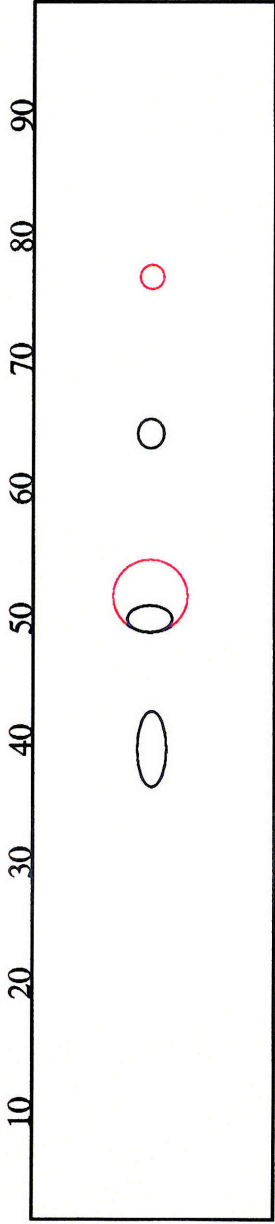
Right Hemisphere



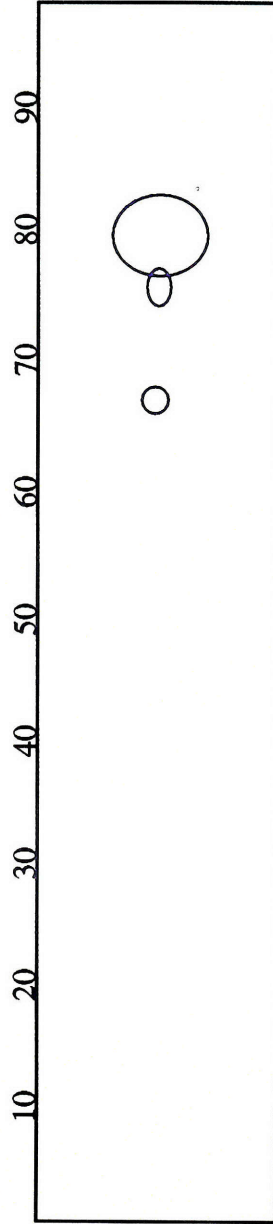
□ = Hand Activation

□ = Hand Inhibition

Subject3 : Hand/Base Comparison



Right Hemisphere

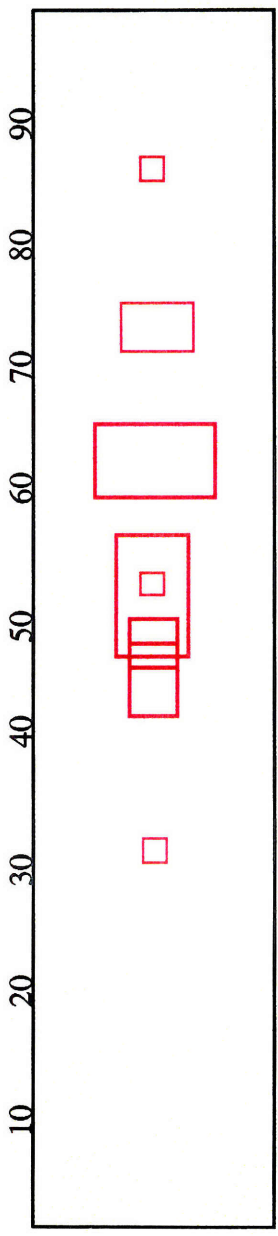


Left Hemisphere

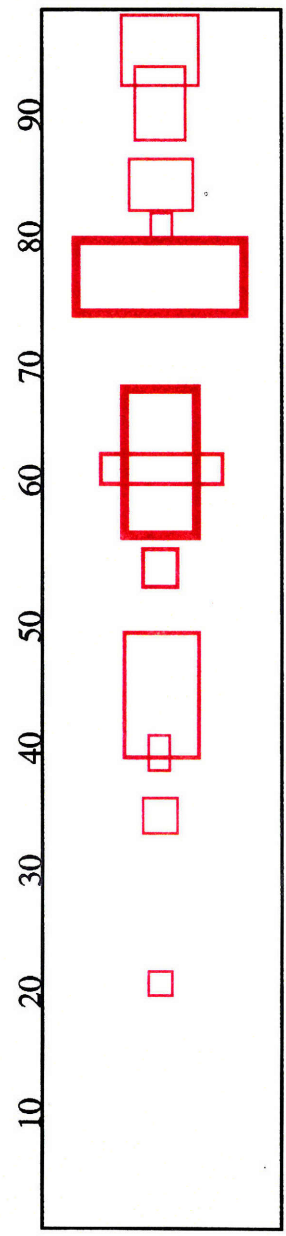
 = Arm Activation

 = Arm Inhibition

Subject3 : Arm/Base Comparison



Right Hemisphere

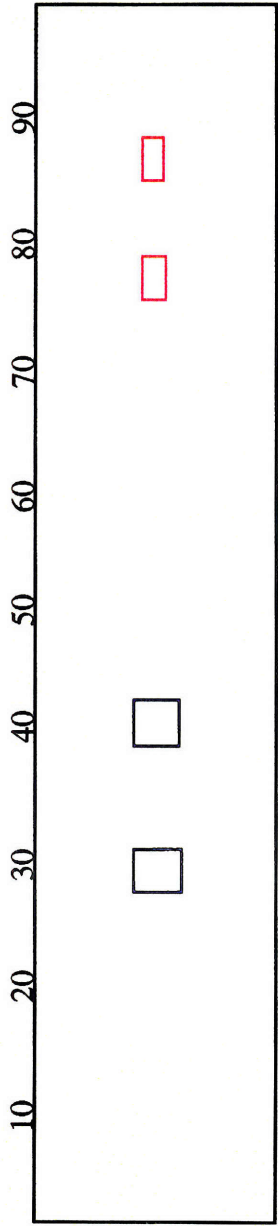


Left Hemisphere

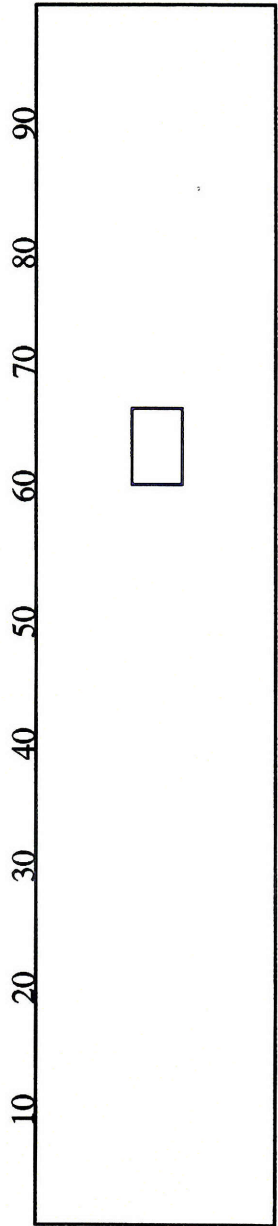
□ = Hand Activation

○ = Arm Activation

Subject3 : Hand/Arm Comparison



Right Hemisphere

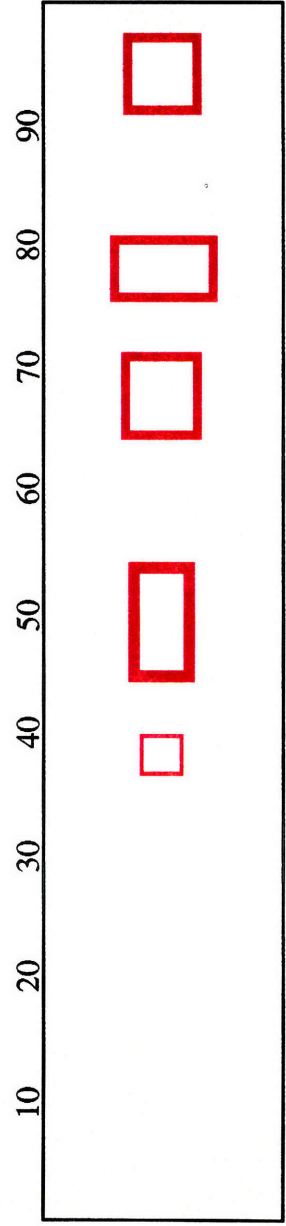
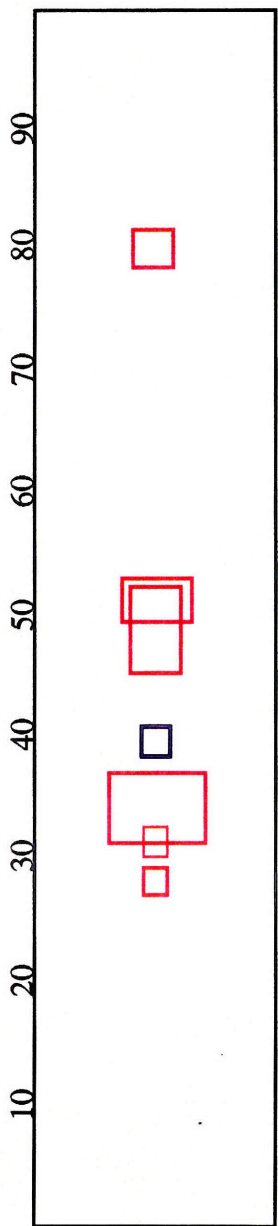


Left Hemisphere

 = Hand+Arm Activation

 = Hand+Arm Inhibition

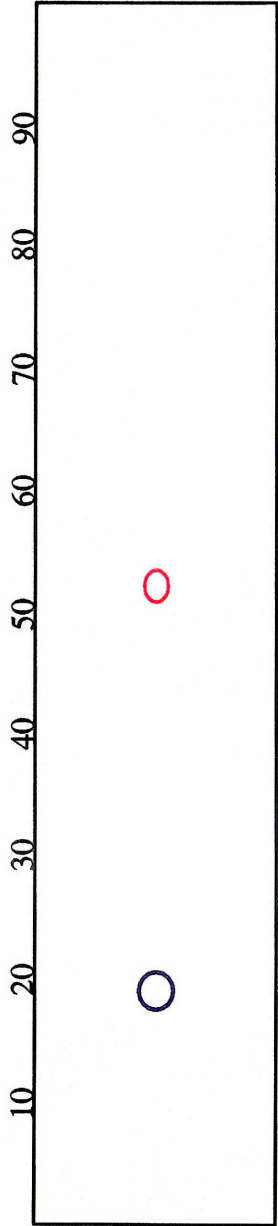
Subject3 : Hand+Arm/Base Comparison



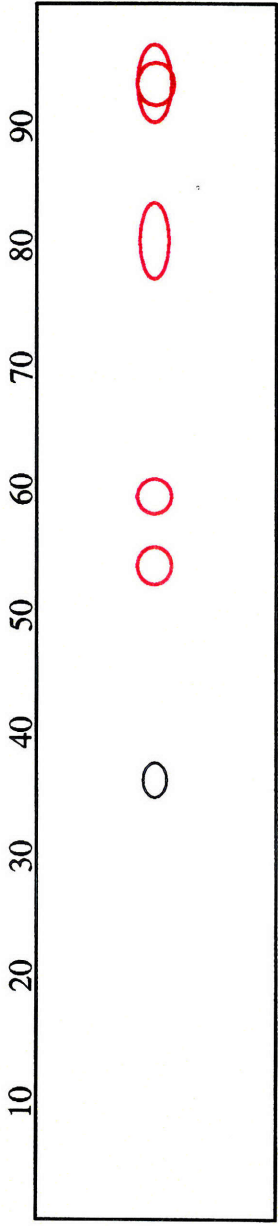
 = Hand Activation

 = Hand Inhibition

Subject4 : Hand/Base Comparison



Right Hemisphere

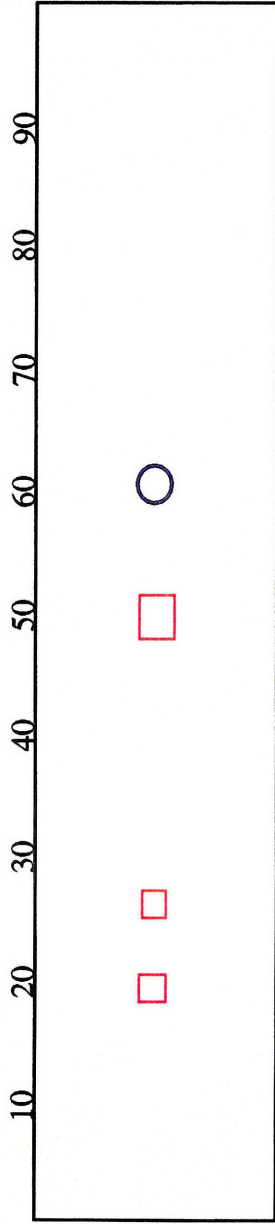


Left Hemisphere

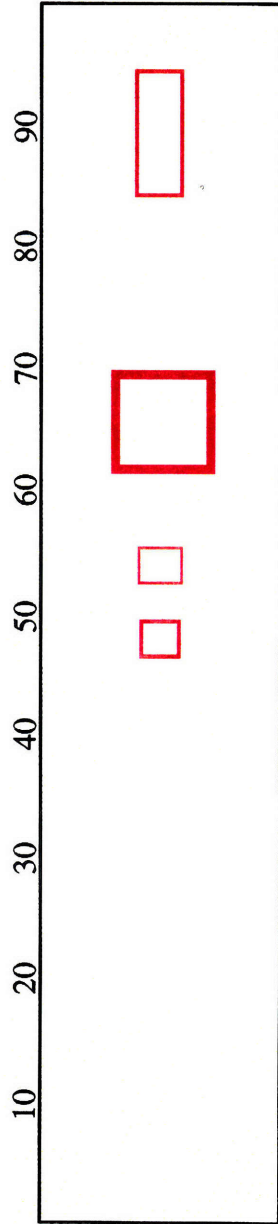
 = Arm Activation

 = Arm Inhibition

Subject4 : Arm/Base Comparison



Right Hemisphere

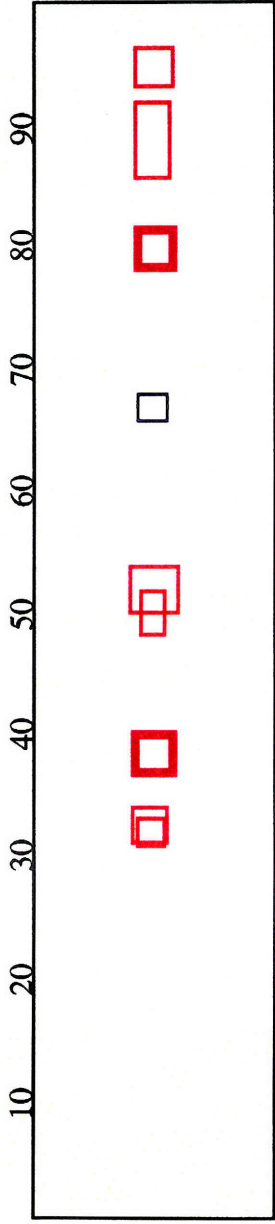


Left Hemisphere

□ = Hand Activation

○ = Arm Activation

Subject4 : Hand/Arm Comparison



Right Hemisphere

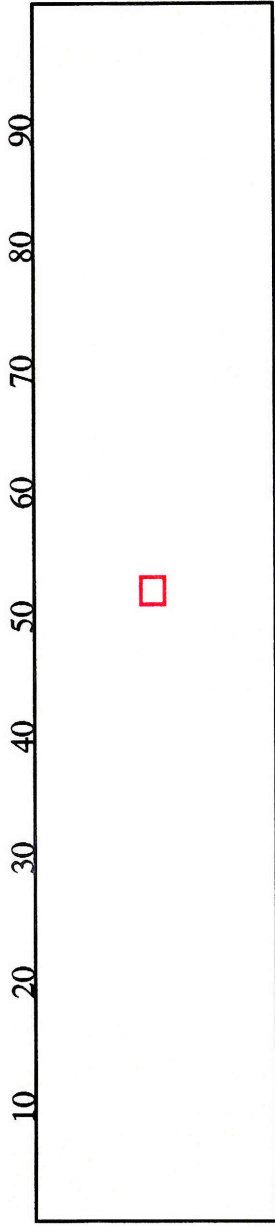


Left Hemisphere

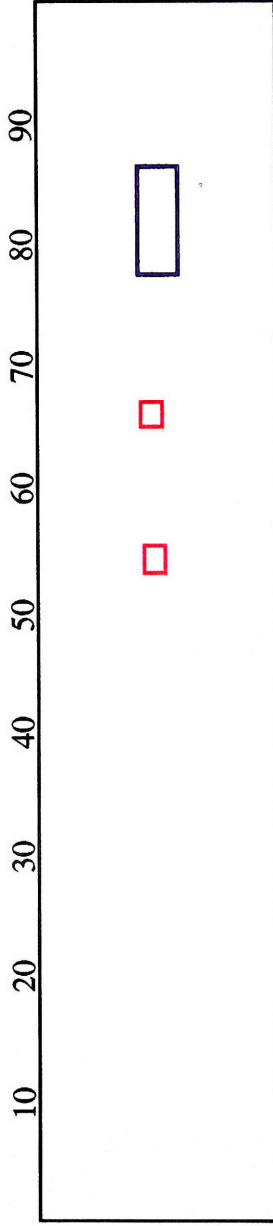
□ = Hand+Arm Activation

□ = Hand+Arm Inhibition

Subject4 : Hand+Arm/Base Comparison



Right Hemisphere

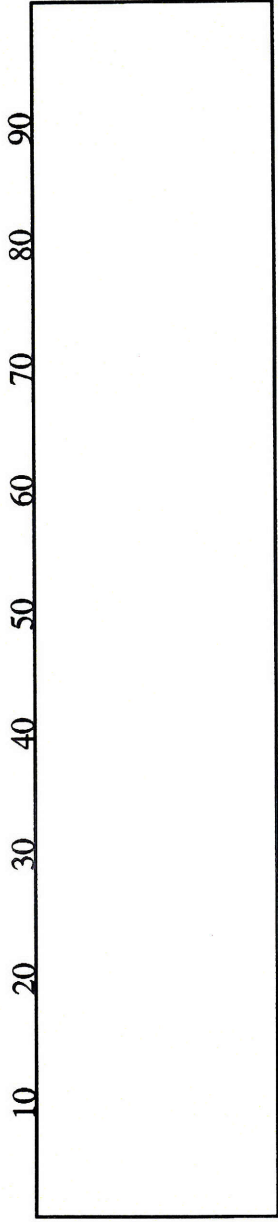


Left Hemisphere

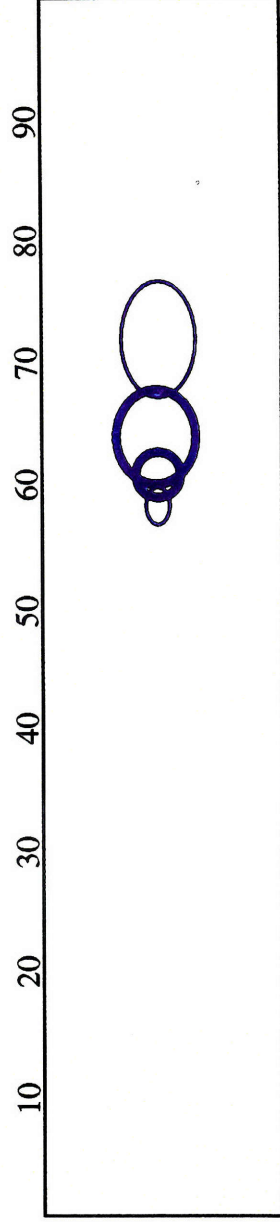
□ = Hand Activation

□ = Hand Inhibition

Subject5 : Hand/Base Comparison



Right Hemisphere

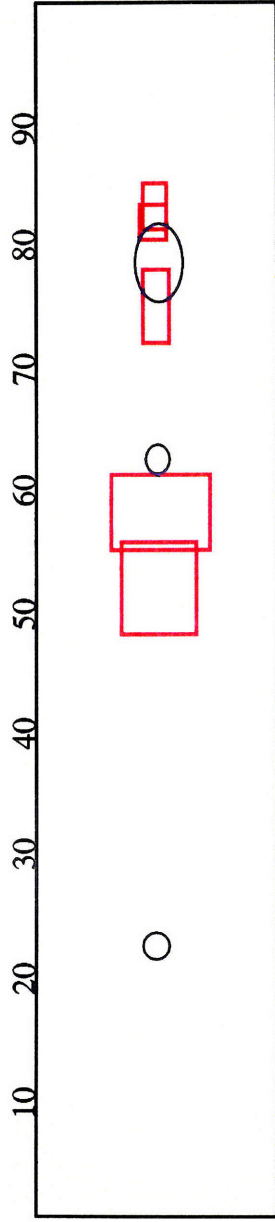


 = Arm Activation

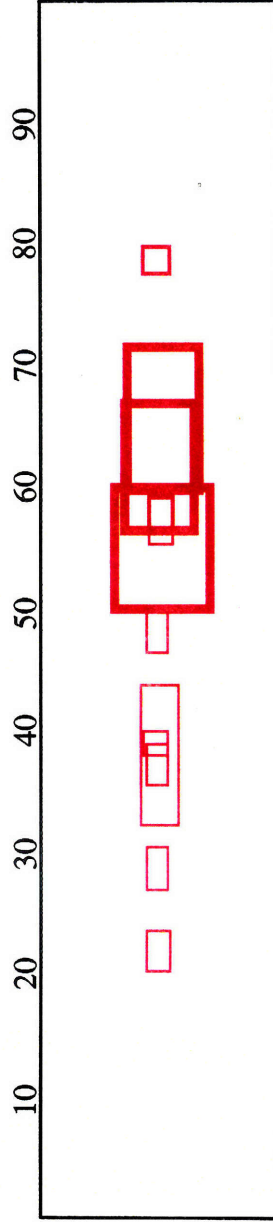
 = Arm Inhibition

Left Hemisphere

Subject5 : Arm/Base Comparison



Right Hemisphere

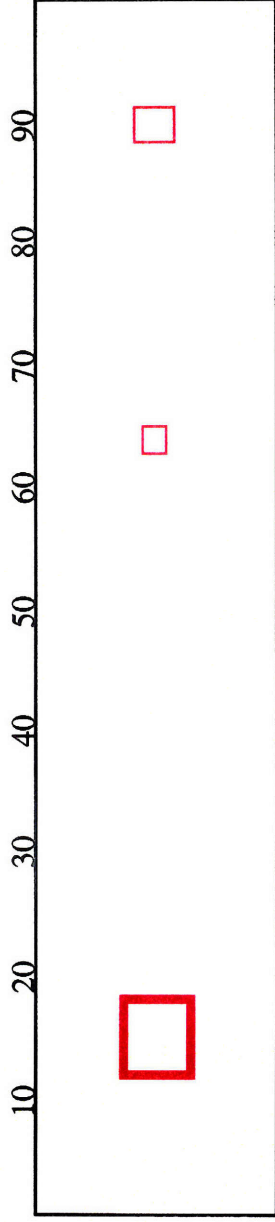


Left Hemisphere

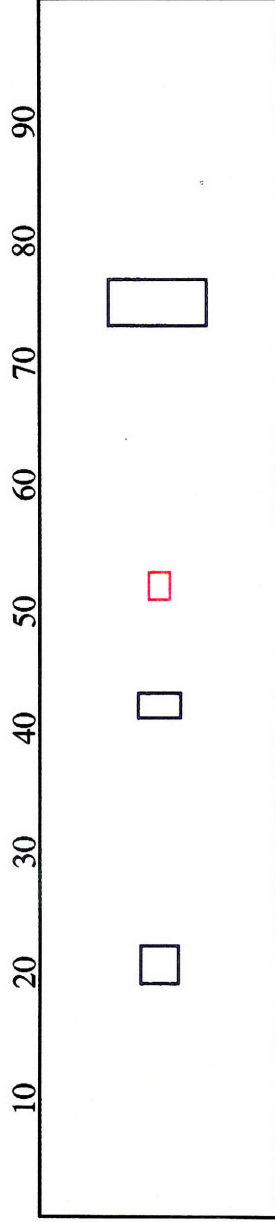
□ = Hand Activation

○ = Arm Activation

Subject5 : Hand/Arm Comparison



Right Hemisphere



Left Hemisphere

 = Hand+Arm Activation

 = Hand+Arm Inhibition

Subject5 : Hand+Arm/Base Comparison